(2)

March 1992
(Revised: Aug. 1992)

ANNUAL TECHNICAL REPORT

to

US AIR FORCE OFFICE OF SCIENTIFIC RESEARCH

Bolling Air Force Base
Washington DC 20332-6448

AFOSR-TR- 92 0890

AFOSR Grant No.91-0170

TRANSPORT PHENOMENA AND INTERFACIAL KINETICS IN MULTIPHASE COMBUSTION SYSTEMS

Principal Investigator: Daniel E. Rosner

Period Covered: 15 February 1991 to 14 February 1992

Yale University
High Temperature Chemical Reaction Engineering Laboratory
Department of Chemical Engineering
PO Box 2159 YS, New Haven CT 06520 USA

APPROVED FOR PUBLIC RELEASE: DISTRIBUTION UNLIMITED

REPORT DOCUMENTATION PAGE

Form Approved
OMB No. 0704-0188

1. AGENCY USE ONLY (Leave blank)	2. REPORT DATE	3. REPORT TYPE AND DATES COVERED
	MARCH 1992	Annual Tech. Rep. 2/15/91 - 2/14/92

4. TITLE AND SUBTITLE

TRANSPORT PHENOMENA AND INTERFACIAL KINETICS IN MULTIPHASE COMBUSTION SYSTEMS (u)

5. FUNDING NUMBERS

PE - 61102F
PR - 2308
SA - BS
G - AFOSR 91-0170

6. AUTHOR(S)

Principal Investigator: **Daniel E. Rosner**

7. PERFORMING ORGANIZATION NAME(S) AND ADDRESS(ES)

HIGH TEMPERATURE CHEMICAL REACTION ENGINEERING LABORATORY
YALE UNIVERSITY
BOX 2159, YALE STATION
NEW HAVEN, CONNECTICUT 06520 U.S.A.

8. PERFORMING ORGANIZATION REPORT NUMBER

9. SPONSORING/MONITORING AGENCY NAME(S) AND ADDRESS(ES)

AFOSR/NA
Building 410
Bolling AFB DC 20332-6448

10. SPONSORING/MONITORING AGENCY REPORT NUMBER

11. SUPPLEMENTARY NOTES

12a. DISTRIBUTION/AVAILABILITY STATEMENT

Approved for public release; distribution is unlimited

12b. DISTRIBUTION CODE

13. ABSTRACT (Maximum 200 words)

This *annual technical report* summarizes Yale High Temperature Chemical Reaction Engineering Laboratory research activities (under Grant AFOSR 91-0170) for the one-year period ending 14 February 1992. Among our research results described in detail in the cited references (Section 5). Perhaps the most notweworthy are the development of:

R1 rational correction factors to account for the effects of suspended particle morphology on convective-diffusion mass deposition rates

R2 quantitative criteria for influence of particle thermophoresis on the structure of two-phase laminar counterflow diffusion flames (potentially useful to predict IR radiation from such flames and optimize particle properties in synthesis applications)

R3 quantitative methods for predicting/correlating the effects of particle inertia on thermophoretic deposition across laminar boundary layers on targets with streamwise curvature (experimentally verified by our seeded micro-combustor experiments on concave ribbon targets)

15 presentations and 2 PhD dissertations have resulted from this research program. Copies of 3 reprints appearing during this period are included in the Appendices (Section 6) of this report.

14. SUBJECT TERMS

Key words Soot, aggregated particles, mass transport, thermophoresis, agglomerates, Brownian diffusion.

15. NUMBER OF PAGES 67

16. PRICE CODE

17. SECURITY CLASSIFICATION OF REPORT	18. SECURITY CLASSIFICATION OF THIS PAGE	19. SECURITY CLASSIFICATION OF ABSTRACT	20. LIMITATION OF ABSTRACT
Unclassified	Unclassified	Unclassified	UL

TRANSPORT PHENOMENA AND INTERFACIAL KINETICS IN MULTIPHASE COMBUSTION SYSTEMS

1. INTRODUCTION

The performance of ramjets burning slurry fuels (leading to condensed oxide aerosols and liquid film deposits), gas turbine engines in dusty atmospheres, or when using fuels from non-traditional sources , depends upon the formation and transport of small particles across non-isothermal combustion gas boundary layers (BLs). Even airbreathing engines burning "clean" hydrocarbon fuels can experience *soot* formation/deposition problems (*e.g.*, combustor liner burnout, accelerated turbine blade erosion and "hot" corrosion). Moreover, particle formation and transport are important in many chemical reactors used to synthesize or process aerospace materials (turbine blade coatings, optical waveguides, ceramic precursor powders,...). Accordingly, our research is directed toward providing chemical propulsion systems engineers and materials-oriented engineers with new techniques and quantitative information on important particle- and vapor-mass transport mechanisms and rates.

The purpose of this report is to summarize our research methods and accomplishments under AFOSR Grant 91-0170 (Technical Monitor: J.M.Tishkoff) during the 1-year period: 15 February '91-14 February '92. Readers interested in greater detail than contained in Section 2 are advised to consult the published papers explicitly cited in Sections 2 and 5. Copies of any of these published papers (Section 5.2) or preprints (Section 5.3) can be obtained by writing to the PI: Prof. Daniel E. Rosner, at the Department of Chemical Engineering, Yale University, Box 2159 Yale Station, New Haven CT 06520-2159 USA. Comments on, or examples of, the applications of our research (Section 3.4.) will be especially welcome.

An interactive experimental/theoretical approach has been used to gain understanding of performance-limiting chemical-, and mass/energy transfer-phenomena at or near interfaces. This included the development and exploitation of seeded laboratory flat flame burners (Section 2.1), and new optical diagnostic/spectroscopic techniques. Resulting experimental rate data, together with the predictions of asymptotic theories (Section 2), were used as the basis for proposing and verifying simple viewpoints and effective engineering correlations for future design/optimization studies.

2 RESEARCH ACCOMPLISHMENTS AND PUBLICATIONS

Most of the results we have obtained under Grant AFOSR 91-0170 can be divided into the subsections below:

2.1. TRANSPORT OF AGGREGATED PARTICLES

The Brownian diffusion-, inertial-, and optical-properties of *aggregated* particles, as formed in sooting diffusion flames, are quite *sensitive* to size (*eg.* number N of "primary" particles) and morphology (configuration of the N particles). In Fig. 1 (*eg.*) we summarize the orientation-averaged Brownian diffusivity of aggregates in the continuum (high presure) limit. Of interest are methods for anticipating coagulation and deposition rates of *populations* of such particles, especially in non-isothermal flow systems. We predict that capture rates from "coagulation-aged" polydispersed aerosols of a particular morphology by the mechanisms of convective-diffusion and, especially, thermophoresis will be close to those calculated if all such particles had the mean particle volume ϕ_p/N_p ,where ϕ_p is the particle *volume fraction* and N_p the *aggregate number density*. Correction factors (Fig.2) for convective-diffusion are found to be *ca.* 0.9 for a surprisingly wide range of gas-dynamic/environmental conditions, and particle morphologies. However, clearly, if one does not know the suspended particle morphology (distribution), a knowledge of volume- (or mass-) fraction alone is not enough to accurately predict *convective-diffusion* deposition rates, with (Section 2.2) or without simultaneous *inertial* effects.

The ability to reliably measure and predict the *thermophoretic* properties of aggregated flame-generated particles (carbonaceous soot, Al_2O_3, ...) is important to many technologies, including chemical propulsion and refractory materials fabrication. We are now completing a manuscript describing our measurements of the size- and morphology insensitive *thermophoretic diffusivity* of flame-generated submicron TiO_2(s) "soot" particles using $TiCl_4$(g)-seeded low strain-rate counterflow laminar diffusion flame (CDF-) techniques (Fig. 3, Gomez and Rosner, 1992)). One of our important conclusions is that engineering calculations of thermophoretically dominated soot deposition rates will usually *not* require details of the aggregate size- and morphology- distribution. Depending on the sharpness of the gas temperature and velocity gradients in counterflow diffusion flames there are one or more *particle stagnation planes*.(PSPs, Fig.4). A knowledge of the relative positions of the gas and particle stagnation planes (shown (Fig.5) *vs.* flame stoichiometry), and the associated chemical environments, can be used to control the composition and morphology of flame-synthesized particles. These factors should also influence particle production and radiation from *turbulent* non-premixed "sooting" flames, as will be discussed further in Gomez and Rosner, 1992

2.2. MULTIPHASE BOUNDARY LAYER THEORY: THERMOPHORESIS AND INERTIA

The results of seeded micro-combustor experiments, and ancillary theoretical calculations on the interesting competition between particle *inertia* and particle *thermophoresis* for the case of laminar gaseous boundary layers on surfaces with streamwise curvature (*eg.*, turbine blades) are shown in Fig.6 (from Konstandopoulos and Rosner, 1992; Rosner *et. al.* 1991). The combined effects of thermophoretic- and inertial-particle drift (here for compact aggregates of MgO(s) with volume mean diameter of *ca.* 0.8 μm) toward a concave, "cold" target are seen to substantially augment local particle deposition rates, in excellent accord with the predictions of two-phase laminar boundary layer theory. As implied by Fig.1, morphology will influence inertially modified deposition rates, reported here in terms of the dimesionless Stanton number (Rosner,1986). Indeed, if these MgO(s) particles were "open" agglomerates of equal mass the relevant dimensionless stopping time parameter: $Stk \cdot Re^{1/2}$ (where Stk is the ordinary *Stokes number* (Rosner,1986) and Re the prevailing length-Reynolds number evaluated at the deposition location) would have been too small to have a measureable effect for the cases shown. On *convex* cooled surfaces (*eg.* the "suction" side of a GT blade) our prediction-correlation methods predict the *competing* effects of thermophoretically-augmented capture and inertial drift *away* from the target. Instructive results for the angular distribution of mass transfer to cooled cylinders and spheres are displayed in Fig. 7. Our recommended correlation/prediction techniques for high Schmidt number combined inertia/phoretic deposition will be the subject of a follow-on paper.

2.3. HEAT TRANSFER EFFECTS ON COAGULATION DYNAMICS

Our continuing studies of submicron particle motion in host-gas temperature gradients and radiation fields (see, *eg.*, Mackowski *et.al.*1992, Rosner, *et. al.*,1992, Mackowski, D.W.,1990) have demonstrated that even spherical particles thermally out of equilibrium with their local host gas will coagulate with particle-particle encounter rate constants quite different from their usual "isothermal" Brownian values (see, *eg.*, the "correction" factors of Fig.8 for unequal-sized carbonaceous particles in a black-body radiation environment with the stated temperatures). This leads to *unusual population dynamics*, including the strong tendency of radiatively *cooled* large particles to grow still larger by rapidly "scavenging" smaller ones. Localized radiative cooling can also thermophoretically concentrate the radiating particles, with interesting stability consequences (Mackowski *et.al.* 1992

2.4. KINETICS AND MORPHOLOGY OF CVD-MATERIALS IN MULTI-PHASE ENVIRONMENTS

A small impinging jet (stagnation flow) reactor is being used to study the CVD-rates of refractory layers on inductively heated substrates, including those deliberately "pre-loaded" with

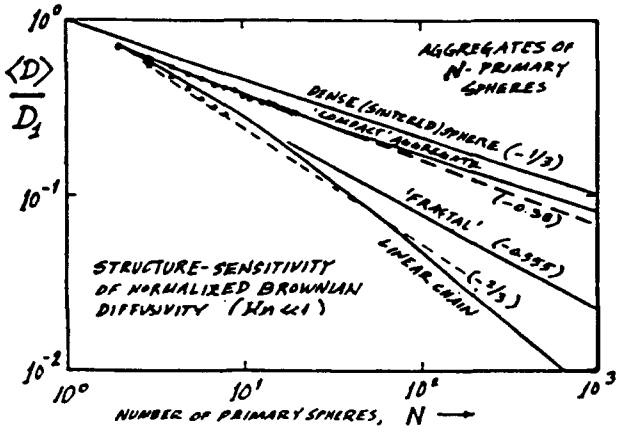

Fig.1. Predicted normalized orientation-averaged Brownian diffusivity of *aggregated* particles containing N-primary spheres in the near-continuum limit; Normalization: Brownian diffusion coefficient, D_1, of *primary sphere* in the same local environment (after Rosner *et.al.* 1991)

Aggregate Particle Morphology	Sc>>1 Convective-diffusion				Turbulent Eddy Impaction
	LDL		TBL		
	fm	c	fm	c	(c)
dense single spheres[d]	0.905	0.942	0.904	0.940	2.94
compact aggregates	?	0.936	?	0.934	2.62
fractal aggregates	0.925	0.922	0.933	0.921	1.79
linear chains[e]	0.914	0.918	0.919	0.917	1.47

a Thermophoretically-dominated deposition rate ratios (closer to unity) not reported here; present values are for negligible transport by non-convective mechanisms other than Brownian diffusion (numerical columns 1-4) or inertia (column 5)

b log-normal orientation averaged populations with $\sigma_g(fm)=2.46$ and $\sigma_g(c)=2.30$ (see,e.g. Rosner & Tassopoulos(1989))

d Reference case; sintered single spheres with abovementioned σ_g-values for PSD

e For continuum cases not strictly a power-law (Fig. 1), however, values stated are for approximate power-law representation for $\langle D_p(N)\rangle$

Fig. 2 Predicted values of $[-\dot{m}''_p/(-\dot{m}''_p(\bar{v}))]$ for isothermal deposition from coagulation-aged aggregated particle populations (after Rosner *et.al.*,1992)

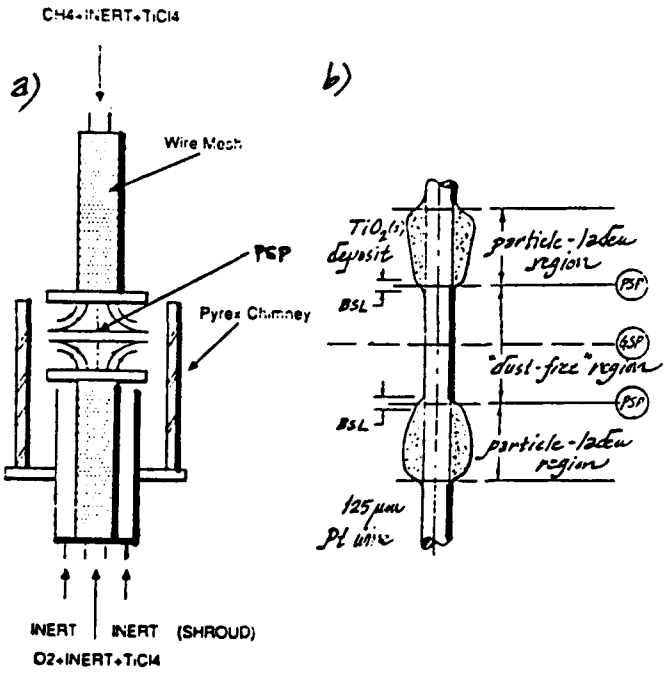

Fig.3 a). Axisymmetric counterflow diffusion flame (CDF) burner configuration used for experimental determination of particle thermophoretic diffusivity based on observed axial position of "particle stagnation planes" (PSPs); b) Appearance of axially mounted 125 μm diam. filament revealing existence of dust-free region straddling the flat diffusion flame (after Gomez and Rosner,1992)

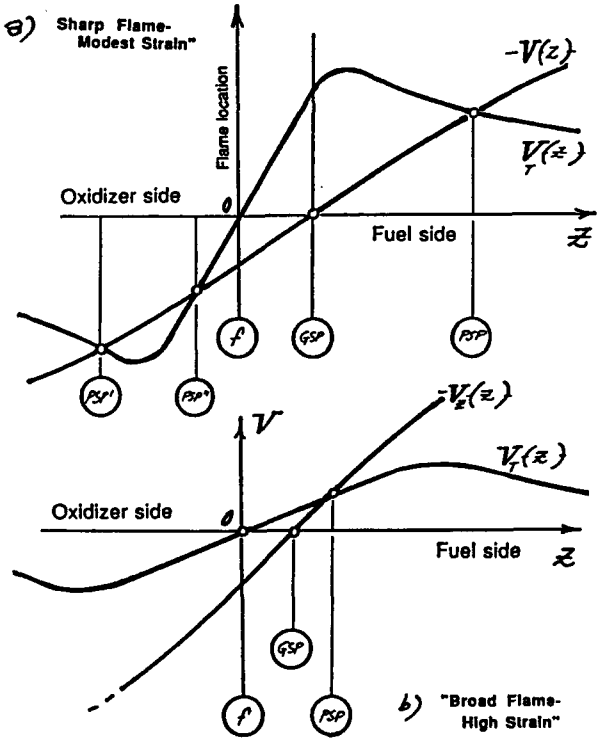

Fig.4 Axial gas velocity and particle thermophoretic velocity profiles in near-stoichiometric counterflow laminar diffusion flames; a) "Sharp flame-modest strain" case with *three* eligible particle stagnation planes (PSPs); b) Broad flame-high strain" case with *one* eligible particle stagnation plane (after Gomez and Rosner,1992)

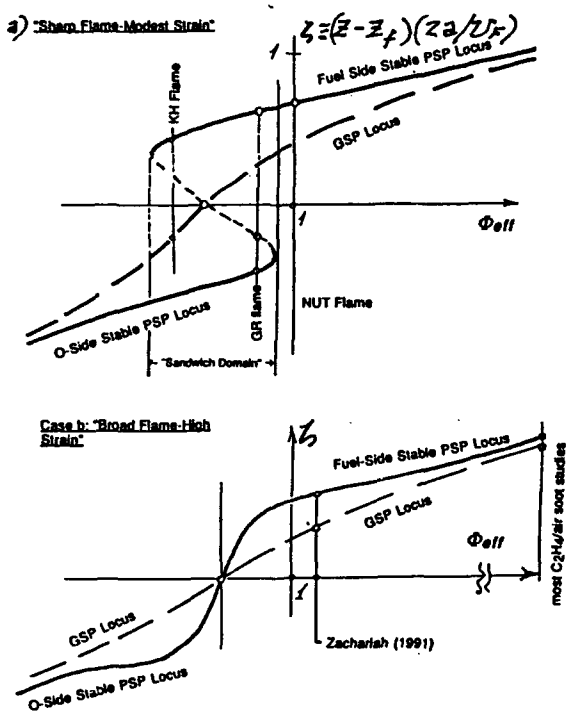

Fig.5 Locus of dimensionless axial positions of *particle stagnation plane*(s) (PSP) and *gas* stagnation plane (GSP) (relative to the flame location, z_f) for laminar counterflow. diffusion flames with fuel velocity U_F as a function of the effective fuel vapor *equivalence ratio*; Φ_{eff}.Case a) "Sharp flame-modest strain rate *a*", Case b "Broad flame-high strain rate *a*" (after Gomez and Rosner, 1992)

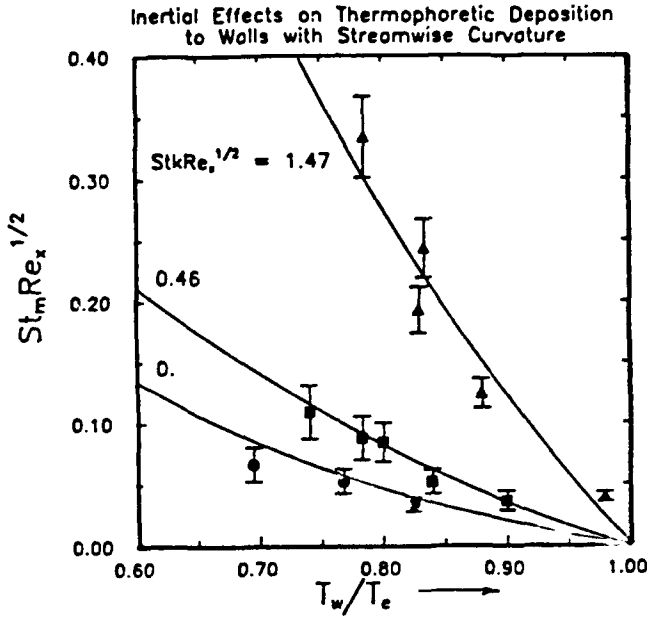

Fig.6 Experimental and theoretical dimensionless particle deposition rate coefficient (Stanton number) $St_mRe_x^{1/2}$ *vs.* surface-to-gas temperature ratio: T_w/T_e and the relevant particle relaxation time parameter (effective Stokes number) $StkRe_x^{1/2}$; laminar boundary layer flow, concave circular arc solid target (after Konstandopoulos and Rosner, 1992)

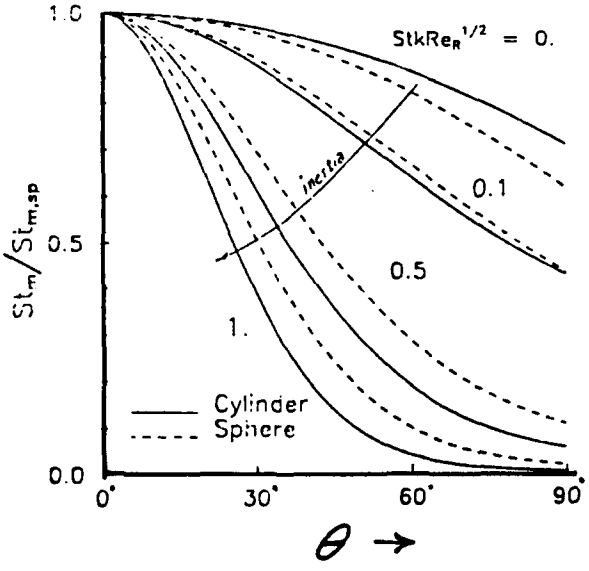

Fig. 7 Predicted inertial effects on thermophoretic-convective mass transfer rates to cooled convex objects at subcritical Stokes numbers; angular distribution of mass transfer coefficient for spheres and cylinders at high Reynolds numbers (Normalization: Stagnation point value at the prevailing value of Stk) (after Konstandopoulos(1991))

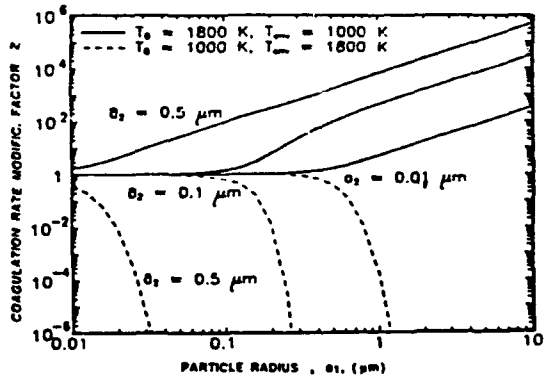

Fig. 8. Multiplicative "correction" to the Brownian (Smoluchowski isothermal) coagulation rate constant due to energy exchange to/from spherical particles of unequal radius (after Rosner *et.al.*,1992, Mackowski *et.al.* 1992)

porous particulate deposits. These measurements and associated "chemical vapor infiltration" theory will be useful to understand deposition rates and deposit microstructures that have been observed in particle-containing CVD environments. Analogous questions arise in anticipating the vapor scavenging- (or sorption-) ability of coagulation-aged populations of *suspended* aggregated particles, on which we are also working.

****

In our OSR-sponsored Yale HTCRE Lab research during the past year, briefly reviewed here, we have shown that new methods for rapidly measuring particle-mass transfer rates combined with recent advances in transport theory, provide useful means to identify and incorporate important, but previously neglected, mass transport phenomena in many propulsion engineering and materials engineering design/optimization calculations.

Despite the formidable complexities to be overcome in the design and operation of air-breathing propulsion power plants utilizing a broad spectrum energetic fuels these particular techniques and results are indicative of the potentially useful simplifications and generalizations which have emerged from our present fundamental AFOSR-funded research studies of combustion-generated particle transport mechanisms. It is hoped that this presentation and its supporting (cited) papers will facilitate the refinement and/or incorporation of some of the present ideas into engineering design procedures of much greater generality and reliability. This work has alredy helped identify new directions where research results would have a significant impact on engineering practice.

3. ADMINISTRATIVE INFORMATION: PERSONNEL, PRESENTATIONS, APPLICATIONS, "COUPLING' ACTIVITIES

The following sections summarize some pertinent 'non-technical' facets of the abovementioned Yale HTCRE Lab/AFOSR research program:

3.1 Personnel

The present results (Sections 2,4 and 5) are due to the contributions of the personnel listed in Table 3.1-1, which also indicates the role of each researcher and the relevant time interval of the activity. It will be noted that, in addition to the results themselves, this program has simultaneously contributed to the research training of a number of students and fresh PhDs, who will now be in an excellent position to make future contributions to technologies oriented toward air-breathing chemical propulsion, and high-tech materials processing.

3.2 Cooperation with US Industry

The research summarized here was supported by AFOSR under Grant 91-0170 (2/15/91-2/14/92). The Yale HTCRE Laboratory has also been the beneficiary of continuing smaller grants from U.S. industrial corporations, including GE-Schenectady, DuPont, and Shell as well as the feedback and advice of principal scientists/engineers from each of these corporations and Combustion Engineering-ABB. We appreciate this level of collaboration, and expect that it will accelerate inevitable applications of our results in areas relevant to their technological objectives (see, also, Section 3.4, below).

3.3 Presentations and Research Training

Apart from the publications itemized in Section 4 and our verbal presentations (of progress) at regular AFOSR Contractors Meetings, our results have also been presented at annual or topical conferences of the following professional organizations:

AAAR	Combustion Inst.(Central States Section)
AIChE	ASME-Engrg. Fdtn.
MRS	

Indeed, our paper on the subject matter of Section 2.3 was awarded first prize at the April '91 annual meeting of the Central States Section of the Combustion Inst.

Table 3.1-1 Summary of *Research Participants*[a] on AFOSR Grant :
TRANSPORT PHENOMENA AND INTERFACIAL KINETICS IN MULTIPHASE COMBUSTION SYSTEMS

Name	Status[a]	Date(s)	Principal Research Activity[b]
Castillo, J.	VS	3/15-4/15	interface stability
Collins,J.	GRA	'91,'92	CVD of ceramic coatings
Garcia-Ybarra, P.	VS	3/15-4/15	thermophoresis (kin.theory)
Gomez,A.	I-Asst.Prof.	'91,'92	meas. of particle transp. props.(CDFs)
Konstandopoulos,A†.	GRA	'91	thermophoresis/inertia coupling
Kho,T.	GRA	'92	chemical vapor infiltration (coatings)
Labowsky,M.	VS	'91,'92	method of images calculations
Papadopoulos,D	GRA	'92	transport phenomena in CVD reactors
Rosner, D.E.	PI	'91-'92	program direction-dep.theory/exp
Tassopoulos,M.†	GRA	'91	aggregate particle deposition
Tandon, P.	GRA	'91-'92	transport phenomena in BLs and CDFs
Tsang,J.	UGRA	Summer '91	CVD of TiO_2(s) Films

a PDRA=Post-doctoral Research Asst (arrival delayed to '92) GRA= Graduate Research Assistant
PI = Principal Investigator....VS = Visiting Scholar
b See Section 5 for specific references cited in text (Section 2); † PhD work completed during '91

In addition, during the period: 2/15/91 -2/14/92, the PI presented seminars at the following Universities:

U. Wisconsin	Waterloo	Trondheim-SINTEF
U. Oslo	KTH-Stockholm	U.Limoges
U.Toulouse	Technion (Haifa)	U. Paris-Nord
NTU-Athens		

In all, a total of about 15 talks were given by Yale-HTCRE people based in part on the results of this AFOSR research program.

This program involved the dissertation research of two graduate students (A.G.Konstandopoulos and M. Tassopoulos; cf.Table 3.1-1) who completed their PhD degree requirements in 1991.

3.4 Known Applications of Yale-HTCRE Lab Research Results

It has been particularly gratifying to see direct applications of some of this AFOSR-supported particle and vapor mass transfer research in more applications-oriented investigations reported in recent years. Indeed, the writer would appreciate it if further examples known to the reader can be brought to his attention.

Explicit examples are provided in ongoing work at MIT, and Sandia CRF, both groups having incorporated our rational correlation of *inertial particle impaction* (*e.g.* a cylinder in crossflow) in terms of an effective Stokes number.

This PI was also pleased to confirm applications of our AFOSR and DOE-supported research (on the correlation of inertial impaction by cylinders in crossflow) by the National Engineering Laboratory (NEL) of Glasgow Scotland (Contact: Dr. Andrew Jenkins). NEL is apparently collaborating with Marchwood Labs-CEGB on developing mass-transfer prediction methods applicable to waste-heat recovery systems in incinerators, as well as pulverized coal-fired boilers. These applications are somewhat similar to those reported by the Combustion Lab R&D group at MIT

In the area of alkali sulfate vapor deposition in combustion systems additional applications of our predictive methods (for "chemically frozen" and LTCE multicomponent laminar boundary

layers) continue to be made by British Coal Corporation-Power Generation Branch (I. Fantom, contact) in connection with their topping cycles which run gas turbines on the products of fluidized bed coal combustors/gasifiers. Our Poster in the 1988 Combustion Symposium (Seattle) appears to have motivated Prof. Takeno (Nagoya) to initiate experiments using a laminar counterflow

diffusion flame to estimate the thermophoretic diffusivity of LDV seed particles. Our paper on the experimental determination of smaller aggregated particle thermophoretic diffusivities using CDF/LDV/Laser Light Scattering techniques is nearing completion, and will be submitted to *Combustion Science and Technology* early in our next year's program. Also, in combustion research many groups (eg. Dobbinbs *et.al.* (Brown U.), Faeth *et.al.* (U. Mich.), Katz *et al.* (J.Hopkins U.)) are now utilizing "thermophoretic sampling" techniques to exploit the size- and morphology-insensitive capture efficiency characteristics that we have proven in our AFOSR research (Section 2.1).

Explicit use of our studies of self-regulated "capture" of incident impacting particles (Rosner and Nagaragan,1987) is being made in current work on impact separators and ceramic heat exchangers for coal-fired turbine systems in high performance stationary power plants. Other potential applications arise in connection with "candle filters" used to remove fines (sorbent particles,...) upstream of the turbines. A useful summary of work in these interrelated areas (Solar Turbines, Textron Defense Systems, Hague International,...) was presented at the Engineering Foundation Conference (Palm Coast, FL for March 1991): *Inorganic Transformations and Ash Deposition During Combustion.* , to appear (ASME/EF) in 1992.

Clearly, fruitful *opportunities* for the application of our recent "non-Brownian" convective mass transfer research now exist in many of the programs currently supported by the US Air Force.

4. CONCLUSIONS

In the OSR-sponsored Yale HTCRE Lab research during the period: 2/15/91-2/14/92, briefly described above, we have shown that new methods for rapidly measuring particle-mass transfer rates , combined with our recent advances in mass transport theory, provide useful means to identify and incorporate important, but previously neglected, mass transport phenomena in many propulsion engineering and materials engineering design/optimization calculations.

Despite formidable complexities to be overcome in the design and operation of mobile and stationary power plants utilizing a broad spectrum energetic fuels the abovementioned techniques and results (Section 2) are indicative of the potentially useful simplifications and generalizations which have emerged from our present fundamental AFOSR-funded research studies of combustion-generated particle transport mechanisms and interfacial reactions. It is hoped that this report and its supporting (cited) papers will facilitate the refinement and/or further incorporation of many of the present ideas into design and test procedures of greater generality and reliability. This work has also helped identify new directions where it is anticipated that research results will have a significant impact on future engineering practice.

5.REFERENCES

5.1 CITED BACKGROUND PUBLICATIONS (Predecessor OSR, DOE- Grants)

Eisner, A.D. and Rosner, D.E., Experimental Studies of Soot Particle Thermophoresis in Non-Isothermal Combustion Gases Using Thermocouple Response Techniques", *Combustion and Flame* **61**, 153-166(1985); see,also: *J. PhysicoChemical Hydrodynamics* **7** ,91-100 (1986)

Rosner, D.E. and Kim,S.S., "Optical Experiments on Thermophoretically Augmented Submicron Particle Deposition From 'Dusty' High Temperature Gas Flows", *The Chemical Engrg. J.*(Elsevier) **29**,[3].147-157 (1984)

Rosner, D.E. and Nagarajan. R.,"Toward a Mechanistic Theory of Net Deposit Growth from Ash-Laden Flowing Combustion Gases: Self-Regulated Sticking of Impacting Particles and Deposit Erosion in the Presence of Vapor 'Glue'", *Proc. 24th National Heat Transfer Conf.*, AIChE Symposium Series, Vol.**83** [257], pp.289-296, (1987)

Rosner, D.E., **Transport Processes in Chemically Reacting Flow Systems**, Butterworth-Heinemann, Stoneham MA, 1986; 3d Printing 1990.

5.2 PUBLICATIONS WHICH APPEARED* BASED IN PART ON AFOSR 91-0170

Castillo, J.L., Garcia-Ybarra, P., and Rosner, D.E.,"Morphological Instability of a Thermophoretically Growing Deposit", *J. Crystal Growth* **116**, 105-126, (1992)

Rosner, D.E., Mackowski,D.W,. Tassopoulos,M., Castillo,J.L., and Garcia-Ybarra, P., "Effects of Heat Transfer on the Dynamics and Transport of Small Particles in Gases", *I/EC -Research (ACS)* **31**,760-769 (1992)

Rosner, D.E.and Tassopoulos,M.," Correction for Sampling Errors due to Coagulation and Wall Loss in Laminar and Turbulent Duct Flow: Direct Solution to the Canonical 'Inverse' Problem for Log-Normal Size Distributions , *J. Aerosol Sci.* **22** (7) 843-867,(1991)

5.3 PAPERS SUBMITTED FOR PUBLICATION OR IN PREPARATION

Gomez, A., and Rosner, D.E., "Thermophoretic Effects on Particles in Counterflow Laminar Diffusion Flames " (in preparation, 1992 for submission to CST)

Gomez, A., Rosner, D.E. and Zvuloni, R., "Recent Studies of the Kinetics of Solid Boron Gasification by $B_2O_3(g)$ and Their Chemical Propulsion Implications", *Proc. 2d Int. Sympos. on Special Topics in Chemical Propulsion*: **Combustion of Boron-Based Solid Propellants and Solid Fuels**, (in press 1992)

Konstandopoulos, A.G.and Rosner, D.E.,"Inertial Effects on Thermophoretic Transport of Small Particles to Walls With Streamwise Curvature---I. Experiment, II. Theory", Submitted to *Int. J. Heat Mass Transfer* (Pergamon)

Mackowski, D.W., Tassopoulos, M. and Rosner, D.E.,"Effect of Radiative Heat Transfer on the Coagulation Rates of Combustion-Generated Particulates", Central States Mtg.-The Combustion Inst., April 1991, Nashville, TN.; (to be submitted to *Aerosol Sci. Technol.(AAAR)* (1992))

Park, H.M., and Rosner, D.E., "Thermophoretically Induced Phase Separation in Highly-Loaded 'Dusty' Gas Mixtures"(Revised version of HTCRE #162, in preparation 1992)

Rosner, D.E., Konstandopoulos, A.G., Tassopoulos, M., and Mackowski,D.W, "Deposition Dynamics of Combustion-Generated Particles: Summary of Recent Studies of Particle Transport Mechanisms, Capture Rates, and Resulting Deposit Microstructure/Properties", *Proc. Engineering Foundation Conference*: **Inorganic Transformations and Ash Deposition During Combustion**, (in press,1992)

Rosner, D.E. and Tandon, P., "The Effective Area/Volume and Sorptive Capacity of Populations of Micro-porous Aerosol Particles Distributed With Respect to Both Size (Volume) and Shape", ((in preparation, 1992 for submission to AIChE J.)

Zvuloni, R., Rosner, D.E., and Gomez, A., "Role of Water Vapor on the Gasification Kinetics of Solid Boron by its Higher Oxide $B_2O_3(g)$", *A.I.A.A. J. Propuls. Power* (in press (1989b)

Zvuloni, R., Rosner, D.E., and Gomez, A., "OBOBO(g) as a Gasifier of Graphite: Measurements and Implications", (in preparation, 1992); also:"High Temperature Kinetics of Solid Boron Gasification By its Higher Oxide $B_2O_3(g)$: Flow Reactor Techniques, Rate Measurements and Their Chemical Implications", *J. Phys. Chem.* (to be submitted, 1992)

*Full papers appear in Section 6

Journal of Crystal Growth 116 (1992) 105–126
North-Holland

JOURNAL OF CRYSTAL GROWTH

Morphological instability of a thermophoretically growing deposit

José L. Castillo, Pedro L. García-Ybarra

Departamento Física Fundamental, UNED, Apdo 60141, Madrid 28080, Spain

and

Daniel E. Rosner

High Temperature Chemical Reaction Engineering Laboratory, Department of Chemical Engineering, Yale University, New Haven, Connecticut 06520-2159YS, USA

Received 15 May 1990; manuscript received in final form 15 April 1991

The stability of the planar interface of a structureless solid growing from a depositing component dilute in a carrier fluid is studied when the main solute transport mechanism is thermal (Soret) diffusion. A linear stability analysis, carried out in the limit of low growth Peclet number, leads to a dispersion relation which shows that the planar front is unstable either when the thermal diffusion factor of the condensing component is positive and the latent heat release is small or when the thermal diffusion factor is negative and the solid grows over a thermally-insulating substrate. Furthermore, the influence of interfacial energy effects and constitutional supersaturation in the vicinity of the moving interface is analyzed in the limit of very large Schmidt numbers (small solute Fickian diffusion). The analysis is relevant to physical vapor deposition of very massive species on cold surfaces, as in recent experiments of organic solid film growth under microgravity conditions.

1. Introduction

The growth of solid deposits from the vapor phase is a technique widely used for the fabrication of thin layers of metals, insulators, and semiconductor materials; see, for instance, the review papers by Stringfellow [1] and Bryant [2]. Even though crystal growth from melts may be a more "efficient" process (usually giving growth rates several orders of magnitude larger than vapor phase growth), the latter is often preferred because of film quality considerations. In particular, new pharmacological and electro-optical applications demand the production of crystalline films of organic and organometallic macromolecules. The optimal growth of these materials from the vapor phase is now under intense experimental investigation internationally, even in microgravity environments to avoid crystal imperfections induced by buoyancy-driven instabilities, see Walter [3].

Especially since the pioneering work of Mullins and Sekerka [4,5] and the review by Langer [6], it is well known that planar crystal growth may be *morphologically unstable* during the solidification of a supercooled liquid (i.e., in the absence of capillarity, a forward-facing bulge in the interface steepens the thermal gradient in the fluid ahead of it, so that latent heat is more rapidly removed from the surface and the bulge amplifies unstably), and in the similar case of isothermal solidification of a liquid mixture (respectively, directional solidification of a binary liquid) due to the *constitutional supersaturation* (respectively, consti-

tutional supercooling) induced ahead of the advancing solidification front. In the above-mentioned cases, the morphological instability arises as a consequence of the existence of a metastable liquid phase near the fluid–solid interface.

A simplified criterion for the existence of constitutional supersaturation was given by Reed and LaFleur [7] and reconsidered by Rosenberger et al. [8]. This criterion leads to the existence of a critical temperature gradient reached when the concentration gradient at the interface just overcomes the gradient of the saturation concentration. Temperature and concentration gradients increase with the growth velocity; then, for a large enough crystal growth velocity constitutional supersaturation appears and the planar growth may become unstable. The criterion may easily be extended to account for the thermal diffusion transport of solute (i.e., the cross diffusion of solute driven by the temperature gradient). Consider a planar crystal–fluid interface with the fluid consisting of an inert (carrier) component and a dilute component which forms a solid deposit with total rejection of the carrier species. The advance of the interface is linked to the diffusive arrival of depositing material, resulting in

$$\rho_d V_{growth} = \rho D\left(\frac{d\omega}{dY} + \alpha_T \frac{\omega}{T}\frac{dT}{dY}\right)_{Y=0}, \qquad (1)$$

where ρ_d is the solid deposit density, V_{growth} the interface advance velocity, ρ the fluid density, $\omega \equiv \rho_1/\rho$ the solute mass fraction, T the temperature and Y the coordinate normal to the interface. The right-hand side in eq. (1) stands for the mass diffusion flux and it is comprised of the Fickian diffusion flux (with D being the binary diffusion coefficient) plus the thermal diffusion contribution (with α_T being the thermal diffusion factor). In the high dilution limit, the solute mass fraction relates to its partial vapor pressure p_v by $\omega = (M_1/M_2)p_v/p$, where M_1 and M_2 are the molar masses of the solute component and carrier species, respectively, and p is the total pressure. The equilibrium partial vapor pressure over a flat solid is temperature dependent and assuming that the total pressure is constant, we can write

$$\frac{d\omega^{eq}}{dY} = \frac{M_1}{M_2 p}\frac{dp_v^{eq}}{dT}\frac{dT}{dY} = \omega^{eq}\frac{\Delta H}{RT^2}\frac{dT}{dY}, \qquad (2)$$

where the Clausius–Clapeyron relation has been used and the solid molar volume has been neglected. ΔH is the latent heat per mole of depositing species converted to solid and R is the universal gas constant. When the mass fraction gradient at the interface is equal to this equilibrium mass fraction gradient, we obtain

$$\rho_d V_{growth} = \left[\rho D\frac{\omega^{eq}}{T}\left(\frac{\Delta H}{RT} + \alpha_T\right)\frac{dT}{dY}\right]_{Y=0}. \qquad (3)$$

For a constant temperature gradient, an increase of the crystal growth velocity beyond this value will produce a mass fraction gradient at the interface larger than the equilibrium mass fraction gradient indicated in eq. (2). Then, the fluid ahead of the front becomes locally supersaturated. This local supersaturation is a necessary condition for the appearance of morphological instability. Thus, for any growth velocity slower than the value given by eq. (3) the planar interface remains stable. eq. (3) shows that the range of stable growth velocities increases when the thermal diffusion factor takes on positive values. In fact, α_T is positive for massive species in light carrier gases, which is a usual characteristic of fluid mixtures in crystal growth from the vapor phase.

As will be shown below, this oversimplified analysis provides only a rough lower bound for the instability threshold. Dissipative effects as well as the effects of latent heat release and surface tension are stabilizing mechanisms which may delay the instability onset well beyond this local supersaturation criterion. Nevertheless, although the planar interface may remain morphologically stable due to these stabilizing mechanisms, the existing supersaturation may lead to nucleation phenomena on the fluid side. Under these circumstances, depositing material arrives to the interface by diffusion, as indicated in eq. (1), and also by thermophoretic transport of the nucleated particles. Even if crystalline, these par-

ticles would deposit at random orientations onto the interface and reduce the quality of the growing crystal. This combined transport of nucleated particles and vapors was analyzed by Castillo and Rosner [9], although in a different physical problem; namely, the deposition of vapors on to cold surfaces across laminar thermal boundary layers. The velocity given by eq. (3) provides, in practice, an upper limit below which no nucleation can occur. In any case, we will not consider further the possibility of homogeneous nucleation in the fluid side.

The case of crystal growth from the *vapor* phase presents some other particularly interesting features. Due to the high density difference between gas and solid phases, the growth process can usually be taken as quasi-stationary. Moreover, in dilute systems, the Stefan flow induced by the advancing front is negligible compared to the diffusive transport and fluid-dynamics often plays a secondary role; see, e.g., Rosner [10]. For condensing macromolecules dilute in a light carrier gas, an interesting limiting case is the so-called quasi-Lorentzian gas mixture, analyzed by Mason [11], for which the Schmidt number Sc (ratio of momentum-diffusivity to mass-diffusivity) and the thermal diffusion factor α_T take on very large values, but their ratio remains of order unity (e.g., α_T/Sc tends to 3/4 for hard spheres undergoing elastic specular collisions, see also García-Ybarra and Rosner [12]). Therefore, when such a gas mixture is subjected to a temperature gradient, thermal diffusion (Soret "cross" mass transport) [#1] becomes the dominant mass transfer mechanism, overwhelming the more familiar Fickian (concentration) diffusion everywhere in the bulk (although the latter must be retained in the vicinity of vapor/solid interfaces to fulfill the required boundary conditions).

In two recent papers [14,15], the authors have shown than in crystal growth from quasi-Lorentzian gas mixtures (when Fickian mass diffusion plays a minor role) there exists a new type of morphological instability. In these mixtures, the mass deposition rate is directly proportional to the temperature gradient normal to the interface. When the thermal conductivity of the solid is larger than that of the fluid mixture, a deformation of the solid–gas interface induces a deformation of the gas phase isotherms that increases the local thermal gradients and therefore increases the local mass deposition rate at the crests and reduces them in the valleys. Thus, any initial surface deformation is enhanced by the modified deposition rates. Planar growth is then always unstable (only the large wavenumber disturbances are stabilized by surface energy effects) and the system tends to present as large an interfacial area as possible. This is the morphological instability induced by thermal mass diffusion. In the opposite case $(\lambda/\lambda_d) > 1$ (a rather unphysical situation), the planar front would be linearly stable. However, latent heat effects were not considered in our previous analyses. This heat release is proportional to the local mass deposition rate and will play a stabilizing role by increasing locally the temperature at the crests (thus reducing the temperature gradients and therefore the local deposition rates) and decreasing the local temperature at the valleys (increasing temperature gradients and deposition rates).

In this paper we study morphological instabilities that may appear during planar growth of a solid deposit generated from a quasi-Lorentzian vapor mixture. The condensate is assumed to be comprised exclusively of the heavier component, which drifts towards the gas–solid interface due to the thermal diffusion induced by some externally imposed thermal gradient. Latent heat release will be taken into account, as well as the influence of surface energy and Fickian diffusion for large wavenumber disturbances. Hurle [16] presented a similar analysis of the opposite limit; that is, the influence of thermal diffusion on the morphological instability of a crystal growing

[#1] Due to the Onsager reciprocal relation (see, e.g., De Groot and Mazur [13]) use of the simple Fourier law for heat diffusion could apparently be questioned, but the ratio of Dufour cross heat transfer contribution to the Fourier heat diffusion is proportional not only to α_T but also to the mass fraction of the heavy component. Under conditions of high dilution, the Dufour effect can therefore be neglected.

mainly by Fickian solute diffusion. Thus, this paper was focused on the influence of thermal diffusion on the supersaturation-induced instability, but its effects were assumed to be rather small and he did not consider the thermophoretically induced instability emphasized here.

This paper is organized as follows. In section 2 we establish the governing equations for the local fields of velocity, temperature and mass fraction of the depositing species in the fluid phase as well as for the temperature field in the solid deposit, using a reference system in which the solid moves at the constant velocity V_d. In section 3 we detail the boundary conditions that must be satisfied at the moving vapor–solid interface. In section 4 the equations and boundary conditions are rendered dimensionless and the relevant dimensionless parameters are identified. The fluid Peclet number (based on the fluid velocity for a planar solidification front) is shown to be a small number (proportional to the mass fraction of the dilute depositing species) and an expansion in the Peclet number is formally carried out. To leading order, convective as well as unsteady terms are negligible in the governing equations compared to the diffusive terms. Since the Schmidt number is a large parameter, a matched asymptotic expansion in the inverse of the Schmidt number is performed. As done by Goren [17], we consider an outer region far from the interface where Fickian (Brownian) diffusion can be neglected and an inner region (a Brownian sublayer, see Gokoglu and Rosner [18]) adjacent to the solid–vapor interface, where concentration diffusion becomes important, bringing the mass fraction from the value required to match with the outer region to the value required by the boundary conditions. The temperature and mass fraction fields (in both outer and inner regions) in the stationary state of planar growth are given in section 5. The remainder of the paper is devoted to a study of the stability of this stationary state with respect to small unavoidable disturbances. A linear stability analysis is provided in section 6, giving a *dispersion relation* linking the disturbance amplification factor with the corresponding wavenumber. Since this analysis breaks down when the disturbance wavelength is comparable to the Brownian sublayer thickness, it is supplemented in section 7 to take into account the case of very large wavenumber disturbances. Section 8 contains remarks on the implications of our results, necessary extensions, and general conclusions.

2. Governing equations

We consider a binary fluid mixture with a depositing species (density ρ_1 and velocity V_1) and a *carrier* component (density ρ_2 and velocity V_2). The total density is $\rho = \rho_1 + \rho_2$ and the mixture barycentric velocity $V = (\rho_1 V_1 + \rho_2 V_2)/\rho$. The depositing (active) component drifts by the combined effect of Fickian and thermal diffusion towards a solid surface where a solid deposit forms with total rejection of the carrier species. The governing equations for the fluid mixture, considered incompressible and with constant thermophysical properties, are (see, e.g., the book by Rosner [10]):

$$\nabla \cdot V = 0, \tag{4}$$

$$\rho \frac{\partial V}{\partial t} + \rho V \cdot \nabla V = -\nabla p + \mu \nabla^2 V, \tag{5}$$

$$\rho c_p \frac{\partial T}{\partial t} + \rho c_p V \cdot \nabla T = \lambda \nabla^2 T, \tag{6}$$

$$\frac{\partial \rho_1}{\partial t} + \nabla(\rho_1 V_1) = 0. \tag{7}$$

In the above equations, μ is the dynamic viscosity, c_p the specific heat of the fluid mixture at constant pressure, and λ the Fourier thermal conductivity. The mass flux of the depositing species relates the velocity V_1 to the barycentric velocity V and the concentration and thermal gradients. This relation, as given by De Groot and Mazur [13] (see also Rosenberger [19]), is

$$\rho \omega V_1 = \rho \omega V - \rho D \nabla \omega - \rho \alpha_T D \omega (1 - \omega) \frac{\nabla T}{T}. \tag{8}$$

The first term on the right hand side is the convective flux, the second term represents the

direct Fickian diffusion flux and the third term represents the thermal diffusion (Soret) effect.

For the temperature field in the solid deposit, the governing equation is

$$\rho_d c_d \frac{\partial T_d}{\partial t} + \rho_d c_d \boldsymbol{V}_d \cdot \nabla T_d = \lambda_d \nabla^2 T_d. \tag{9}$$

where the subscript "d" refers to the deposit and all symbols have their usual meaning.

The above set of equations must be solved subject to appropriate boundary conditions on the fluid and solid sides and at the moving boundary between the two phases.

3. Boundary conditions at the solid–fluid interface

For simplicity we restrict ourselves to a two-dimensional geometry (X, Y) and consider a reference system in which the solid deposit moves with constant velocity V_d directed along the Y axis.

The separation line between the fluid mixture and the solid deposit is defined by the position vector $\boldsymbol{r}_\zeta$:

$$\boldsymbol{r}_\zeta = (X, \zeta\{X, t\}). \tag{10}$$

The locus $\boldsymbol{r}_\zeta$ is an unknown of the problem, as in other problems with free moving boundaries (for example, combustion fronts in Clavin and García-Ybarra [20], liquid–gas interfaces in García-Ybarra et al. [21], or solidification fronts in Langer [6]). Then, the unit normal vector pointing towards the fluid side and the unit tangent vector are

$$\boldsymbol{n} = \left(-\frac{1}{N}\frac{\partial \zeta}{\partial X}, \frac{1}{N}\right), \quad \boldsymbol{t} = \left(\frac{1}{N}, \frac{1}{N}\frac{\partial \zeta}{\partial X}\right), \quad \text{with}$$

$$N \equiv \left[1 + \left(\frac{\partial \zeta}{\partial X}\right)^2\right]^{1/2}. \tag{11}$$

The normal component of the local interfacial velocity V_ζ is related to the evolution of the interface location, $\zeta(X, t)$, via the kinematic condition:

$$\frac{\partial \zeta}{\partial t} = N V_\zeta \cdot \boldsymbol{n}. \tag{12}$$

We assume that the inert component of the fluid mixture does not penetrate the deposit, that is, it moves with the same speed as the interface. Therefore:

$$\boldsymbol{V}_2 \cdot \boldsymbol{n} = \boldsymbol{V}_\zeta \cdot \boldsymbol{n}. \tag{13}$$

Moreover, the no-slip condition at the interface corresponds to continuity of tangential velocities, that is:

$$\boldsymbol{V} \cdot \boldsymbol{t} = \boldsymbol{V}_d \cdot \boldsymbol{t}. \tag{14}$$

On the other hand, continuity of mass flux across the interface implies:

$$\rho(\boldsymbol{V} - \boldsymbol{V}_\zeta) \cdot \boldsymbol{n} = \rho\omega(\boldsymbol{V}_1 - \boldsymbol{V}_\zeta) \cdot \boldsymbol{n} = \rho_d(\boldsymbol{V}_d - \boldsymbol{V}_\zeta) \cdot \boldsymbol{n}. \tag{15}$$

By using relations (12), (13) and (8) in boundary condition (15), we obtain:

$$\frac{\partial \zeta}{\partial t} = \boldsymbol{V}_d \cdot \boldsymbol{n} N + \frac{\rho N}{\rho_d} \boldsymbol{n} \cdot \left(\frac{D}{1-\omega}\nabla\omega + \alpha_1 D\omega \frac{\nabla T}{T}\right). \tag{16}$$

and from eqs. (12) and (15),

$$\boldsymbol{V} \cdot \boldsymbol{n} N = \frac{\rho_d}{\rho} \boldsymbol{V}_d \cdot \boldsymbol{n} N + \left(1 - \frac{\rho_d}{\rho}\right) \frac{\partial \zeta}{\partial t}. \tag{17}$$

Note that the unknown V_d can be removed by choosing a reference system in which the solid is at rest and the solid–fluid interface is moving. In that case, $V_d = 0$, but this is not the most convenient reference system because then there is no steady state solution. Instead, we use a reference system linked to the interface in which the solid is retreating with the crystal growth velocity. Once V_d has been specified by a proper selection of the reference system, eq. (16) determines the evolution of the fluid–solid interface location and the boundary conditions (14) and (17) give the fluid velocity (tangential and normal component, respectively) at the interface.

Regarding the associated thermal conditions, we consider that the temperature and the energy flux are continuous across the interface, so that:

$$T = T_d,$$
$$-\lambda \boldsymbol{n}\cdot\nabla T + \frac{\Delta H}{M_1}\rho(\boldsymbol{V}-\boldsymbol{V}_\zeta)\cdot\boldsymbol{n} = -\lambda_d \boldsymbol{n}\cdot\nabla T_d, \tag{18}$$

where $\boldsymbol{V}_\zeta\cdot\boldsymbol{n}$ is given by (12) and $(\Delta H/M_1)$ is the latent heat per unit mass converted into solid.

Finally, local thermochemical equilibrium at the fluid–solid interface will be assumed, i.e.:

$$\omega\{X,\zeta\} = \omega^{eq}\{T, \text{local curvature}\}, \tag{19}$$

where the functional dependence of ω^{eq} is governed by thermodynamic considerations. We assume that ω^{eq} depends only on the local interface curvature and temperature, see, for instance, the book by Frenkel [22].

4. Dimensionless equations and boundary conditions

At this point it is quite useful to normalize and make dimensionless the variables of the problem, by defining $\tau \equiv tV_{ref}/L$, $x \equiv X/L$, $y \equiv Y/L$, $\boldsymbol{v} \equiv \boldsymbol{V}/V_{ref}$, $\Theta \equiv T/T_{ref}$, $\Theta_d \equiv T_d/T_{ref}$, $\Omega = \omega/\omega_{ref}$, and $\eta\{x,\tau\} \equiv \zeta\{X,t\}/L$, where the reference values will be selected later. Also, we define the dimensionless distance from the interface:

$$z \equiv y - \eta\{x,\tau\} \tag{20}$$

and rewrite our equations in x, z coordinates. Then, the governing equations on the fluid side ($z > 0$), eqs. (4) to (7), transform to

$$\nabla\cdot\boldsymbol{v} = 0, \tag{21}$$

$$\mathrm{Pr}^{-1}\,\mathrm{Pe}\left(\frac{\partial \boldsymbol{v}}{\partial\tau} - \frac{\partial\eta}{\partial\tau}\frac{\partial \boldsymbol{v}}{\partial z} + \boldsymbol{v}\cdot\nabla\boldsymbol{v}\right) = -\nabla\Pi + \nabla^2\boldsymbol{v}, \tag{22}$$

$$\mathrm{Pe}\left(\frac{\partial\Theta}{\partial\tau} - \frac{\partial\eta}{\partial\tau}\frac{\partial\Theta}{\partial z} + \boldsymbol{v}\cdot\nabla\Theta\right) = \nabla^2\Theta, \tag{23}$$

$$\mathrm{Pr}^{-1}\,\mathrm{Pe}\left(\frac{\partial\Omega}{\partial\tau} - \frac{\partial\eta}{\partial\tau}\frac{\partial\Omega}{\partial z} + \boldsymbol{v}\cdot\nabla\Omega\right) = \frac{1}{\mathrm{Sc}}\nabla^2\Omega + \alpha\nabla\left[\Omega(1-\omega_{ref}\Omega)\nabla\ln\Theta\right], \tag{24}$$

where eq. (8) has been used in eq. (7) to obtain eq. (24).

Whereas, in the solid ($z < 0$), from eq. (9), we find:

$$\mathrm{Pe}\left(\frac{\rho_d c_d}{\lambda_d}\frac{\lambda}{\rho c_p}\right)\left(\frac{\partial\Theta_d}{\partial\tau} - \frac{\partial\eta}{\partial\tau}\frac{\partial\Theta_d}{\partial z} + \boldsymbol{v}_d\cdot\nabla\Theta_d\right) = \nabla^2\Theta_d. \tag{25}$$

We have introduced the dimensionless pressure $\Pi \equiv pL/\mu V_{ref}$, and the dimensionless parameters $\mathrm{Pe} \equiv V_{ref}L/[\lambda/(\rho c_p)]$ (thermal Peclet number), the Prandtl number $\mathrm{Pr} = \nu/[\lambda/(\rho c_p)]$, the Schmidt number $\mathrm{Sc} \equiv \nu/D$, the parameter $\alpha \equiv \alpha_T D/\nu$ that determines the importance of thermophoresis (Soret effect), and ν is the kinematic viscosity (momentum diffusivity), $\nu \equiv \mu/\rho$.

Note that due to our selection of the x, z coordinate system, the operators ∇ and ∇^2 are, respectively, given by:

$$\nabla = \left(\frac{\partial}{\partial x} - \frac{\partial\eta}{\partial x}\frac{\partial}{\partial z}, \frac{\partial}{\partial z}\right), \tag{26a}$$

$$\nabla^2 = \left\{\frac{\partial^2}{\partial x^2} - \frac{\partial^2\eta}{\partial x^2}\frac{\partial}{\partial z} - 2\frac{\partial\eta}{\partial x}\frac{\partial^2}{\partial x\partial z} + \left[1+\left(\frac{\partial\eta}{\partial x}\right)^2\right]\frac{\partial^2}{\partial z^2}\right\}. \tag{26b}$$

Therefore the fluid–solid interface is located at $z = 0$, and the following boundary conditions must be fulfilled:

$$\boldsymbol{v}\cdot\boldsymbol{t} = \boldsymbol{v}_d\cdot\boldsymbol{t}, \tag{27}$$

$$\boldsymbol{v}\cdot\boldsymbol{n}N = \left(\frac{\rho_d}{\rho}\right)\boldsymbol{v}_d\cdot\boldsymbol{n}N + \left(1-\frac{\rho_d}{\rho}\right)\frac{\partial\eta}{\partial\tau}, \tag{28}$$

$$\frac{\partial\eta}{\partial\tau} = \boldsymbol{v}_d\cdot\boldsymbol{n}N + \frac{\rho}{\rho_d}\frac{\omega_{ref}\mathrm{Pr}}{\mathrm{Pe}}Nn\cdot\left[\frac{1}{\mathrm{Sc}}\nabla\Omega + \Omega(1-\omega_{ref}\Omega)\alpha\nabla\ln\Theta\right]. \tag{29}$$

$$\Theta = \Theta_d, \tag{30}$$

$$-Nn\cdot\Gamma\Theta + \mathcal{L}\frac{\rho_d}{\rho}\left(v_d\cdot nN - \frac{\partial\eta}{\partial\tau}\right) = -\frac{\lambda_d}{\lambda}Nn\cdot\Gamma\Theta_d, \tag{31}$$

$$\Omega = \Omega^{eq}\{\Theta\} - \gamma K, \tag{32a}$$

with $\mathcal{L} \equiv \mathrm{Pe}(\Delta H/M_1)/(c_p T_{ref})$, Ω^{eq} the equilibrium mass fraction over a flat surface, K the local curvature and γ a dimensionless parameter that takes into account the interfacial energy. Using the Gibbs–Kelvin relation (see, for instance, the book by Frenkel [22]), this parameter can be written as

$$\gamma = 2\sigma_T M_1/\rho_d RT\omega_{ref} L, \tag{32b}$$

where σ_T is the interfacial tension of the solid–fluid interface.

As in the problem of directional solidification, a stationary state can be achieved by imposing the remaining boundary conditions at constant distances from the fluid–solid front, let us say, at a distance L on the fluid side (that, is at $y = 1$) and at a different distance L_d on the solid side (that is, at $y = -\delta$, where $\delta \equiv L_d/L$). Therefore, we assume that the mass fraction at $y = 1$ is kept fixed and the temperature, at $y = 1$ and $y = -\delta$, reaches some particular values during the stationary state. That is

$$\Omega\{y = 1\} = \Omega_e \equiv \frac{\omega_e}{\omega_{ref}}, \quad \Theta\{y = 1\} = \Theta_e + \mathrm{nst},$$
$$\Theta\{y = -\delta\} = \Theta_\delta + \mathrm{nst}, \tag{33}$$

with the subscript e denoting values at $y = 1$, and subscript δ values at $y = -\delta$. The notation nst stands for nonstationary terms corresponding to disturbances of the stationary state. For these nst, Biot type boundary conditions will be used and discussed later on (see eqs. (58) and (59)).

As mentioned before, v_d is only a function of the reference system. In the case of a planar growing interface, a useful reference system is that in which the interface does not move at all and is always located at $y = 0$. Then $\partial\eta/\partial\tau = 0$ and v_d is found to compensate the otherwise secular growth of η given by boundary condition (29). In that case, from eq. (28) and taking into account that v is of order unity, and eq. (29), it is clear that $\mathrm{Pe} \sim \mathrm{Pr}\ \omega_{ref}$. In many practical cases the depositing species is very dilute in the carrier fluid, so that ω_{ref} is quite small and therefore $\mathrm{Pe} \ll 1$ provided that the Prandtl number Pr is of order unity (as in gases). To leading order in a small Peclet number expansion, the physical problem described by eqs. (21) to (25) with boundary conditions (27) to (33) becomes a purely diffusive (negligible advection) problem and the flow field in the gas plays no role. In the following we restrict ourselves to this case (i.e., $\omega_{ref} \ll 1$ and $\mathrm{Pe} \ll 1$). Note that we have incorporated the Peclet number into the definition of the latent heat parameter $\mathcal{L}$, because we are interested in emphasizing the stabilizing effects of latent heat release on the thermophoretically induced instability, as mentioned in the introduction.

We focus here on cases in which the main transport mechanism of the depositing species toward the solid is thermal (Soret) diffusion, with Fickian diffusion playing a minor role. This situation corresponds to high values of the Schmidt number. Then Fickian diffusion effects become important only in a very thin region (the Brownian sublayer) surrounding the fluid–solid interface. This sublayer *allows* the mass fraction profile to satisfy boundary condition (32a). To deal with this situation, we develop a boundary layer analysis, as indicated in the book by Van Dyke [23]. Thus, we define an inner region near the interface using the stretched variable:

$$\xi = \mathrm{Sc}\cdot z. \tag{34}$$

Therefore, in the limit $\mathrm{Pe} \ll 1$, eqs. (21) to (24) transform to

$$\Gamma\cdot v = 0, \tag{35}$$

$$\Gamma^2 v = \Gamma\Pi, \tag{36}$$

$$\Gamma^2\Theta = 0, \tag{37}$$

$$\frac{1}{\mathrm{Sc}}\Gamma^2\Omega + \alpha\Gamma(\Omega/\Theta)\cdot\Gamma\Theta = 0, \tag{38}$$

$$\Gamma^2\Theta_d = 0, \tag{39}$$

with the operators Γ and Γ^2, in the outer region given by (26a) and (26b), respectively. Whereas in the inner region (Brownian sublayer) they are given by:

$$\Gamma = \left(\frac{\partial}{\partial x} - \mathrm{Sc}\frac{\partial \eta}{\partial x}\frac{\partial}{\partial \xi} \quad \mathrm{Sc}\frac{\partial}{\partial \xi} \right), \tag{40a}$$

$$\Gamma^2 = \frac{\partial^2}{\partial x^2} - \mathrm{Sc}\frac{\partial^2 \eta}{\partial x^2}\frac{\partial}{\partial \xi} - 2\mathrm{Sc}\frac{\partial \eta}{\partial x}\frac{\partial^2}{\partial x \partial \xi} + \mathrm{Sc}^2\left[1 + \left(\frac{\partial \eta}{\partial x}\right)^2\right]\frac{\partial^2}{\partial \xi^2}. \tag{40b}$$

The boundary conditions at $\xi = 0$ are still given by eqs. (27) to (32) with the terms $\omega_{\mathrm{ref}}\Omega$ in (29) being negligibly small.

5. Stationary state

Under the above-mentioned circumstances, there exists a steady solution with a planar interface moving at constant velocity. We choose our reference system such that the planar interface does not move and remains at $y = 0$. Therefore $\eta = 0$ and $z = y$.

Then the solution of eq. (37) and eq. (39) with boundary conditions (30) and (33b) may be written:

$$\Theta^{\mathrm{st}} = \Theta_{\mathrm{c}} + \beta(z - 1), \tag{41}$$

$$\Theta_{\mathrm{d}}^{\mathrm{st}} = \Theta_{\mathrm{c}} - \beta + \beta_{\mathrm{d}} z, \tag{42}$$

with $\Theta_{\mathrm{c}} \equiv T_{\mathrm{c}}/T_{\mathrm{ref}}$ and β and β_{d}, the dimensionless temperature gradients in the fluid and solid phase, respectively. At this point we select the reference velocity V_{ref} as the fluid velocity during the stationary growth, then $v^{\mathrm{st}} = (0, -1)$ and $v_{\mathrm{d}} = (\rho/\rho_{\mathrm{d}})v^{\mathrm{st}}$. Therefore, from boundary conditions (31) and (33c), we obtain the dimensionless stationary temperature gradients

$$\beta \equiv \frac{L}{T_{\mathrm{ref}}}\frac{\mathrm{d}T^{\mathrm{st}}}{\mathrm{d}Y} = \frac{\Theta_{\mathrm{c}} - \Theta_{\delta} - \delta\mathscr{L}(\lambda/\lambda_{\mathrm{d}})}{1 + \delta(\lambda/\lambda_{\mathrm{d}})},$$
$$\beta_{\mathrm{d}} \equiv \frac{L}{T_{\mathrm{ref}}}\frac{\mathrm{d}T_{\mathrm{d}}^{\mathrm{st}}}{\mathrm{d}Y} = \frac{\lambda}{\lambda_{\mathrm{d}}}\frac{\Theta_{\mathrm{c}} - \Theta_{\delta} + \mathscr{L}}{1 + \delta(\lambda/\lambda_{\mathrm{d}})}. \tag{43}$$

For the mass fraction in the outer region, to leading order in a Sc expansion, eq. (38) leads to the solution:

$$\Omega_{\mathrm{out}}^{\mathrm{st}} \equiv \frac{\Omega_{\mathrm{c}}}{\Theta_{\mathrm{c}}}\Theta^{\mathrm{st}}, \tag{44}$$

where the boundary condition (33a) has been imposed. In order to satisfy the mass fraction boundary condition at the solid interface (32a), the inner diffusion layer must be considered. In this Brownian sublayer, eq. (38) taking into account (40) and (41) becomes (to leading order in Sc):

$$\frac{\mathrm{d}^2\Omega_{\mathrm{in}}^{\mathrm{st}}}{\mathrm{d}\xi^2} + \frac{\alpha}{\Theta_0}\beta\frac{\mathrm{d}\Omega_{\mathrm{in}}^{\mathrm{st}}}{\mathrm{d}\xi} = 0, \tag{45}$$

with $\Theta_0 = \Theta_{\mathrm{c}} - \beta$, being the temperature (in dimensionless form) of the planar interface.

The solution of eq. (45) satisfying boundary condition (32a) at $\xi = 0$, and matching with the outer solution, $(\Omega_{\mathrm{in}}^{\mathrm{st}}\{\xi \to \infty\} = \Omega_{\mathrm{out}}^{\mathrm{st}}\{z = 0\})$ is:

$$\Omega_{\mathrm{in}}^{\mathrm{st}} = \left(\Omega_0^{\mathrm{eq}} - \Omega_{\mathrm{c}}\frac{\Theta_0}{\Theta_{\mathrm{c}}}\right)\exp\left(-\frac{\alpha}{\Theta_0}\beta\xi\right) + \Omega_{\mathrm{c}}\frac{\Theta_0}{\Theta_{\mathrm{c}}}. \tag{46}$$

with $\Omega_0^{\mathrm{eq}} \equiv \Omega^{\mathrm{eq}}\{\Theta_0\}$.

On the other hand, because $v^{\mathrm{st}} = (0, -1)$, from the boundary conditions (28) and (29) with $\partial\eta/\partial\tau = 0$, we find

$$\mathrm{Pe} = \omega_{\mathrm{ref}}\mathrm{Pr}\,\Omega_{\mathrm{c}}(\alpha\beta/\Theta_{\mathrm{c}}). \tag{47}$$

Because the velocity of the solid deposit, from boundary condition (14) is $V_{\mathrm{d}} = V_{\mathrm{ref}}(\rho/\rho_{\mathrm{d}})v^{\mathrm{st}}$, it turns out that

$$V_{\mathrm{d}} = \frac{\rho}{\rho_{\mathrm{d}}}\alpha_{\mathrm{T}}D\omega_{\mathrm{c}}\frac{1}{T_{\mathrm{c}}}\frac{\mathrm{d}T^{\mathrm{st}}}{\mathrm{d}Y}v^{\mathrm{st}}. \tag{48a}$$

with $\mathrm{d}T^{\mathrm{st}}/\mathrm{d}Y$ the constant temperature gradient in the fluid mixture indicated in eq. (43). Note that $-V_{\mathrm{d}}$ is the velocity of the moving solid–fluid front measured in a reference system in which the solid deposit remains at rest, that is V_{growth}. Then, from eq. (48a) the product $\alpha_{\mathrm{T}}(\mathrm{d}T^{\mathrm{st}}/\mathrm{d}Y)$ (and therefore $\alpha\beta$) is positive for a growing solid (and it will be negative for a subliming solid).

We can also imagine that in some actual experiments what is fixed instead of the distances L and L_d is the total distance $l = L + L_d$ over which the temperature and mass fractions are controlled. In that case, from eqs. (43a) and (48a) depending on the crystal growth velocity, the location of the solid–fluid interface can be obtained; i.e., the relative value of L. One finds

$$L = \frac{l\frac{\lambda}{\lambda_d}\left(1+\frac{\Delta H}{M_1}\frac{\alpha_T D\rho\omega_c}{\lambda T_c}\right) - \frac{\rho}{\rho_d}\frac{\alpha_T D\omega_c}{V_d}\frac{T_c - T_\infty}{T_c}}{\frac{\lambda}{\lambda_d}\left(1+\frac{\Delta H}{M_1}\frac{\alpha_T D\rho\omega_c}{\lambda T_c}\right) - 1}. \quad (48b)$$

The thickness of the fluid layer may vary from the maximum value $L = l$ to its minimum value $L = 0$. These two extreme values provide limiting crystal growth velocities, resulting

$$V_{growth}\{L = l\} = \frac{\rho}{\rho_d}\frac{\alpha_T D\omega_c}{l}\frac{T_c - T_\infty}{T_c},$$
$$V_{growth}\{L = 0\} = \frac{\lambda_d}{\lambda}\frac{V_{growth}\{L = l\}}{1+\frac{\Delta H}{M_1}\frac{\alpha_T D\rho\omega_c}{\lambda T_c}}. \quad (48c)$$

This result can be used as a quasisteady approximation to the nonstationary growth when the concentration and temperatures are kept constant at fixed locations. The growth is assumed to accommodate at every instant to the new interface location, with a growing velocity varying from $V_{growth}\{L = l\}$, at the beginning, when no solid is present, to the value $V_{growth}\{L = 0\}$, when the solid occupies the entire cavity.

We are now interested in finding under what conditions the solution given by eqs. (41), (42), (44) and (46) is *stable* and when an initially infinitesimal disturbance will grow to a finite amplitude.

6. Linear stability analysis

We assume that stationary planar growth is perturbed, so that the interface deforms and the fields become $\Theta = \Theta^{st} + \theta$, $\Theta_d = \Theta_d^{st} + \theta_d$, $\Omega_{out} = \Omega_{out}^{st} + \Gamma_{out}$ and $\Omega_{in} = \Omega_{in}^{st} + \Gamma_{in}$. When the amplitudes of the disturbances are infinitesimally small, the corresponding governing equations and boundary conditions can be linearized around the initial undisturbed state, resulting from eqs. (37) to (39) with Γ and Γ^2 given by eqs. (26)

$$\left(\frac{\partial^2}{\partial x^2}+\frac{\partial^2}{\partial z^2}\right)\theta = \beta\frac{\partial^2\eta}{\partial x^2}, \quad (49)$$

$$\left(\frac{\partial^2}{\partial x^2}+\frac{\partial^2}{\partial z^2}\right)\theta_d = \beta_d\frac{\partial^2\eta}{\partial x^2}, \quad (50)$$

$$\frac{\partial}{\partial z}\left(\frac{\Gamma_{out}}{\Theta^{st}} - \frac{\Omega_c}{\Theta_c}\frac{\theta}{\Theta^{st}}\right) = 0, \quad (51)$$

whereas in the Brownian sublayer, from eqs. (38) and (40)

$$\frac{\partial^2}{\partial\xi^2}\Gamma_{in} + \frac{\alpha\beta}{\Theta_0}\frac{\partial\Gamma_{in}}{\partial\xi} = \alpha\beta\frac{\theta\{z=0\}}{\Theta_0^2}\frac{\partial\Omega_{in}^{st}}{\partial\xi} - \frac{\alpha}{\Theta_0}\left(\frac{\partial\theta}{\partial z}\right)_{z=0}\frac{\partial\Omega_{in}^{st}}{\partial\xi}. \quad (52)$$

The boundary conditions for the temperature disturbances at the interface are

$$\theta = \theta_d \quad \text{at} \quad z = 0, \quad (53)$$

$$\frac{\partial\theta}{\partial z} + \mathcal{S}\frac{\rho_d}{\rho}\frac{\partial\eta}{\partial\tau} = \frac{\lambda_d}{\lambda}\frac{\partial\theta_d}{\partial z} \quad \text{at} \quad z = 0. \quad (54)$$

The matching condition between the inner and the outer mass fraction disturbances corresponds to

$$\Gamma_{in}\{\xi\to\infty\} = \Gamma_{out}\{z\to 0\}. \quad (55)$$

Linearizing eq. (29) with respect to the disturbances and taking into account (47), we obtain

$$\frac{\partial\eta}{\partial\tau} = \frac{\rho}{\rho_d}\frac{\Theta_c}{\Omega_c\alpha\beta} \times\left[\frac{\partial\Gamma_{in}}{\partial\xi} + \frac{\alpha\beta}{\Theta_0}\Gamma_{in} + \frac{\alpha}{\Theta_0}\Omega_{in}^{st}\left(\frac{\partial\theta}{\partial z} - \beta\frac{\theta}{\Theta_0}\right)\right] \quad \text{at} \quad \xi = z = 0, \quad (56)$$

and from boundary condition (32a)

$$\Gamma_{in} = \chi\theta - \gamma\frac{\partial^2\eta}{\partial x^2} \quad \text{at} \quad \xi = 0, \tag{57}$$

with

$$\chi \equiv \left(\frac{d\Omega^{eq}}{d\Theta}\right)_{\omega,\,\omega_0} = \frac{\Delta H T_{ref}\omega_0^{eq}}{RT_0^2\omega_{ref}}$$

the parameter that measures the variation of the equilibrium mass fraction with temperature, see eq. (2).

Finally, we must specify the disturbances boundary conditions at the fluid side, $y = 1$ (i.e., $z = 1 - \eta\{x, \tau\}$) and at the solid side, $y = -\delta$ (i.e., $z = -\delta - \eta\{x, \tau\}$). For the temperature, we consider Biot type boundary conditions, that is, the local heat flux perturbation is taken to be proportional to the local temperature field disturbance, then, we obtain the linearized conditions

$$\frac{\partial\theta}{\partial z} = -\mathrm{Bi}(-\beta\eta + \theta) \quad \text{at} \quad z = 1, \tag{58}$$

$$\frac{\partial\theta_d}{\partial z} = \mathrm{Bi}_d(-\beta_d\eta + \theta_d) \quad \text{at} \quad z = -\delta. \tag{59}$$

The terms proportional to η arise from the apparent displacement of the boundaries with respect to the fluid–solid interface. The Biot number at the upper (Bi) and lower (Bi_d) boundaries are defined positive and measure the thermal resistance of the boundaries. The limit of a very large Biot number corresponds to a perfectly conducting boundary where the temperature remains constant and thermal disturbances vanish. The opposite limit of very small Biot numbers corresponds to an thermally insulating boundary where the heat flux is kept fixed.

The mass fraction is assumed to remain constant at $y = 1$, therefore

$$-\beta\frac{\Omega_e}{\Theta_e}\eta + \Gamma_{out} = 0, \quad \text{at} \quad z = 1, \tag{60}$$

where we have used the value of Ω^{st} given by eq. (44).

The system of eqs. (49) to (52) with boundary and matching conditions (53) to (60) can be solved by expanding each variable in a Fourier series. As the system is linear, we can study the behavior of the stationary state (41), (42), (44) and (46) via each Fourier mode. Therefore, we consider

$$F\{x, z, \tau\} = \hat{F}\{z\}\exp(ikx + \sigma\tau), \tag{61}$$

where F stands for θ, θ_d, Γ_{out}, Γ_{in} and η (this last one without the z dependence). By using (61) in eq. (49), we find that the solution is given by

$$\hat{\theta} = \beta\hat{\eta} + A\,e^{kz} + B\,e^{-kz}. \tag{62}$$

From Eqs. (50) and (51) we obtain, respectively,

$$\hat{\theta}_d = \beta_d\hat{\eta} + A_d\,e^{kz} + B_d\,e^{-kz}, \tag{63}$$

$$\hat{\Gamma}_{out} = \beta\frac{\Omega_e}{\Theta_e}\hat{\eta} + A\frac{\Omega_e}{\Theta_e}\,e^{kz} + B\frac{\Omega_e}{\Theta_e}\,e^{-kz} + C\Theta^{st}. \tag{64}$$

Eq. (52) may be integrated once, yielding

$$\frac{d}{d\xi}\hat{\Gamma}_{in} + \frac{\alpha\beta}{\Theta_0}\hat{\Gamma}_{in} = \frac{\alpha\Omega_{in}^{st}}{\Theta_0}\left[\beta\frac{\theta\{z=0\}}{\Theta_0} - \left(\frac{\partial\theta}{\partial z}\right)_{z=0}\right] + \sigma\hat{\eta}\frac{\rho_d}{\rho}\frac{\Omega_e\alpha\beta}{\Theta_e}, \tag{65}$$

where the second term on the right-hand side of the equation is an integration constant which has been obtained by using boundary condition (56).

The solution of eq. (65) with Ω_{in}^{st} given by eq. (46) is

$$\hat{\Gamma}_{in} = \frac{\Omega_e}{\Theta_e}\Theta_0\left[\hat{\eta}\left(\frac{\sigma\rho_d}{\rho} + \frac{\beta}{\Theta_0}\right) + A\left(\frac{1}{\Theta_0} - \frac{k}{\beta}\right) + B\left(\frac{1}{\Theta_0} + \frac{k}{\beta}\right)\right] + \left\{\alpha\left(\frac{\Omega_0^{eq}}{\Theta_0} - \frac{\Omega_e}{\Theta_e}\right) \times\left[\frac{\hat{\eta}}{\Theta_0}\beta^2 + A\left(\frac{\beta}{\Theta_0} - k\right) + B\left(\frac{\beta}{\Theta_0} + k\right)\right]\xi + E\right\}\exp\left(-\frac{\alpha}{\Theta_0}\beta\xi\right). \tag{66}$$

The values of A, B, A_d, B_d, C, E and $\hat{\eta}$ must satisfy the boundary conditions (58) and (60) at $z = 1$, (59) at $z = -\delta$, the matching condition given by (55), and the conditions (53), (54) and (57) at $z = 0$. By substitution of (62), (63), (64) and (66) in the boundary conditions, the following homogeneous system of algebraic equations is obtained:

$$A(k + \mathrm{Bi})\, e^{k} + B(\mathrm{Bi} - k)\, e^{-k} = 0, \tag{67}$$

$$A\, e^{k} + B\, e^{-k} + C\frac{\Theta_c^2}{\Omega_c} = 0, \tag{68}$$

$$A_d(\mathrm{Bi}_d - k)\, e^{-k\delta} + B_d(\mathrm{Bi}_d + k)\, e^{k\delta} = 0, \tag{69}$$

$$-A\frac{k}{\beta} + B\frac{k}{\beta} + \hat{\eta}\sigma\frac{\rho_d}{\rho} - C\frac{\Theta_c}{\Omega_c} = 0, \tag{70}$$

$$A + B - A_d - B_d + \hat{\eta}(\beta - \beta_d) = 0, \tag{71}$$

$$A - B - \frac{\lambda_d}{\lambda}A_d + \frac{\lambda_d}{\lambda}B_d + \mathscr{S}\frac{\rho_d}{\rho}\frac{\sigma}{k}\hat{\eta} = 0, \tag{72}$$

$$A\left[\left(\frac{1}{\Theta_0} - \frac{k}{\beta}\right)\frac{\Omega_c}{\Theta_c}\Theta_0 - \chi\right] + B\left[\frac{\Omega_c}{\Theta_c}\Theta_0\left(\frac{1}{\Theta_0} + \frac{k}{\beta}\right) - \chi\right] + \hat{\eta}\left[\frac{\Omega_c}{\Theta_c}\Theta_0\left(\frac{\sigma\rho_d}{\rho} + \frac{\beta}{\Theta_0}\right) - \gamma k^2\right] + E = 0. \tag{73}$$

Note that eq. (73) is needed just to specify the value of E which determines the inner mass fraction disturbance $\hat{I}_{in}$ by eq. (66). This value of E is such that the equilibrium condition at the solid interface is fulfilled. As a consequence, the Brownian sublayer has no influence *at all* on the stability of the planar front as long as the disturbance wavenumbers are not too large (see next section). No matter how complicated the mass fraction boundary condition is at the fluid–solid interface, Fickian diffusion will bring the mass fraction from its value at the outer edge region of the Brownian sublayer to the required value at the interface.

Thus, the value of σ given below is not affected by the boundary condition corresponding to the mass fraction at the interface, eq. (32a). The system (67) to (72) is a homogeneous algebraic system of six equations with six unknowns (A, B, A_d, B_d, C and $\hat{\eta}$). The determinant of the coefficients must vanish in order to have a non-trivial solution. Imposing this condition, the following *dispersion* relation is obtained:

$$\sigma = \left[\frac{\rho}{\rho_d}\frac{\beta - \beta_d}{\beta}k\left(\frac{\beta}{\Theta_c} + k\sinh k + \mathrm{Bi}\cosh k\right)\right] \times \left\{k\cosh k + \mathrm{Bi}\sinh k + \frac{\lambda}{\lambda_d} \times \left[(k\sinh k + \mathrm{Bi}\cosh k)\left(1 + \frac{\mathscr{S}}{\beta}\right) + \frac{\mathscr{S}}{\Theta_c}\right] \times \frac{k\cosh k\delta + \mathrm{Bi}_d\sinh k\delta}{k\sinh k\delta + \mathrm{Bi}_d\cosh k\delta}\right\}^{-1}. \tag{74}$$

Recalling eq. (61), the sign of σ determines the stability of the stationary state against infinitesimal disturbances of wavenumber k. The stationary state, with a planar interface, is unstable when $\sigma > 0$ and an initially small disturbance will grow until the non-linear terms become important and determine the new shape of the advancing front. When the amplification factor, σ, is negative the planar front is linearly stable against infinitesimally small disturbances, although it may be destabilized by finite amplitude disturbances.

The value of σ in eq. (74) depends on the density ratio ρ/ρ_d (only as a multiplicative factor), the thermal Biot numbers, Bi and Bi_d, the thermal conductivity ratio λ/λ_d, the depth ratio δ, and the dimensionless groups

$$\frac{\beta}{\Theta_c} \equiv \frac{L}{T_c}\frac{\mathrm{d}T^{st}}{\mathrm{d}Y} = \frac{\rho_d}{\rho}\frac{LV_{growth}}{\alpha_T D\omega_c},$$

$$\frac{\mathscr{S}}{\beta} = \frac{\Delta H}{M_1 T_c}\frac{\rho\alpha_T D}{\lambda}\omega_c = \frac{\rho_d V_{growth}(\Delta H/M_1)}{\lambda\,\mathrm{d}T^{st}/\mathrm{d}Y}, \tag{75a}$$

for quasi-Lorentzian gas mixtures ($\alpha_T > 0$) all the mentioned parameters are positive definite, and except for β/Θ_c and $\mathscr{S}/\beta$, which depend on

growth conditions, all others are determined by material properties. Note that $\mathscr{S}/\beta$ is the ratio of latent heat release (due to the mass deposition flux) to the diffusive heat flux towards the interface from the fluid side.

For positive values of α_1 (i.e. $\beta > 0$), all the mentioned parameters are positive and therefore, the sign of σ is the same as the sign of the group

$$\frac{\beta - \beta_d}{\beta} = 1 - \frac{\lambda}{\lambda_d}\left(1 + \frac{\mathscr{S}}{\beta}\right). \tag{75b}$$

When this group is positive, σ given by eq. (74) is a *monotonically increasing function* of k. Planar growth is always unstable for perturbations of any wavenumber and the system tends to present as large surface as possible. A deformation of the solid–gas interface induces a deformation of the isotherms in the gas phase that increases the thermal gradients and therefore the local mass deposition rate at the crests and reduces them in the valleys. Thus, the initial surface deformation is enhanced by the modified deposition rates. In the opposite case, $(\beta - \beta_d)/\beta) < 0$, the planar front is linearly stable. Therefore, we can conclude that

for $\alpha_1 > 0$, planar growth is unstable when

$$\frac{\mathscr{S}}{\beta} < \frac{\lambda_d}{\lambda} - 1. \tag{75c}$$

Thus, for negligible latent heat release planar growth is always unstable because $\lambda_d/\lambda > 1$ under usual conditions. Latent heat plays a stabilizing role, as pointed out in the introduction of this paper. Eq. (75c), with the value of $\mathscr{S}/\beta$ given by eq. (75a), provides a minimum value of the group $\rho\omega_c/T_c$ for stable planar growth and shows that, for sufficiently low dilution, planar growth is unstable.

The result indicated in eq. (75c) shows that when thermophoretically growing planar deposits are stable, from eq. (48c), it appears that $V_{growth}\{L = 0\} > V_{growth}\{L = l\}$. Therefore, for the case of thermal boundary conditions imposed at fixed locations and quasisteady growth, the stable thermophoretic planar growth corresponds to a solid–fluid front which starts moving at the velocity, $V_{growth} = V_{growth}\{L = l\}$, and accelerates as the solid deposit depth increases. As the growth velocity increases, constitutional supersaturation may build up in the neighborhood of the advancing interface (i.e., in the Brownian sublayer) rendering unstable this planar growth. To account for this possibility we have to study very large wavenumber disturbances which are strongly affected by the Brownian sublayer structure. However, short wavenumber disturbances are not affected in the linear stage by supersaturation effects and the above results remain valid.

On the other hand, the analysis carried out here predicts that the planar front is unstable when α_1 (and therefore β) is negative, and $-(\beta/\Theta_c) > \mathrm{Bi}$, as could be the case in some liquid mixtures. There is a singular value of k, denoted by k^*, for which the numerator in eq. (74) vanishes (that is, $k^* \sinh k^* + \mathrm{Bi} \cosh k^* = -(\beta/\Theta_c)$, and thus $\sigma\{k^*\} = 0$). Thus for $(\beta - \beta_d)/\beta) < 0$ (respectively, $(\beta - \beta_d)/\beta) > 0$), the planar interface is unstable for wavenumber smaller (respectively, larger) than k^* and linearly stable otherwise. Therefore

for $\alpha_1 < 0$, planar growth is unstable when

$$\mathrm{Bi} < -\frac{\beta}{\Theta_c}, \tag{75d}$$

that is, planar growth is unstable when the upper boundary is a thermal insulator.

It should be kept in mind that in liquid mixtures Fickian (concentration) diffusion is usually more important than thermal mass diffusion and the present analysis must therefore be extended to take this into account. Ordinarily the velocity of planar deposit growth from liquids will be determined principally by direct Fickian transport. Nevertheless thermal mass diffusion can play a non-negligible role in influencing the stability properties of such systems; see, by analogy, García-Ybarra et al. [23].

Eq. (74) extends our preliminary results, Castillo et al. [14,15], to arbitrary Biot numbers at both ends and also incorporates the influence of the latent heat. We proceed now to analyze the most important features of the dispersion rela-

tion, eq. (74). The growth rate of a planar disturbance (zero wavenumber) is

$$\sigma\{\mathrm{Bi}_d \neq 0,\ k = 0\} = \frac{\rho}{\rho_d}\left(\frac{\beta - \beta_d}{\beta}\right) \times \frac{\mathrm{Bi} + \beta/\Theta_c}{1 + \mathrm{Bi} + \frac{\lambda}{\lambda_d}\left[\mathrm{Bi} + \frac{\mathscr{L}}{\beta}\left(\mathrm{Bi} + \frac{\beta}{\Theta_c}\right)\right]\frac{1 + \delta\mathrm{Bi}_d}{\mathrm{Bi}_d}} \tag{76a}$$

Note, however, that this growth rate vanishes in the limit of a perfect insulating support, when a quadratic dependence for small wavenumbers is obtained

$$\sigma\{\mathrm{Bi}_d = 0,\ k \to 0\} \approx \frac{\rho}{\rho_d}\left(\frac{\beta - \beta_d}{\beta}\right) \times \frac{\mathrm{Bi} + \beta/\Theta_c}{\frac{\lambda}{\lambda_d}\left[\mathrm{Bi} + \frac{\mathscr{L}}{\beta}\left(\mathrm{Bi} + \frac{\beta}{\Theta_c}\right)\right]}\delta k^2. \tag{76b}$$

On the other hand, in the opposite limit of very large wavenumbers, eq. (74) leads to a linear behavior

$$\sigma\{k \to \infty\} \approx \frac{\rho}{\rho_d}\left(\frac{\beta - \beta_d}{\beta}\right) \times \frac{k}{1 + \frac{\lambda}{\lambda_d}\left(1 + \frac{\mathscr{L}}{\beta}\right)} = \frac{\rho}{\rho_d}\left(\frac{\beta - \beta_d}{\beta + \beta_d}\right)k, \tag{77}$$

which coincides (for $\rho_d = \rho$) with the Hurle [16] dispersion relation in the limit of very high Soret effect (once the several misprints in Hurle's equations are corrected: using his notation, NG_L/k should be replaced by NG_L in his eq. (11), in his eq. (23) a minus sign in the first contribution to ω^* is forgotten, and in his dispersion relation, eq. (24), a ω in the left-hand side of the numerator should be in the denominator, the bracket in the right hand side numerator is missing and in the denominator, G_c must be replaced by $G_c + NG_L$).

Eq. (77) shows that when $(\beta - \beta_d)/(\beta + \beta_d) > 0$, the amplification factor σ increases linearly with k and the smaller wavelength disturbances are the most dangerous to the planar growth because they amplify faster. However, in this analysis, the value of the disturbance wavenumber has been assumed to be of order unity in the Schmidt number expansion. This assumption fails when the wavenumber takes on large values and a different scaling law is required to improve the result shown in eq. (74). This new scaling is presented in the next section.

7. Study of large wavenumber disturbances

In the case of very large wavenumber disturbances (i.e. when $k = \mathrm{Sc}\ a$, with $a = O(\mathrm{Sc}^0)$), the stability analysis performed in section 6 is no longer valid. The variations with x become more important and a new scaling is needed. Therefore, we define the new rescaled coordinate φ and time τ' via:

$$\varphi \equiv \mathrm{Sc}\ x, \quad \tau' \equiv \mathrm{Sc}\ \tau. \tag{78}$$

It can be shown that for a given order of the mass fraction disturbance amplitude, the disturbances in the front shape and in the temperature fields are Sc^{-1} times smaller. The mass fraction field in the vicinity of the interface is very sensitive to front corrugations. Then, different expansions are needed for the temperature fields in the inner and outer regions. Therefore we take:

$$\eta = \frac{1}{\mathrm{Sc}}\bar{\eta}, \tag{79a}$$

$$\Theta_{\mathrm{out}} = \Theta^{*1} + \frac{1}{\mathrm{Sc}}\bar{\theta}_{\mathrm{out}} \qquad 0 \leq z \leq 1 - \eta, \tag{79b}$$

$$\Theta_{\mathrm{in}} = \Theta_0 + \frac{1}{\mathrm{Sc}}\left(\beta\xi + \bar{\theta}_{\mathrm{in}}\right) \qquad 0 \leq \xi \leq \infty, \tag{79c}$$

$$\Theta_{d,out} = \Theta_d^{st} + \frac{1}{Sc}\tilde{\theta}_{d,out} \qquad -\delta - \eta \le z \le 0, \tag{79d}$$

$$\Theta_{d,in} = \Theta_0 + \frac{1}{Sc}\left(\beta_d \xi + \tilde{\theta}_{d,in}\right) \qquad -\infty \le \xi \le 0, \tag{79e}$$

$$\Omega_{out} = \Omega_{out}^{st} + \tilde{\Gamma}_{out} \qquad 0 \le z \le 1 - \eta, \tag{79f}$$

$$\Omega_{in} = \Omega_{in}^{st} + \tilde{\Gamma}_{in} \qquad 0 \le \xi \le \infty, \tag{79g}$$

Eqs. (79) define the tilde-quantities. Then the operators Γ and Γ^2 in the outer regions become

$$\Gamma = \left(Sc\frac{\partial}{\partial\varphi} - \frac{\partial\tilde{\eta}}{\partial\varphi}\frac{\partial}{\partial z}, \frac{\partial}{\partial z}\right), \tag{80}$$

$$\Gamma^2 = Sc^2\frac{\partial^2}{\partial\varphi^2} - Sc\frac{\partial^2\tilde{\eta}}{\partial\varphi^2}\frac{\partial}{\partial z} - 2Sc\frac{\partial\tilde{\eta}}{\partial\varphi}\frac{\partial^2}{\partial z\,\partial\varphi} + \left[1 + \left(\frac{\partial\tilde{\eta}}{\partial\varphi}\right)^2\right]\frac{\partial^2}{\partial z^2}, \tag{81}$$

and in the inner regions

$$\Gamma = \left(Sc\frac{\partial}{\partial\varphi} - Sc\frac{\partial\tilde{\eta}}{\partial\varphi}\frac{\partial}{\partial\xi}, Sc\frac{\partial}{\partial\xi}\right), \tag{82}$$

$$\Gamma^2 = Sc^2\frac{\partial^2}{\partial\varphi^2} - Sc^2\frac{\partial^2\tilde{\eta}}{\partial\varphi^2}\frac{\partial}{\partial\xi} - 2Sc^2\frac{\partial\tilde{\eta}}{\partial\varphi}\frac{\partial^2}{\partial\xi\,\partial\varphi} + Sc^2\left[1 + \left(\frac{\partial\tilde{\eta}}{\partial\varphi}\right)^2\right]\frac{\partial^2}{\partial z^2}. \tag{83}$$

Then to lowest order in the Schmidt number expansion, the linearized equations for the disturbances, from eqs. (37) to (39) with (80) and (81) in the outer region, become

$$\frac{\partial^2\tilde{\theta}_{out}}{\partial\varphi^2} - \frac{\partial^2\tilde{\eta}}{\partial\varphi^2}\beta = 0, \tag{84}$$

$$\frac{\partial^2\tilde{\theta}_{d,out}}{\partial\varphi^2} - \frac{\partial^2\tilde{\eta}}{\partial\varphi^2}\beta_d = 0, \tag{85}$$

$$\frac{\partial^2\tilde{\Gamma}_{out}}{\partial\varphi^2} = 0, \tag{86}$$

whereas, taking into account (82) and (83), in the inner regions, we obtain:

$$\frac{\partial^2\tilde{\theta}_{in}}{\partial\varphi^2} - \frac{\partial^2\tilde{\eta}}{\partial\varphi^2}\beta + \frac{\partial^2\tilde{\theta}_{in}}{\partial\xi^2} = 0, \tag{87}$$

$$\frac{\partial^2\tilde{\theta}_{d,in}}{\partial\varphi^2} - \frac{\partial^2\tilde{\eta}}{\partial\varphi^2}\beta_d + \frac{\partial^2\tilde{\theta}_{d,in}}{\partial\xi^2} = 0, \tag{88}$$

$$\frac{\partial^2\tilde{\Gamma}_{in}}{\partial\xi^2} + \frac{\partial^2\tilde{\Gamma}_{in}}{\partial\varphi^2} - \frac{\partial^2\tilde{\eta}}{\partial\varphi^2}\frac{d\Omega_{in}^{st}}{d\xi} + \frac{\alpha\beta}{\Theta_0}\frac{\partial\tilde{\Gamma}_{in}}{\partial\xi} + \frac{\alpha}{\Theta_0}\frac{\partial\tilde{\theta}_{in}}{\partial\xi}\frac{d\Omega_{in}^{st}}{d\xi} = 0. \tag{89}$$

The boundary conditions at the interface, from eqs. (53), (54), (56) and (57) are

$$\tilde{\theta}_{in} = \tilde{\theta}_{d,in} \qquad \text{at} \quad \xi = 0; \tag{90}$$

$$\frac{\partial\tilde{\theta}_{in}}{\partial\xi} + \mathscr{L}\frac{\rho_d}{\rho}\frac{\partial\tilde{\eta}}{\partial\tau} = \frac{\lambda_d}{\lambda}\frac{\partial\tilde{\theta}_{d,in}}{\partial\xi} \qquad \text{at} \quad \xi = 0; \tag{91}$$

$$\frac{\partial\tilde{\eta}}{\partial\tau} = \frac{\rho}{\rho_d}\frac{\Theta_c}{\Omega_c\alpha\beta}\left(\frac{\partial\tilde{\Gamma}_{in}}{\partial\xi} + \frac{\alpha\beta}{\Theta_0}\tilde{\Gamma}_{in} + \frac{\alpha}{\Theta_0}\Omega_{in}^{st}\frac{\partial\tilde{\theta}_{in}}{\partial\xi}\right) \qquad \text{at} \quad \xi = 0; \tag{92}$$

$$\tilde{\Gamma}_{in} = \chi_S\tilde{\theta}_{in} - \gamma_S\frac{\partial^2\tilde{\eta}}{\partial\varphi^2} \qquad \text{at} \quad \xi = 0; \tag{93}$$

with $\chi_S \equiv \chi/Sc$ and $\gamma_S \equiv \gamma Sc$, taken to be of order unity.

As in the case studied in section 6, the system of linear equations can be analyzed in a Fourier series, by considering any disturbance in the form

$$\tilde{F}\{\varphi, Z, \tau'\} = \hat{F}\{Z\}\exp(ia\varphi + \Sigma\tau'), \tag{94}$$

where $\tilde{F}$ stands for $\tilde{\eta}$, $\tilde{\theta}$, $\tilde{\theta}_d$ and $\tilde{\Gamma}$, and Z for z (for the outer quantities) or ξ (for the inner variables).

Then the solution of eqs. (84), (85), (87) and (88) satisfying boundary conditions (90) and (91) and the matching principle is

$$\hat{\theta}_{out} = \beta\hat{\eta}, \tag{95}$$

$$\hat{\theta}_{in} = \beta\hat{\eta}\left[1 + \left(\frac{\mathscr{S}}{\beta}\frac{\Sigma}{a}\frac{\rho_d}{\rho}\frac{\lambda}{\lambda_d} - \frac{\beta-\beta_d}{\beta}\right) \times (1+\lambda/\lambda_d)^{-1}\,e^{-a\xi}\right]. \quad (96)$$

$$\hat{\theta}_{d,out} = \beta_d\hat{\eta}. \quad (97)$$

$$\hat{\theta}_{d,in} = \beta\hat{\eta}\left[\frac{\beta_d}{\beta} + \frac{\lambda}{\lambda_d}\left(\frac{\mathscr{S}}{\beta}\frac{\Sigma}{a}\frac{\rho_d}{\rho} + \frac{\beta-\beta_d}{\beta}\right) \times (1+\lambda/\lambda_d)^{-1}\,e^{a\xi}\right]. \quad (98)$$

Also, from eq. (86), we obtain

$$\hat{I}_{out} = 0. \quad (99)$$

Note that, to leading order, the boundary conditions (58) to (60) are automatically satisfied, irrespective of the Biot numbers. Thus, the outer regions act as a thermal bath for the inner region and the boundary conditions far from the interface play no role.

The solution to eq. (89) which vanishes when ξ goes to infinity (to match with the outer solution (99)) is

$$\hat{I}_{in} = \left\{A\,e^{r\xi} - \alpha\beta\hat{\eta}\left(\frac{\Omega_0^{eq}}{\Theta_0} - \frac{\Omega_c}{\Theta_c}\right) \times\left[1 + \left(\frac{\mathscr{S}}{\beta}\frac{\Sigma}{a}\frac{\rho_d}{\rho}\frac{\lambda}{\lambda_d} - \frac{\beta-\beta_d}{\beta}\right) \times (1+\lambda/\lambda_d)^{-1}\,e^{-a\xi}\right]\right\} \times \exp\left(-\frac{\alpha}{\Theta_0}\beta\xi\right), \quad (100)$$

with

$$r \equiv \frac{1}{2}\frac{\alpha\beta}{\Theta_0} - \left[\left(\frac{1}{2}\frac{\alpha\beta}{\Theta_0}\right)^2 + a^2\right]^{1/2}. \quad (101)$$

The constants A and $\hat{\eta}$ in eq. (100) should satisfy two different conditions, coming from eqs. (92) and (93). The resulting algebraic system has a solution different from the trivial one when the following compatibility condition is fulfilled:

$$\frac{\rho_d}{\rho}\Sigma = \left\{a\frac{\beta-\beta_d}{\beta} - r\left[\frac{\lambda}{\lambda_d}\left(2+\frac{\mathscr{S}}{\beta}\right) \times\left(1 - \frac{\Theta_c}{\Omega_c}\left(\frac{\chi_S}{\alpha} + \frac{\Omega_0^{eq}}{\Theta_0}\right)\right) - a^2\frac{\gamma_S\Theta_c}{\Omega_c\alpha\beta}\left(1+\frac{\lambda}{\lambda_d}\right)\right]\right\} \times\left\{1 + \frac{\lambda}{\lambda_d}\left(1+\frac{\mathscr{S}}{\beta}\right) + \frac{r}{a}\frac{\mathscr{S}}{\beta}\frac{\lambda}{\lambda_d}\left[1 - \frac{\Theta_c}{\Omega_c}\left(\frac{\chi_S}{\alpha} + \frac{\Omega_0^{eq}}{\Theta_0}\right)\right]\right\}^{-1}. \quad (102)$$

In the limit of small values of a, this expression reduces to

$$\frac{\rho_d}{\rho}\Sigma\{a\to 0\} \approx \frac{\beta-\beta_d}{\beta\left[1+\frac{\lambda}{\lambda_d}\left(1+\frac{\mathscr{S}}{\beta}\right)\right]}a = \frac{\beta-\beta_d}{\beta+\beta_d}a. \quad (103)$$

Comparing this result with the asymptotic limit of eq. (74) for very large wavenumbers (which is given by eq (77)), clearly shows the same trends. Therefore, both dispersion relations, eq. (74) and eq. (102), match perfectly in the intermediate wavenumber range and a composite relation can be written down as usual, just by adding the right-hand side of both dispersion relations and subtracting the common part given by the right-hand side of eq. (103).

In order to present the results in a simple way, we define the saturation parameter

$$\mathscr{S} \equiv \frac{\frac{\lambda}{\lambda_d}\left(2+\frac{\mathscr{S}}{\beta}\right)}{\gamma_S\left(1+\frac{\lambda}{\lambda_d}\right)}\frac{4\Theta_0\Omega_0^{eq}}{\alpha\beta}S. \quad (104a)$$

with

$$S \equiv \frac{\Theta_0}{\Omega_0^{eq}\alpha\beta}\left(\frac{d\Omega_{in}^{st}}{d\xi} - \frac{d\Omega^{eq}}{d\xi}\right)_{\xi=0}. \quad (104b)$$

Note that $\mathscr{S}$ can also be written

$$\mathscr{S} = \frac{\frac{\lambda}{\lambda_d}\left(2+\frac{\mathscr{S}}{\beta}\right)}{\gamma_S\left(1+\frac{\lambda}{\lambda_d}\right)}\frac{4\Omega_c\Theta_0^2}{\alpha\beta\Theta_c}\left[1-\frac{\Theta_c}{\Omega_c}\left(\frac{\chi_S}{\alpha}+\frac{\Omega_0^{eq}}{\Theta_0}\right)\right]. \quad (104c)$$

Both parameters S and $\mathscr{S}$ have the same sign and they measure the degree of saturation in the vicinity of the growing deposit. Note that when $\mathscr{S}$ is negative the Brownian sublayer is undersaturated ahead of the moving fluid–solid interface whereas positive values of $\mathscr{S}$ correspond to constitutional supersaturation.

On the other hand, the parameter

$$\mathscr{G} \equiv \frac{\beta-\beta_d}{\beta}\frac{4\Omega_c\Theta_0^2}{\gamma_S\Theta_c\alpha\beta(1+\lambda/\lambda_d)} \quad (105)$$

provides a measure of the thermophoretically induced instability. When $\mathscr{G}$ is positive, planar crystal growth is unstable, as indicated in section 6.

In terms of the parameters $\mathscr{S}$ and $\mathscr{G}$, the dispersion relation expressed by eq. (102) can be rewritten in a simplified manner by using the new normalized amplification factor Σ^* and wavenumber a^*

$$\Sigma^* \equiv \frac{\rho_d}{\rho}\frac{2\Theta_0}{\alpha\beta}\Sigma, \quad a^* \equiv 2\frac{\Theta_0}{\alpha\beta}\frac{k}{Sc}, \quad (106)$$

and defining the parameter

$$\Lambda \equiv \frac{4\Omega_c\Theta_0^2}{\Theta_c\alpha\beta}\frac{1+\frac{\lambda}{\lambda_d}\left(1+\frac{\mathscr{S}}{\beta}\right)}{\gamma_S(1+\lambda/\lambda_d)}, \quad (107)$$

then, eq. (102) becomes

$$\Sigma^* \equiv \frac{a^*\mathscr{G}+\left(\sqrt{1+a^{*2}}-1\right)(\mathscr{S}-a^{*2})}{\Lambda-\frac{\sqrt{1+a^{*2}}-1}{a^*}\frac{\mathscr{S}/\beta}{2+\mathscr{S}/\beta}\mathscr{S}}. \quad (108)$$

Within the range of validity of the present analysis, the sign of Σ^* in eq. (108) is given by the numerator of the last fraction (occasionally, the denominator may vanish or become negative, but this happens either for unrealistically large values of the surface tension parameter or for very large values of the wavenumber and, in both cases, the expansion in the Schmidt number we have performed breaks down). When the numerator is positive for some wavenumber a^*, planar growth is unstable. Therefore the stability of the front is governed by only two parameters, the thermophoretic parameter $\mathscr{G}$ defined in eq. (105) and the saturation parameter $\mathscr{S}$ defined in eq. (104). These parameters account for the two morphological instabilities which may arise during planar growth of a solid deposit by thermal diffusion mass transport.

When $\mathscr{G}$ is positive, the amplification factor Σ^* is positive, at least for the small values of a^*. This is the thermophoretically-induced morphological instability pointed out in the previous section. Besides, eq. (108) shows that for very large wavenumbers, a^*, the stabilizing effect of surface energy, measured by the parameter γ_S and represented by the last term in $-a^{*2}$, is dominant, and Σ^* becomes negative. Therefore large wavenumber disturbances are always damped out by their excess in surface energy.

On the other hand, whenever $\mathscr{S}$ is positive there exists a constitutional supersaturation in the Brownian sublayer. As it was schematically pointed out in the Introduction and shown by Hurle [25] and Sekerka [26], this is a potentially unstable situation. This is the constitutional supersaturation-induced morphological instability. However, when $\mathscr{S}$ is negative, interface protuberances have more difficulty in developing into the fluid region because it is a thermodynamically stable phase.

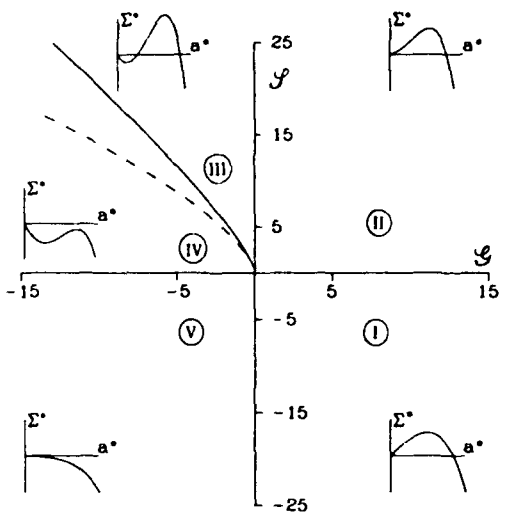

Fig. 1. Stability diagram of thermophoretically growing deposits. Planar growth is unstable in regions I, II and III and stable in regions IV and V. In each region a schematic representation of the amplification factor Σ^*, as a function of the disturbance wavenumber a^*, is presented. The solid line separating regions III and IV corresponds to the critical values given by eqs. (110) whereas the dashed line is the asymptotic result given by eq. (111).

The main features of the dispersion relation (108) are depicted in fig. 1. There exist five different regions in the parameter space labeled I to V in fig. 1. The behavior of the linear amplification factor, Σ^*, as a function of the disturbance wavenumber, a^*, is schematically indicated in each region.

In region I, $\mathcal{G}$ is positive and the planar growth is unstable due to the morphological instability indicated in section 6, but $\mathcal{Y}$ is negative, therefore the fluid ahead of the interface is undersaturated. For large values of a^*, the stabilizing influence of the undersaturation overcomes the destabilizing effect of thermal diffusion within the diffusive boundary layer. The right-hand side term of eq. (108) becomes negative and large wavenumber disturbances are damped out. Therefore, only disturbances with wavelengths larger than the diffusive boundary layer thickness are expected to develop. Thus, the undersaturation modifies the result given by eq. (77), which predicted a monotonic increase of the amplification factor with the disturbance wavenumber when Brownian diffusion and surface energy effects were not taken into account. Only disturbances with wavenumbers ranging from $a^* = 0$ to the value at which Σ^* (a^*) vanishes again, are linearly unstable.

In region II, both parameters $\mathcal{G}$ and $\mathcal{Y}$ are positive. The planar front is already unstable for the thermal diffusion-driven morphological instability indicated in the previous section, and a positive value of $\mathcal{Y}$ results in even higher amplification factors for intermediate wavenumber disturbances. This is the most unstable situation. Both effects cooperate to render the planar growth unstable until surface energy effects take over and stabilize the very large wavenumbers.

In region III, $\mathcal{G}$ is a negative quantity and the planar front is stable for thermal diffusion instability, but a high enough supersaturation (that is, a positive and large value of $\mathcal{Y}$) render the value of Σ^* in eq. (108) positive for some intermediate values of the wavenumber, a^*. Then a supersaturation induced morphological instability appears. The small wavenumber disturbances are stabilized by latent heat release but at an intermediate range of wavenumbers, supersaturation overcomes these stabilizing effects and makes unstable the planar growth. Again, surface energy effects stabilize the very large wavenumbers.

In region IV, $\mathcal{G}$ is negative and $\mathcal{Y}$ is positive but is not large enough to overcome the stabilizing effects of both latent heat release and surface energy excess. Planar growth is stable.

Finally, in region V, both $\mathcal{G}$ and $\mathcal{Y}$ are negative and the planar interface during the growth of a solid deposit by thermophoretic transport is linearly stable. Disturbances of any wavenumber are damped out.

All these mentioned features are clearly pointed out when the dispersion relation is expanded, around the origin in the parameter space, for small values of the wavenumber as

$$\Sigma^* = \frac{1}{\Lambda}\left(\mathcal{G}a^* + \frac{\mathcal{Y}}{2}a^{*2} - \tfrac{1}{2}a^{*4}\right), \tag{109}$$

this simple expression incorporates the whole qualitative description of the morphological insta-

bility in the five distinctive regions of the parameter space.

Over the line separating region III from region IV, Σ^* starts at a zero value at $a^* = 0$ and decreases as a^* increases due to the stabilizing role of latent heat release. Further increases of a^* tend to increase the value of Σ^* due to the constitutional supersaturation, but Σ^* reaches a maximum value equal to zero and comes down back again due to the surface energy stabilizing influence. Therefore, the locus of this critical line may be easily obtained by noting that Σ^* vanishes when it is also a maximum respect to a^*. Imposing these two conditions ($\Sigma^* = 0$ and $d\Sigma^*/da^* = 0$), we obtain the critical values for the saturation parameter, $\mathscr{S}_{crit}$, and the critical wavenumber, a^*_{crit}, as functions of the thermal parameter $\mathscr{G}$. It results that

$$\mathscr{S}_{crit} = (a^*_{crit})^2\left[1 + 2\sqrt{1 + (a^*_{crit})^2}\right], \tag{110a}$$

$$-\mathscr{G} = 2a^*_{crit}\left[1 + (a^*_{crit})^2 - \sqrt{1 + (a^*_{crit})^2}\right]. \tag{110b}$$

Thus, given a negative value of $\mathscr{G}$, eq. (110b) provides the critical wavenumber, a^*_{crit}, and eq. (110a) the critical value of the saturation parameter, $\mathscr{S}_{crit}$ which corresponds to the separation line between region III and region IV in fig. 1. For positive values of $\mathscr{G}$ or values of $\mathscr{S}$ larger than the critical value (which is a function of $\mathscr{G}$ only), planar growth is unstable.

The behavior of the critical values, for small negative values of $\mathscr{G}$ can easily be obtained from eqs. (109) and (110), resulting in

$$\mathscr{S}_{crit} = 3(-\mathscr{G})^{2/3}, \quad a^*_{crit} = (-\mathscr{G})^{1/3} \quad \text{when} \quad 0 < -\mathscr{G} \ll 1. \tag{111}$$

This asymptotic results is plotted in fig. 1 as a dashed line.

The critical wavenumber, a^*_{crit}, is plotted in fig. 2 as a function of the thermal parameter $\mathscr{G}$. The solid line corresponds to the exact result given by eq. (110) and the dashed line gives the asymptotic limit for small values of the thermal parameter provided by eq. (111).

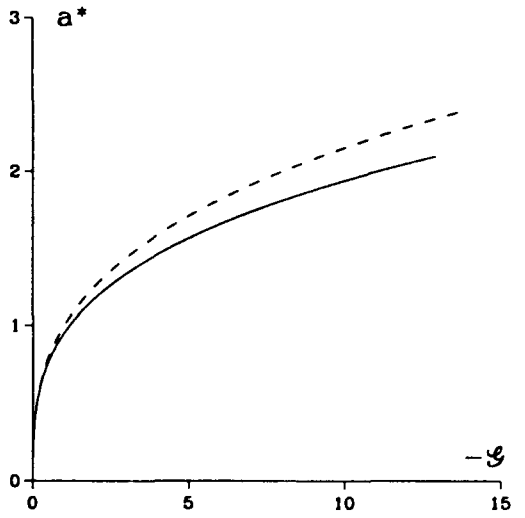

Fig. 2. Normalized critical wavenumber a^*, as a function of the thermophoretic parameter $\mathscr{G}$. Solid line represents the exact result from eq. (110b), whereas dashed line is the asymptotic result given by eq. (111).

Also the line corresponding to $\mathscr{G} = 0$, and negative values of the saturation parameter $\mathscr{S}$ (i.e. $\mathscr{G} = 0$ and $\mathscr{S} < 0$), is a critical line because it separates stable and unstable regions of planar growth. Over this line, the critical wavenumber, a^*_{crit}, is always equal to zero.

When $\mathscr{G}$ is negative, the critical value of the saturation parameter, $\mathscr{S}_{crit}$, provided by eq. (109a) is a monotonically increasing function of $(-\mathscr{G})$. Therefore, the range of experimental operation conditions for stable planar growth is enlarged beyond the limit growth velocity given by the oversimplified criterion, eq. (3), due to the stabilizing influence of both latent heat release and interfacial energy. Thus, we can conclude that for negative values of $\mathscr{G}$, the maximum growth velocity for stable planar growth is

$$\rho_d V_{growth} = \rho\alpha_T D\frac{\omega_c}{T_e}\left(\frac{dT}{dY}\right)_{Y=0} = \left\{\rho D\frac{\omega^{eq}}{T}\left[\frac{\Delta H}{RT} + \alpha_T(1 + S_{crit})\right]\frac{dT}{dY}\right\}_{Y=0}. \tag{112}$$

where the critical value S_{crit} may be obtained from the definition (109a) once $\mathcal{S}_{crit}$ is known. As S_{crit} is always positive (when the planar growth is thermophoretically stable; i.e., for negative values of $\mathcal{S}$) the limit velocity is larger than the given by the simplified criterion. However, for positive values of the thermophoretic parameter $\mathcal{S}$, planar growth is unstable for any given velocity.

8. Discussion of results and conclusions

We have performed a linear stability analysis of a solid deposit with a planar interface growing from a fluid mixture. The depositing species is considered to be dilute in the carrier fluid and the growth limited by thermal diffusive (Soret) transport, with Brownian diffusion playing a minor role (restricted to a boundary (sub-)layer in the immediate vicinity of the solid–liquid interface) and without considering interfacial kinetic limitations. Due to the diluteness assumption, the Peclet number associated with the advancing solidification front is quite small and the unsteady term as well as the convective terms have been neglected in the governing equations.

The resulting dispersion relation between the disturbance amplification rate σ and the disturbance wavenumber k is given by eq. (74), which describes a new type of *morphological* instability. The driving mechanism is the thermal (Soret) diffusion phenomenon. Sufficient conditions for the appearance of the instability are explicitly given by eq. (75c) and eq. (75d). Planar growth is unstable either when the thermal diffusion factor α_T of the depositing species is positive (as is the case for very massive molecules in a light carrier gas) and the latent heat release is very small, or when α_T is negative and the upper boundary is a good thermal insulator. To be consistent with the assumption of a comparatively small diffusive (Fickian) mass transport, α_T should be considered positive, Rosner [27]. This situation corresponds to large depositing molecules dilute in a light carrier gas. Such *particles* drift by thermal diffusion towards cooler regions, that is, the deposit should then be colder than the fluid mixture. In that case, eq. (74) shows that, subject to our present model idealizations, when the latent heat release is very small (and the thermal conductivity of the solid is larger than the fluid thermal conductivity, as it usually happens), there is no possibility of stable planar growth – i.e., disturbances of any wavenumber will be magnified, with the amplification factor being a monotonically increasing function of wavenumber. However, the analysis leading to eq. (74) breaks down when the disturbance wavelength is of the order of the thickness of the diffusive boundary layer [that is, when $k = O(Sc)$]. Then, transverse diffusive fluxes should be taken into account and eq. (102) provides the corresponding dispersion relation. The implemented dispersion relation incorporates a second type of morphological instability induced by constitutional supersaturation. The two kinds of instabilities may compete or cooperate in this interval of large wavenumber disturbances. Thus, when the diffusion sublayer is stable by itself (that is, when there is no constitutional supersaturation near the interface), this stabilization mechanism may provide a cutoff to the instability induced by thermophoresis. On the other hand, when constitutional supersaturation is present, the band of unstable wavenumber is enlarged up to the scale where interfacial energy phenomena take over and the smaller wavelengths are damped out. When the latent heat release is able to stabilize the small wavenumbers disturbances but supersaturation exists, the destabilizing effect of supersaturation may render unstable the planar growth for some wavenumber of the order of the Schmidt number. Under these circumstances, a front corrugated on very small length scales is expected.

Debe and Poirier [28] have recently reported some experimental results on the physical vapor deposition of dilute copper phtalocyanine under microgravity and ground-based conditions. Although in the latter case buoyancy currents [#2] appearing in the bulk may alter the resulting crystallization pattern, they observed in both cases

[#2] Gas "creep" along the non-isothermal solid sidewalls is also expected to drive an appreciable convection, even under microgravity conditions (Rosner [29]).

the formation of a very corrugated front, leading finally to the development of non-linear structures of finger-shaped form, with an average size of the order of 10^3 Å. Copper phtalocyanine molecules are very large and in the usual gas carriers they exhibit a low Fickian mobility (with Schmidt numbers about 10) and a large thermal diffusion effect (with thermal diffusion factors about 7). Thus, the solid growth was actually controlled by thermal diffusion. Under their experimental conditions, constitutional supersaturation was actually present (see, e.g. Rosner and Keyes [30]). Moreover, the copper phthalocyanine was very dilute in the gas mixture and, then, the latent heat release rate was very small and unable to stabilize the small wavenumber disturbances. Therefore, planar growth was unstable against both types of morphological instabilities. To avoid or reduce the instability one might use a carrier of larger molecular size (comparable to that of the depositing species) although the "price" paid would be a notable decrease in the molecular diffusion-limited growth rate. In any case, our approach predicts an important dependence of surface morphology on the nature of the carrier gas, which may have interesting practical implications.

On the other hand, the experiments conducted by Reed and LaFleur [7] on the growth of iodine solids from iodine–helium mixtures were carried out for heavy mass-loaded mixtures and, in spite of the molar dilution, the mass diluteness assumption can not be applied and the Stefan flow must play a non-negligible role. Furthermore, the Schmidt number was of the order of the unity and Fickian diffusion transport was as important as thermal diffusion mass transfer. In any case, the planar growth was found to be initially stable, becoming unstable only for sufficiently large growth velocities. The experimentally observed critical growth velocity, as indicated by Rosenberger et al. [8], was one order of magnitude larger than the value predicted for the oversimplified criterion, eq. (3). Our result (eq. (112)) explains qualitatively this discrepance because α_T as well as S_{crit} are positive and a larger growth velocity may be achieved with a planar interface still remaining stable.

It is clear that the additional mechanisms of Fickian diffusion and Stefan flow cannot be neglected in many practical situations, and the present analysis should be extended to account for mixtures in which both diffusive mass fluxes (Fickian diffusion and thermal (Soret) diffusion) as well as the deposition-induced convective mass transport have comparable importance throughout the domain. It would be also interesting to relate this class of continuum models to *discrete* computer simulations of deposit formation (see, e.g., Tassopoulos et al. [31] and Rosner et al. [32]) which predict deposit microstructural properties (surface roughness, porosity, etc.). Our further studies will be directed along these lines.

Acknowledgments

Two of the authors (J.L.C. and P.L.G.-Y.) acknowledge partial support by the Dirección General de Investigatión Científica y Técnica (DGICYT), Spain, under contracts PB87-0588 and PB88-0159.

Nomenclature

A, B, C, E	Integration constants
a	Rescaled disturbance wavenumber, $a = k/\mathrm{Sc}$
Bi	Biot numbers introduced in eqs. (58) and (59)
c_d	Deposit specific heat
c_p	Fluid specific heat at constant pressure
D	Binary diffusion coefficient

$\mathscr{E}$	Thermophoretic parameter defined in eq. (105)
ΔH	Molar heat of solid deposit sublimation
K	Dimensionless local surface curvature
k	Dimensionless disturbance wave-number
$\mathscr{L}$	Dimensionless latent heat parameter $\mathscr{L} \equiv \Delta H\ \mathrm{Pe}/(M_1 c_p T_{\mathrm{ref}})$
L	Fluid layer thickness
L_d	Deposit thickness
l	$l = L + L_d$
M	Molar mass
N	Normalization factor defined by eq. (11)
n	Unit vector normal to the fluid–solid interface, eq. (11)
Pe	Fluid thermal Peclet number, $\mathrm{Pe} \equiv V_{\mathrm{ref}} L/[\lambda/(\rho c_p)]$
Pr	Prandtl number, $\mathrm{Pr} \equiv \nu/[\lambda/(\rho c_p)]$
p	Local pressure
R	Universal gas constant
r	Exponential factor defined by eq. (101)
r_s	Interface position vector, eq. (10)
S	Measure of supersaturation defined by eq. (104b)
$\mathscr{S}$	Supersaturation parameter defined by eq. (104a)
Sc	Schmidt number, $\mathrm{Sc} \equiv \nu/D$
T	Local temperature
t	Time
t	Unit vector tangent to the fluid–solid interface, eq. (11)
V	Local velocity
v	Dimensionless velocity, $v \equiv V/V_{\mathrm{ref}}$
X, Y	Space coordinates
x, y	Dimensionless coordinates
z	Dimensionless vertical distance from the interface, $z \equiv y - \eta(x, \tau)$
α	Dimensionless thermophoretic diffusivity, $\alpha = \alpha_T D/\nu$
α_T	Thermal diffusion factor
β	Dimensionless fluid temperature gradient
Γ	Mass fraction disturbance
γ	Dimensionless interfacial energy parameter, $\gamma \equiv 2\sigma_T M_1/(\rho_d RTL\omega_{\mathrm{ref}})$, eq. (32b)
γ_S	Stretched γ, $\gamma_S = \gamma \mathrm{Sc}$
δ	Thickness ratio, $\delta \equiv L_d/L$
ζ	Interfacial deformation, eq. (10)
η	Dimensionless interfacial deformation, $\eta \equiv \zeta/L$
Θ	Dimensionless temperature field, $\Theta \equiv T/T_{\mathrm{ref}}$
θ	Temperature disturbance
λ	Thermal conductivity
Λ	Parameter defined by eq. (107)
μ	Dynamic viscosity
ν	Kinematic viscosity, $\nu = \mu/\rho$
ξ	Inner stretched coordinate, $\xi = \mathrm{Sc}\, z$
Π	Dimensionless pressure field, $\Pi = pL/\mu V_{\mathrm{ref}}$
ρ	Density
Σ	Normalized disturbance amplification factor, $\Sigma = \sigma/\mathrm{Sc}$
σ	Disturbance amplification factor
σ_T	Interfacial tension of the fluid–solid interface
τ'	Stretched dimensionless time, $\tau' = \tau\, \mathrm{Sc}$
τ	Dimensionless time, $\tau = tV_{\mathrm{ref}}/L$
ϕ	Stretched horizontal coordinate, $\phi = \mathrm{Sc}\, x$
χ	$\chi = (\mathrm{d}\Omega^{\mathrm{eq}}/\mathrm{d}\Theta)$ at $\Theta = \Theta_0$
χ_S	Stretched χ, $\chi_S = \chi/\mathrm{Sc}$
Ω	Normalized mass fraction, $\Omega = \omega/\omega_{\mathrm{ref}}$
ω	Depositing species mass fraction, $\omega = \rho_1/\rho$

Subscripts

crit	Critical values, see eqs. (110)
d	Deposit
e	Values at $Y = L$
in	Inner solution
out	Outer solution

ref	Reference values used to nondimensionalize the variables
s	Interface
0	Refers to the value at the interface during stationary growth
1	Refers to the deposit forming fluid component
2	Refers to the inert (carrier) fluid component
δ	Values at $Y = -L_d$

Superscripts

eq	Equilibrium mass fraction values, eq. (19)
st	Stationary state, section 5
*	Normalized values defined by eqs. (106)

Miscellaneous

^	Disturbance z-dependence (see eq. (61))
-	Refers to disturbances defined by eq. (79)
{ }	Functional parentheses
Γ, Γ^2	Gradient and Laplacian operators, respectively
nst	Non-steady terms

References

[1] G.B. Stringfellow, in: Crystal Growth, Ed. B.R. Pamplin (Pergamon, Oxford, 1980) p. 181.
[2] W.A. Bryant, J. Mater. Sci. 12 (1977) 1285.
[3] H.U. Walter, Ed., Fluid Sciences and Material Science in Space (Springer, Berlin, 1987).
[4] W.W. Mullins and R.F. Sekerka, J. Appl. Phys. 34 (1963) 323.
[5] W.W. Mullins and R.F. Sekerka, J. Appl. Phys. 35 (1964) 444.
[6] J.S. Langer, Rev. Mod. Phys. 52 (1980) 1.
[7] T.B. Reed and W.J. LaFleur, Appl. Phys. Letters 5 (1964) 191.
[8] F. Rosenberger, M.C. Delong, D.W. Greenwell, J.M. Olson and G.H. Westphal, J. Crystal Growth 29 (1975) 49.
[9] J.L. Castillo and D.E. Rosner, Chem. Eng. Sci. 44 (1989) 925.
[10] D.E. Rosner, Transport Processes in Chemically Reacting Flow Systems, 3rd printing (Butterworths–Heinemann, London, 1990).
[11] E.A. Mason, J. Chem. Phys. 27 (1957) 782.
[12] P.L. García-Ybarra and D.E. Rosner, AIChE J. 35 (1989) 139.
[13] S.R. de Groot and P. Mazur, Non-Equilibrium Thermodynamics (North-Holland, Amsterdam, 1962).
[14] J.L. Castillo, P.L. García-Ybarra and D.E. Rosner, in: Proc. 7th European Symp. on Materials and Fluid Sciences in Microgravity (European Space Agency SP-295, 1990) p. 167.
[15] J.L. Castillo, P.L. Garcia-Ybarra and D.E. Rosner, Advan. Space Res. 11(7) (1991) 277.
[16] D.T.J. Hurle, J. Crystal Growth 61 (1983) 463.
[17] S. Goren, J. Colloid Interface Sci. 61 (1977) 77.
[18] S.A. Gokoglu and D.E. Rosner, AIAA J. 24 (1986) 172.
[19] F. Rosenberger, Fundamentals of Crystal Growth I (Springer, Berlin, 1981).
[20] P. Clavin and P. García-Ybarra, J. Mécanique 2 (1983) 245.
[21] P.L. García-Ybarra, J.L. Castillo and M.G. Velarde, Phys. Fluids 30 (1987) 2655.
[22] J. Frenkel, Kinetic Theory of Liquids (Dover, New York, 1955).
[23] M. Van Dyke, Perturbation Methods in Fluid Mechanics (Academic Press, New York, 1964).
[24] P.L. García-Ybarra, C. Nicoli and P. Clavin, Combust. Sci. Tech. 42 (1984) 87.
[25] D.T.J. Hurle, in: Crystal Growth: An Introduction, Ed. P. Hartman (North-Holland, Amsterdam, 1973).
[26] R.F. Sekerka, in: Crystal Growth: An Introduction, Ed. P. Hartman (North-Holland, Amsterdam, 1973).
[27] D.E. Rosner, Physico-Chem. Hydrodyn. 1 (1980) 159.
[28] M.K. Debe and R.J. Poirier, Thin Solid Films 186 (1990) 327.
[29] D.E. Rosner, Phys. Fluids A 1 (1989) 1761.
[30] D.E. Rosner and D.E. Keyes, Theoretical Studies in Support of the 3M-Vapor Transport (PVTOS-) Experiments, NASA CR185122 (July 1989).
[31] M. Tassopoulos, J. O'Brien and D.E. Rosner, AIChE J., 35 (1989) 967.
[32] D.E. Rosner, A.G. Konstandopoulos, M. Tassopoulos and D.W. Mackowski, in: Proc. Engineering Foundation Conf. on Inorganic Transformations and Ash Deposition During Combustion, in press.

Reprinted from I&EC RESEARCH, 1992, 31.

Effects of Heat Transfer on the Dynamics and Transport of Small Particles Suspended in Gases

Daniel E. Rosner,* Daniel W. Mackowski,† Menelaos Tassopoulos, Jose Castillo,‡ and Pedro Garcia-Ybarra‡

Chemical Engineering Department, High Temperature Chemical Reaction Engineering Laboratory, Yale University, New Haven, Connecticut 06520-2159

Heat transfer (associated with Fourier diffusion, photon absorption and/or emission, surface chemical reaction, and/or evaporation) can lead to dramatic changes in the motion of small particles in gases, modifying coagulation rates, and/or capture rates. Cases discussed in this review of recent studies include (a) *thermo*phoretic drift of spherical particles in a gas through which energy is diffusing, (b) *photo*phoretic drift of radiation-absorbing suspended spheres, (c) phoresis and apparent Brownian diffusivity of *asymmetric* particles, including spheres with nonuniform accommodation coefficient and unequal primary particle size aggregates, (d) scavenging of fine particles by evaporating droplets, and (e) coagulation rate of unequal temperature spherical particles. These transport phenomena, often associated with the localized "overheating" or "undercooling" of individual particles, have largely been ignored by applied scientists on the (usually implicit) assumption that the more familiar effects of ordinary Brownian diffusion would dominate in near-isothermal laminar gas (sub-)regions. However, we show that even in regions free of macroscopic (bulk) temperature gradients, these phenomena can dominate ordinary Brownian transport by orders of magnitude, with potentially important engineering consequences. General expressions for the relevant particle drift velocities, coagulation rate constants, or effective particle diffusivities are used to carry out illustrative calculations for multiphase systems of current and future engineering interest, including fine particle synthesis/materials processing, and combustion gas cleaning.

1. Introduction, Motivation, and Goals

Technologies that exploit or inadvertently generate particle-laden gases are often also associated with large "convective" and radiative energy fluxes, as in the cases of optical waveguide glass deposition (see, e.g., Rosner and Park, 1988) or pulverized-coal-fired electric power stations (see, e.g., Flagan and Friedlander, 1978). Yet, the science of "aerosols" had its origins in the understanding/control of environmental problems which were relatively uninfluenced by simultaneous *energy* transfer (see, e.g., Whytlaw-Gray and Patterson, 1932; Fuchs, 1964; Friedlander, 1977; Hidy, 1984; Flagan and Seinfeld, 1988). For example, fine particles suspended in isothermal "fluids" undergo Brownian motion due to molecular/particle impacts (Einstein, 1926) and this random walk motion is, in turn, associated with the now well-known phenomena of particle–particle "coagulation" and particle Brownian diffusion to macroscopic solid surfaces (immersed or containment). The simultaneous presence of significant *energy fluxes* (e.g., Fourier conduction or radiative transport through the carrier gas) raises the important question of if and how the familiar laws of particle "diffusive" transport and coagulation are modified from those normally associated with isothermal gases in the absence of a net energy flux.

Our recent research on combustion gases containing suspended spherical or nonspherical particles, briefly summarized in this paper, has provided many examples in which the *mass*-transfer effects of simultaneous *energy* transfer are quite dramatic, because of the onset of "new" mechanisms of particle transport in the presence of gas temperature gradients and/or radiative fluxes. Actually, some of these mechanisms (conventional "thermophoresis" (section 2.1) and "photophoresis" (section 2.2)) are discussed in classical aerosol *science* texts, but, until relatively recently, were not thought to be of *engineering* importance. Others (associated with *asymmetrical* particles in the presence of energy transfer (section 2.3)) are much less familiar and are now under active investigation (Garcia-Ybarra and Rosner, 1989). Moreover, some of the phenomena we describe can be viewed as extreme cases of the Soret effect, which describes the drift of *molecular* species in nonisothermal disparate molecular weight systems (see, e.g., the review of Rosner (1980) and Garcia-Ybarra and Rosner (1989)). In each case we briefly illustrate the consequences of simultaneous energy transfer for determining fine particle deposition rates via transport across gaseous boundary layers (section 3.1), fine particle "scavenging rates" by evaporating droplets (as in "wet scrubbers"; Cooper, 1982) (section 3.2), and the coagulation dynamics of a population of unequal temperature radiation-heated particles (section 3.3). Further details on each of these developing topics will be found under Literature Cited, with our present conclusions and recommendations summarized in section 4. To some extent this paper may also be viewed as a companion to (and extension of) Rosner (1987), which emphasized the non-Fickian (-Brownian) nature of small particle mass transport in the presence of convective energy transfer, with applications to electric power generation and advanced materials processing.

2. Examples of Heat-Transfer Effects on the Dynamics of Small Particles Suspended in Gases

Consider the local environment of a solid particle too small to appreciably "sediment" or depart (due to its inertia) from the local gas mixture mass motion. In the presence of an energy flux it is not difficult to anticipate that its normally "isotropic" Brownian motion becomes "biased" in a direction related to the direction of the local energy flux. When one averages over many gas molecule/particle surface impacts, this "bias" is associated with a net particle "drift" (called *phoresis*) which, for isotropic spheres, is usually in the same direction as the local energy flux vector. The most familar case of Fourier heat conduction through the gas is first briefly discussed in section

*To whom correspondence should be addressed.
†Present address: Department of Mechanical Engineering, Auburn University, Auburn, AL 36849-5341.
‡Visiting Scholar; Permanent address: UNED-Madrid, Spain.

0888-5885/92/2631-0760$03.00/0

2.1, whereas the case of radiation energy flux through a locally isothermal gas containing absorbing particles is taken up in section 2.2. In section 2.3 we consider some unusual properties of *asymmetric* particles (e.g., aggregates of two spheres) not in thermal equilibrium with the local carrier gas. In all cases the resulting particle motion in the direction of the net energy flux is dramatically altered, giving rise to the engineering consequences discussed in section 3.

2.1. Thermophoresis of Spherical Particles Suspended in a Gas. A small spherical particle which finds itself in a radiation-free "fluid" sustaining a temperature gradient (and hence Fourier energy diffusion) comprises the simplest and best-studied case. Two limiting subcases are easiest to visualize, depending on the ratio of the host gas mean free path l_g to the characteristic particle dimension (say the diameter d_p for a sphere). When this ratio (the so-called particle Knudsen number) is very large, the particle behaves like a "giant" (almost stationary) molecule in a disparate molecular weight gas mixture (Garcia-Ybarra and Rosner, 1989). Waldmann (1961) showed that such a particle will drift down the temperature gradient with the quasi-steady velocity (relative to the gas)

$$v_T = (\alpha_T D)_p |\dot{q}''_F/(k_g T)| \tag{1}$$

where $\dot{q}''_F = k_g|-(\text{grad } T)|$ is the Fourier energy flux vector and the "thermophoretic diffusivity" $(\alpha_T D)_p$ was found to be

$$(\alpha_T D)_p = (3/4)\nu_g\{1 + (\pi/8)\alpha_{mom}\}^{-1} \tag{2}$$

$\nu_g = (\mu/\rho)_g$ is the local gas *momentum diffusivity* ("kinematic viscosity") and α_{mom} the gas/solid *momentum accommodation coefficient*. Equation 2 has recently been shown to be consistent with observed "particle-free" zone thicknesses measured using counterflow laminar diffusion flames containing suspended submicron TiO_2 particles (Gomez and Rosner (1992) and section 3.4). In the opposite limit $Kn_p \ll 1$ emphasized in what follows (sections 2.2 and 2.3), the surrounding gas can be treated as a "continuous" fluid but one must abandon the conventional "no-slip" boundary condition of classical fluid mechanics (see, e.g., Rosner, 1986, 1989b). Indeed, J. C. Maxwell in 1879 showed that whenever $\alpha_{mom} \neq 0$ the presence of a *tangential* gas temperature gradient in the vicinity of such a surface will be associated with a local gas motion directed from cold to hot, which will act to "propel" the surface toward the cooler gas. This "pumping" action, which can be viewed as the "mechanism" of thermophoresis (and photophoresis, section 2.2 below) in the $Kn_p \ll 1$ limit, leads to the result (see, e.g., Brock, 1962)

$$(\alpha_T D)_p = \frac{2c_s\nu\left(\frac{k_g}{k_p} + c_t\frac{l_g}{a}\right)\left[1 + \frac{l_g}{a}(A + Be^{-Ca/l_g})\right]}{\left(1 + 3c_m\frac{l_g}{a}\right)\left(1 + 2\frac{k_g}{k_p} + 2c_t\frac{l_g}{a}\right)} \tag{3}$$

for an isotropic sphere of thermal conductivity k_p in a gas of (translational) thermal conductivity k_g. (Remaining quantities are defined in the Nomenclature section).

It is interesting that $(\alpha_T D)_p$ in both Kn_p limits is actually particle size independent, with d_p influencing "only" the nature of the transition between these two limiting values (see, e.g., Figure 1, constructed for silica particles in ca. 1500 K "air" using a semiempirical transition regime relation (Talbot, 1981)). Equation 3 reveals that, unless $Kn_p \gg 1$, particles with the smallest thermal conductivity will experience the largest thermophoretic effects.

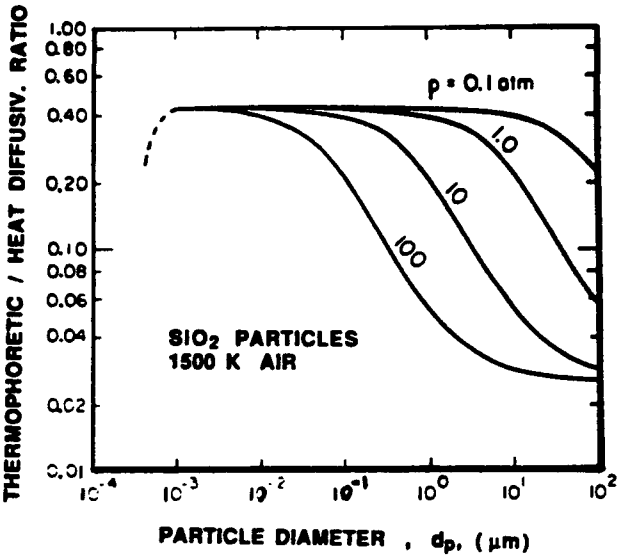

Figure 1. Predicted particle thermophoretic diffusivity (normalized by the gas *thermal* diffusivity) as a function of particle size and pressure level in ca. 1500 K "air" (after Rosner (1980) and Fernandez de la Mora and Rosner (1981)).

2.2. Photophoresis of Spherical Particles Suspended in a Gas. *Photophoresis* of spherical particles is in many respects similar to thermophoresis because the particle motion is induced by a temperature gradient in the gas adjacent to the particle. In *photo*phoresis, however, the gradient arises from nonuniform absorption of incident radiation *within* the particle; i.e., the gas temperature "far" from the sphere can be uniform. Considering that radiative transport is often the dominant mode of heat transfer in large-scale combustors (see, e.g., Viskanta and Menguc, 1987) the "driving force" for particle photophoresis in high-temperature environments can be significant.

In a manner completely analogous to thermophoresis (cf. eq 1), the photophoretic velocity of a particle can be formally expressed:

$$v_P = (\alpha_P D)_p |\dot{q}''_R/(k_g T)| \tag{4}$$

where $\dot{q}''_R$ is the *radiative* energy flux vector and $(\alpha_P D)_p$, *defined* by eq 7, is the *photophoretic diffusivity* (Mackowski, 1989; Castillo et al., 1990). Prediction of $(\alpha_P D)_p$ must take into account the particular Knudsen number regime of the sphere, as well as the nature of radiation absorption within the sphere. For monochromatic radiation the latter is characterized by the size parameter $x = \pi d_p/\lambda$ (where λ is the radiation wavelength) and m, the complex index of refraction $(n + ik)$. Particles having size parameters much less than unity will not undergo appreciable photophoretic motion because radiation absorption within the particle becomes uniform in this limit. Consequently, in typical thermal radiation environments photophoresis will only be significant for super-micron-sized particles, especially in the "window" of particle sizes before the onset of appreciable *inertial impaction* effects (near-critical Stokes number). The analysis of photophoresis under atmospheric pressure (or high pressure) conditions can thus be approached from a near-continuum (i.e., $Kn_p \ll 1$) viewpoint. In this regime (Mackowski, 1989)

$$(\alpha_P D)_p = -\frac{2c_s\nu J_1}{3}\frac{1 + \frac{l_g}{a}(A + Be^{-Ca/l_g})}{\left(1 + 3c_m\frac{l_g}{a}\right)\left(1 + 2\frac{k_g}{k_p} + 2c_t\frac{l_g}{a}\right)} \tag{5}$$

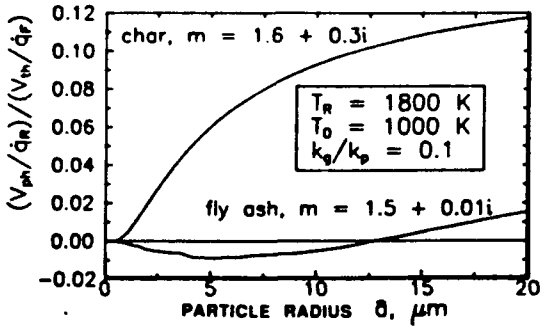

Figure 2. Ratio of *photo*phoretic to *thermo*phoretic "diffusion" factors for equal Fourier and radiative energy fluxes (after Castillo et al. (1990)).

which contains the familiar Cunningham–Millikan correction factor to the Stokes drag (Buckley and Loyolka, 1989). J_1 is the dimensionless *radiative asymmetry factor* (characterizing the degree of nonuniformity of radiation absorption within the particle), defined by (Yalamov et al., 1976)

$$J_1 = (3/(2a^3\dot{q}''_R))\int_0^a\int_0^\pi \dot{Q}'''(r,\theta)r^3 \cos\theta \sin\theta \, d\theta \, dr \quad (6)$$

$\dot{Q}'''(r,\theta)$ is the radiative absorption rate distribution. In the limit $x \gg 1$ most absorption occurs essentially at the sphere surface and J_1 approaches its minimum value, −0.5. Our evaluation of J_1 (analogous to computing radiative cross sections) for arbitrary x and m utilizes Lorentz–Mie theory to calculate $\dot{Q}'''(r,\theta)$, for which eq 6 can be analytically (term by term) integrated. The photophoretic diffusivity for spectrally distributed radiation is obtained through integration of J_1 over the wavelength distribution of the incident radiation.

Presented in Figure 2 is the ratio (α_P/α_T) of the photophoretic and thermophoretic factors vs sphere diameter for both highly absorbing (e.g., carbonaceous) and weakly absorbing (e.g., fly ash) particles. In either case this ratio is equivalent to the ratio of photo- and thermophoretic *velocities* under equal radiative and Fourier (conductive) heat flux conditions. For simplicity, the illustrative results displayed pertain to a wavelength-independent refractive index and a blackbody incident radiation spectrum corresponding to 1800 K. Ashlike particles display the interesting phenomenon of "negative" photophoresis for diameters less than about 25 μm; i.e., the "drift" is directed *toward* the radiation source (a consequence of radiation "focusing" by the particle to the rear (nonilluminated side)). However, phoretic ratios for highly absorbing particles are positive throughout and several times larger than the weak-absorber ratios. Although absolute values of this ratio do not exceed about 0.1, the radiative flux to heat-exchanger surfaces in large furnaces will often exceed the "conductive" flux by over 10-fold. Under such conditions photophoresis can significantly augment the deposition rate of micron-sized absorbing particles (Castillo et al., 1990), as shown in Figure 3.

2.3. "Thermal Phoresis" of Asymmetric Particles. In a general sense photophoresis is the result of thermal nonequilibrium between the particle and surrounding gas (via radiative absorption or emission) and an *asymmetry* in the particle–gas heat-transfer process. In "conventional" photophoresis (outlined above) the asymmetry arises from an anisotropic distribution of radiation absorption and results in a "space-fixed" phoretic motion. But, it is also entirely possible for heat-transfer asymmetry to result from an *inherent asymmetry of the particle*, such as nonspherical shape, and/or nonuniform surface properties.

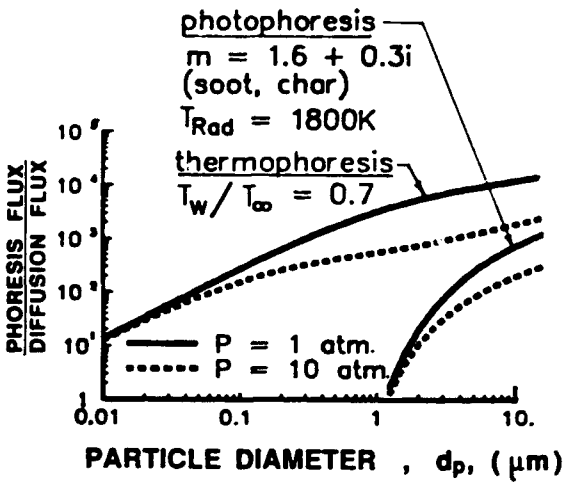

Figure 3. Relative importance of particle mass transport by the mechanisms of *Brownian diffusion* (reference case), *thermo*phoresis, and *photo*phoresis for equal radiative and Fourier energy flux across laminar gaseous boundary layers. Size dependence for absorbing particles. T_∞ = 1000 K, k_g/k_p = 0.1.

Phoresis arising from particle asymmetry will be aligned with respect to the particle, i.e., "body-fixed". Such effects have, indeed, been recently observed in a series of interesting experiments by Rohatschek (1985), who concluded that photophoretic motion of irregularly shaped particles can be 3 or 4 orders of magnitude greater than that predicted for uniform property spherical particles.

Few theoretical investigations of body-fixed photophoresis (BFP) have been published, due, in part, to mathematical difficulties associated with the analysis of nonspherical, nonuniform particles. Rohatschek (1985) presented a free-molecular-limit ($Kn_p \gg 1$) analysis in which the particle was modeled as a perfect sphere but with a nonuniform surface thermal accommodation coefficient. Forces arising from small differences in thermal accommodation were found to be well in excess of those due to nonuniform particle radiation absorption. We recently extended the same model to the near-continuum regime with similar conclusions; i.e., resulting BFP forces greatly exceed space-fixed, conventional photophoretic forces.

One interesting and singular aspect of this sphere-based model is that body- and space-fixed phoretic actions will *not* produce a torque on the particle. Rotation of such a sphere would therefore be due to Brownian action alone, and the resulting BFP motion would be *stochastic* in character. To a fixed observer, the long-time phoretic motion would thus resemble a "diffusion" process. An order-of-magnitude analysis of the "effective" translational diffusion resulting from BFP leads to the expression

$$D_{p,eff} = (v_{BFP})^2/D_{p,rot} \quad (7)$$

where v_{BFP} is the photophoretic velocity and $D_{p,rot}$ the Brownian *rotational* diffusion coefficient. Presented in Figure 4 are near-continuum model predictions for $D_{p,eff}$ (normalized with respect to the gas momentum diffusivity ν_g) vs sphere diameter at several ambient gas temperatures. These results pertain to a difference in thermal accommodation coefficient of only 0.1 between the two halves of the sphere, and particle/gas thermal nonequilibrium resulting from radiative emission from the sphere to a cool environment. Also shown is the "normal" Brownian (translational) diffusion coefficient for a sphere of the same size under the same ambient conditions. Our results indicate that the "effective" diffusion resulting from photophoresis can be several orders of magnitude greater than

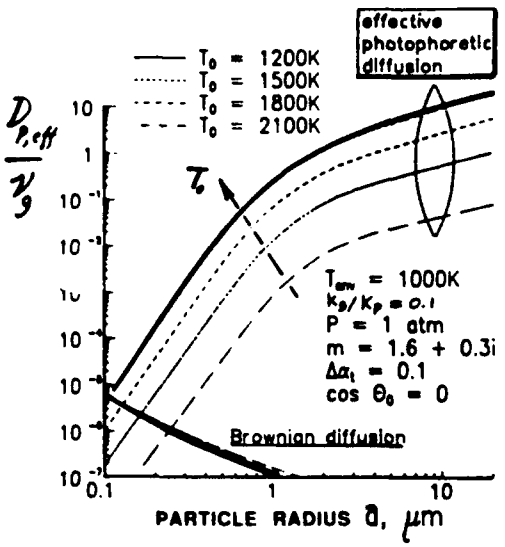

Figure 4. "Effective" particle diffusion coefficient (normalized by gas momentum diffusivity) compared to true Brownian diffusivity; consequences of a 0.1 difference in thermal accommodation coefficient across a spherical particle radiating to an environment at 1000 K.

the radiation-independent Brownian counterpart. Such behavior can have important consequences (section 3) for coagulation and deposition rates of radiation absorbing/emitting "real" particles in high-temperature environments and could also falsify particle size inferences based on the experimental method called "dynamic light scattering".

Analysis of the phoretic behavior of asymmetric-*shaped* particles is considerably more complicated than sphere-based models. As a first step, we recently investigated the behavior of an idealized *two-sphere aggregate* in the near-continuum regime (Mackowski, 1990). In this model each of the two spheres is taken to be completely homogeneous with respect to surface properties and the absorption or emission of radiation. Heat-transfer asymmetry is introduced via differences in properties (i.e., size, thermal conductivity, and/or refractive index) between the two spheres. A semianalytical spherical harmonics-based technique is used to solve the heat conduction- and thermal slip-induced creeping flow equations. Results of this analysis parallel those obtained from the above-mentioned spherical particle/nonuniform accommodation coefficient investigation, in that radiative absorption or emission by the asymmetrical aggregate results in a BFP motion directed along the aggregate axis. In the absence of "external aligning" forces the BFP motion, when combined with inevitable Brownian rotation, will result in an "effective" Brownian (translation) diffusion which can be significantly greater than ordinary Brownian diffusion.

This model also predicts that conventional thermophoresis, due to a temperature gradient in the bulk gas, *will* act to align the axis of the asymmetrical aggregate with the gradient. In so doing the BFP motions become essentially space-fixed and contribute to (or diminish) the thermophoretic velocities—leading to a significant change in the predicted "effective" aggregate thermophoretic diffusivity, $(\alpha_T D)_{p,eff}$. Similar conclusions were reached by Rohatschek (1985) in that space-fixed phoretic forces, while considerably smaller than body-fixed forces, contribute importantly by *aligning* the particles in a particular direction. The phoretic velocity due to aggregate asymmetry may *augment* or sometimes *oppose* the ordinary thermophoretic velocity; e.g., radiative absorption from a hot environment can lead to an overall decrease (even sign reversal) in $(\alpha_T D)_{p,eff}$. Incidentally, our parallel Monte Carlo studies of particulate *deposit microstructure* (Tassopoulos et al., 1989) reveal that the *alignment* of incoming nonspherical particles (relative to $\dot{q}''_F$) will lead to more *anisotropic deposits*.

Currently, we are extending the above-mentioned aggregate model to three or more contacting spheres. These extensions should prove useful because, among other things, they will allow investigation of the transport behavior or particles having no plane or axis of symmetry as well as bridging the wide gap between the properties of small and large "agglomerates" (Mountain et al., 1986; Rosner et al., 1991).

2.4. Effect of Gas/Particle Thermal Nonequilibrium on Coagulation Rates. The previous remarks have interesting consequences for predicting coagulation rates between particles not in local thermal equilibrium with the gas. Several heat-transfer mechanisms act to drive the temperature of a particle above or below the surrounding "transparent" gas, e.g., radiative absorption/emission and heterogeneous chemical reaction. Regardless of the mechanism, energy transfer from/to the particle will perturb the adjacent temperature field and, as a result of thermophoresis, influence encounter rates with neighboring particles. Our analysis (Mackowski et al., 1990a,b; 1991) begins by investigating the thermophoretic attraction (or repulsion) between a pair of particles separated by the distance R. Let $\dot{Q}_i$ (i = 1, 2) denote the net energy transfer rate to each particle i via radiative absorption, emission, etc. Furthermore, we assume that the particles and gas are in a (quasi-) steady state and neglect higher order thermal interactions between the particles. From energy conservation, particle 2 will experience a gas temperature gradient resulting from energy transfer to particle 1 equal to

$$\{dT_g/dx\}_2 = -\dot{Q}_1/(4\pi R^2 k_g) \tag{8}$$

where the direction of the length x is taken to be from particle 1 to particle 2. An equivalent expression is, of course, obtained for the gradient about particle 1 as a result of particle 2, with these results applying in both asymptotic extremes of the particle Knudsen number. Neglecting "hydrodynamic" interactions and inertial effects, we conclude that due to *thermophoresis* the particles will move toward (or away from) each other at the rate

$$v_{T,12} = |(\alpha_T D)_1 \dot{Q}_2 + (\alpha_T D)_2 \dot{Q}_1|/(4\pi R^2 k_g T_0) \tag{9}$$

The motion is *as if* an attractive (or repulsive) force acted between the two particles, of magnitude

$$F_{T,12}\langle R\rangle = v_{T,12}(B_1 + B_2)^{-1} \tag{10}$$

where B_1 and B_2 are the respective particle "mobilities" in the surrounding gas. Introducing this effective thermophoretic force (proportional to R^{-2}), the analysis becomes equivalent to that for coagulation between *electrically charged* particles (Zebel, 1966). Consequently, the ratio, Z, of coagulation rates including thermophoresis to that due to Brownian motion alone can be expressed in the familiar form (cf. eq 14)

$$Z = y/(\exp(y) - 1) \tag{11}$$

where, now

$$y = F_{T,12}\langle R_{12}\rangle R_{12}/(k_B T) \tag{12}$$

and R_{12} is the separation distance at contact (i.e., $a_1 + a_2$). When the particles are cooler than the surrounding gas, the energy transfer rates $\dot{Q}_i$ and the force $F_{T,12}$ are negative and the coagulation "correction" factor Z exceeds unity,

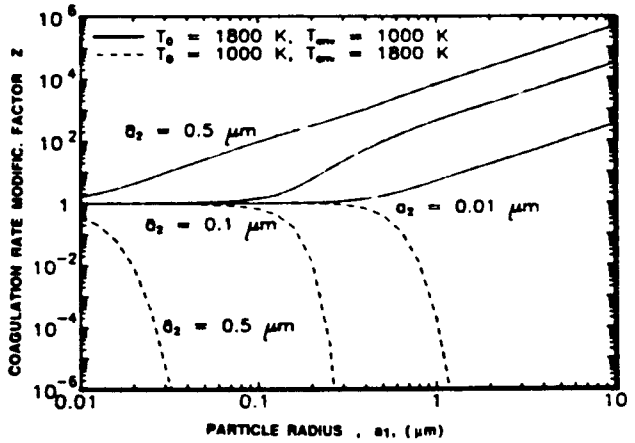

Figure 5. Correction to the Brownian (isothermal) coagulation rate constant due to energy exchange to/from spherical particles of unequal radius (after Mackowski et al. (1990, 1991)).

as expected. Particles hotter than the gas will have a Z-factor less than unity.

Suppose the particles are out of thermal equilibrium with the local gas due to radiative absorption or emission, and radiate from (about) the local gas temperature to a background environment of temperature T_{env}. Then the above-mentioned heat source for either particle will be

$$\dot{Q}_i = 4\pi a_i^2 \sigma_B |\alpha_i T_{env}^4 - \epsilon_i T_0^4| \qquad (13)$$

where ϵ_i and α_i are the particle emittance and absorptance, respectively, estimated from Lorentz–Mie theory at the corresponding radiation emission and absorption temperatures.

A plot illustrating the anticipated effect of radiative heating or cooling on particle coagulation rates is given in Figure 5, in which the coagulation factor Z is given as a function of the two radii, a_1 and a_2. The temperatures T_0 and T_{env} are 1800 and 1000 K (and reversed), and the particle refractive index was taken to be $m = 1.6 + 0.3i$, representative of carbonaceous soot. For radiation *cooling*, this effect leads to preferential growth of large particles via "scavenging" of small particles. The growth of radiatively *heated* particles, on the other hand, is essentially "frozen" for supermicron particle radii (see section 3.3 and Mackowski et al. (1990a,b, 1991) for the startling consequences for PSD evolution. Clearly, similar PSD consequences would follow from the use of the Zebel-corrected Brownian rate constant for unipolar *charged* aerosols, a topic outside of the scope of the present paper).

3. Some Engineering Consequences

The "phoretic" phenomena and "effective" Brownian diffusivities described in section 2 have important consequences in high-temperature "dusty gas" applications, some of which are briefly considered below.

3.1. Fine Particle Deposition Rates on Heat-Exchanger Surfaces. At sufficiently subcritical Stokes numbers (see, e.g., Fernandez de la Mora and Rosner, 1981, Konstandopoulos and Rosner, 1991) particle Brownian diffusion across a thin convective diffusion boundary layer would normally govern local particle deposition rates in nearly isothermal systems (see, e.g., Friedlander, 1977). But in *nonisothermal* forced convection systems with nearly constant thermophysical properties, the order of magnitude of the ratio of the thermophoretic deposition rate to the ordinary convective-Brownian diffusion rate is set by the dimensionless ratio

$$-B_T = (\alpha_T)_p[(T_e - T_w)/T_w][Nu_h(Re,Pr)/Nu_m(Re,Sc)] \qquad (14)$$

where $(\alpha_T)_p$ is the above-mentioned (dimensionless) thermophoretic factor, and the indicated Nu-functions are the corresponding *Nusselt numbers* (*dimensionless coefficients*) for *heat* and *mass transfer*. More generally, Rosner (1980) has shown that $-B_T$ plays the role of a dimensionless "suction" Peclet number, i.e., $v_{T,w}\delta_m/D_p$, with total deposition rates in the presence of heat transfer being augmented by the familiar approximate factor

$$B_T/[\exp\langle B_T\rangle - 1] \qquad (15)$$

For the most commonly encountered systems (with $D_p \ll \nu_{g,e}$) this convenient result is known to overestimate particle deposition rates to cooled solid surfaces by a factor (called F(outer sink) by Rosner (1980) and Gokoglu and Rosner (1984)) equal to the steady-state reduction in particle mass fraction across the thermal boundary layer (smaller than unity but larger than T_w/T_e. Correlations of F(outer sink) can be obtained from the results of Goren (1977), Gokoglu and Rosner (1984, 1986a,b), Batchelor and Shen (1985) and Shen (1985) for *laminar* boundary layers, and Rosner and Fernandez de la Mora (1984) for *turbulent* boundary layers. Noting that, frequently, $Nu_h/Nu_m \sim (Pr/Sc)^{1/3}$, eq 14 can be rewritten in the form

$$-B_T = |(\alpha_T D)_p/\nu_g|[(T_e - T_w)/T_w](Pr)^{1/3}(Sc)^{2/3} \qquad (16)$$

But, since $(\alpha_T D)_p/\nu_g$ and $(Pr)^{1/3}$ are frequently of order unity (cf. eq 2, when $Kn_p \gg 1$), one sees that the magnitude of $-B_T$ is often set by the product $(\Delta T/T_w)(Sc)^{2/3}$, which can be quite large even for submicron particles (e.g., for $d_p = 1$ μm at $p = 1$ atm in 1500 K "air" $Sc = 3 \times 10^6$, so that $(Sc)^{2/3} = 2 \times 10^4$). Indeed, in the experiments of Rosner and Kim (1984) (deposition of ca. 0.7-μm MgO(s) particles from seeded combustion gases to Pt ribbons at $T_w/T_e = 0.7$ *and modest* Reynolds numbers) actual (thermophoretically enhanced) particle deposition rates were found to be over 10^3 times those expected in the corresponding isothermal flow (see, also, Figure 3). It is also significant that absolute soot particle deposition rates of Rosner and Kim (1984), Eisner and Rosner (1985, 1986), and, recently, Makel and Kennedy (1991), as well as "dust-free zone thicknesses" observed near laminar diffusion flame "sheets" (Gomez and Rosner, 1992; see, also, section 3.4 below), are consistent with kinetic theory predictions of $(\alpha_T D)_p$ for single spheres (see eq 2 and Waldmann (1961)) even though it is well established that the particles in such flames are comprised of large numbers of small quasi-spherical "primary" particles bound together (see, e.g., Megaridis and Dobbins, 1990). The explanation for this interesting apparent paradox appears to be that, while the Brownian diffusivity and drag properties of aggregates are quite sensitive to aggregate size (e.g., radius of gyration) and morphology, the orientation-averaged thermophoretic diffusivity, $\langle(\alpha_T D)_p\rangle$, is remarkably *insensitive* to aggregate size and morphology in either the free-molecule or continuum regime (Rosner et al., 1991), a phenomenon which facilitates engineering calculations of total deposition rates and makes "thermophoretic particle sampling" (see, e.g., Dobbins and Megaridis, 1987) particularly attractive.

It should also be remarked that further rate enhancements are expected in "cold-wall" systems with *nonnegligible mainstream particle mass loading* (as in the deposition of optical waveguide "pre-forms" (Rosner and Park, 1988; Park and Rosner, 1989a–c)). Moreover, one expects that the microstructure (and hence microstructure-sensitive properties like the effective thermal conductivity tensor) of such deposits will be different from those grown by ordinary convective diffusion (see, e.g.,

Tassopoulos et al., 1989). This will influence the thermal resistance growth rate, of decisive interest in "fouling" situations (Marner, 1989).

3.2. Hot Dusty Gas "Cleanup": Scavenging of Fine Particles by an Evaporating Droplet. Dust-laden gases are said to be "scrubbed" clean when they are "contacted" by a spray whose droplets capture the suspended dust and concentrate the particulate solids in an effluent slurry. Most discussions and measurements of the performance of *wet scrubbers* (see, e.g., Cooper, 1982; Hidy, 1984) focus on the *inertial capture* of supermicron dust particles which "impact" upon the (much larger) moving droplets—a mechanism only weakly influenced by the energy fluxes necessarily associated with droplet evaporation. In view of the considerations of section 2.1, it is of interest to ask to what extent the *heat* transfer associated with droplet evaporation accelerates the capture of *submicron* dust, i.e., "respirable" dust particles too small to be captured by the mechanism of inertial impaction. The situation has some similarities to that discussed in section 3.1 but with one important distinction, viz., whereas section 3.1 dealt implicitly with an *internally* cooled solid surface, we are now (in the case of each droplet) dealing with an *evaporatively cooled* surface undergoing outward vapor mass transfer. Thus, whereas the temperature gradient associated with the gas supplying the latent heat of evaporation tends to thermophoretically draw small suspended particles into the droplet, the radial outflow of vapor (Stefan flow) tends to "convect" the particles away. The following simple analysis establishes the conditions under which thermophoretic particle capture occurs and predicts the rate of this capture per droplet. While a more general analysis is possible, we limit ourselves here to the simplest case of negligible particle Brownian diffusion, small particle mass loadings ($\omega_p \ll 1$) and negligible "slip" between the local gas and the droplet ($Re^{1/2} \ll 1$). For further details and discussion, see Rosner and Mackowski (1992).

If one considers a quasi-steady evaporating sphere, then the mass flow rates $\dot{m}''_p(4\pi r^2)$ and $\dot{m}''_v(4\pi r^2)$, and the radial energy flow rate $\dot{q}''_F(4\pi r^2)$ are independent of radius, r, where $\dot{q}''_F$ ($=k_g(-\text{grad } T)$) is the local Fourier heat flux and the subscripts p and v refer to suspended particles and vapor, respectively. The Fourier flux at the vapor/liquid interface supplies the required latent heat of evaporation, L (actually, eq 17 below is valid under QS-transient conditions, in which case the effective value L_{eff} ($\equiv(-\dot{q}''_F/\dot{m}''_v)_w$) is the true latent heat L, *plus a contribution associated with droplet heatup*), linking $-\dot{q}''_F$ and $\dot{m}''_v$, but $-\dot{q}''_F$ is also linked to the particle thermophoretic flux $\dot{m}''_p$ via eq 1. Combining these interrelations, and eliminating the energy flux, leads to a remarkably simple and interesting result (Rosner and Mackowski, 1992):

$$-\dot{m}_p = \dot{m}_v\omega_p\left\{\frac{(\alpha_T Le)_p}{Le_v}\frac{L_{eff}}{c_pT} - 1\right\} \tag{17}$$

linking the fine *particle* capture rate $-\dot{m}_p$ with the prevailing single *droplet* evaporation rate $\dot{m}_v$. In the bracketed term appears the thermophoretic diffusivity ratio $\alpha_T Le_p$ displayed in Figure 1, and the more familiar Lewis number for vapor diffusion $D_v/(k/\rho c_p)_{air}$, which is quite near unity (e.g., for water vapor in air). It is interesting that for the bracketed term to be positive the ambient temperature cannot exceed a readily calculated threshold (ca. 900 K for a water droplet collecting submicron particles from ordinary combustion products). For process gas conditions above this threshold, the Stefan flow associated with droplet evaporation prevents the thermophoretic scavenging of dust particles, but much below this threshold ambient temperature droplets will be "surprisingly" effective in removing small suspended particles (in accord with eq 17), far exceeding the performance expected based on fine particle capture by Brownian diffusion alone. Also, below this threshold gas temperature, particles larger than some "cutoff diameter" (obtained via Figure 1, by setting the bracketed term in eq 17 equal to zero) will not be scavenged in this manner. Incidentally, by integrating both sides of eq 17 over the total evaporative lifetime of a droplet, the bracketed factor, which above plays the role of a *discriminant*, can also be shown to be interpretable as the *ratio of the actual total number of particles captured during the evaporative lifetime of an individual motionless droplet to the number of particles initially contained in the volume required to accommodate the initial droplet mass if the droplet density were reduced to the ambient gas density.* Further interesting corollaries of eq 17 will be found in Rosner and Mackowski (1992).

3.3. Coagulation Dynamics of a Population of Unequal Temperature Spherical Particles. To demonstrate the effect of gas/particle thermal nonequilibrium on the evolution of a particle size distribution (PSD), we consider an aerosol comprised of spherical particles (of volume v) evolving due to coagulation only. In this case the PSD $n(v,t) \equiv dN_p/dv$ obeys the integro-differential equation (see, e.g., Friedlander, 1977)

$$\partial n(v,t)/\partial t = (1/2)\int_0^v Z(v,u)\,\beta(v,u)\,n(v-u)\,n(u)\,du - n(v)\int_0^\infty Z(v,u)\,\beta(v,u)\,n(u)\,du \tag{18}$$

where we have introduced Z, the above-mentioned correction factor for thermophoretic scavenging/repulsion (eq 11) and $\beta(v_i,v_j)$ is the coagulation rate constant due to ordinary Brownian coagulation. To account for coagulation in the transition regime, we simply use the "harmonic average approximation" for the collision kernel (see, e.g. Pratsinis, 1988; Rosner and Tassopoulos, 1989), viz., $\beta = \beta_{FM}\beta_C/(\beta_{FM} + \beta_C)$, where β_{FM} and β_C are the coagulation rate constants ("kernels") in the free-molecule and continuum regimes, respectively. The three lowest integral moments of eq 18 satisfy the well-known ODEs (see, e.g., Cohen and Vaughn, 1971)

$$dM_0/dt = -(1/2)\int_0^\infty\int_0^\infty Z(v,u)\,\beta(v,u)\,n(v)\,n(u)\,dv\,du \tag{19}$$

$$dM_1/dt = 0 \tag{20}$$

$$dM_2/dt = \int_0^\infty\int_0^\infty Z(v,u)\,\beta(v,u)\,n(v)\,n(u)\,vu\,dv\,du \tag{21}$$

Here M_k is the kth moment of the distribution defined by

$$M_k \equiv \int_0^\infty v^k n(v)\,dv = M_0 v_g^k \exp((k^2/2)\ln^2\sigma_g) \tag{22}$$

where the second equality in eq 22 is a useful property of "log-normal" distributions. Note that the zeroth and first moments of the PSD correspond, physically, to the total particle *number density*, N_p, and the total particle *volume fraction*, ϕ_p, respectively. In situations for which the PSD *shape* remains "log-normal", eqs 19–21 become a closed set of coupled ODEs (see, also, Rosner and Tassopoulos, 1991), used below to predict the effects of thermophoresis on aerosol population evolution.

In Figure 6 we plot the PSD *standard deviation*, σ_g, and mean particle diameter (corresponding to the median of the log-normal PSD) vs dimensionless time $\tau \sim N_{p,0}t$ (see the Nomenclature section) where the evolution occurs from an initial PSD characterized by $\sigma_g(0) = 3.0$ and $d_g(0) = 0.01$ μm. The curves labeled 1 correspond to the isothermal

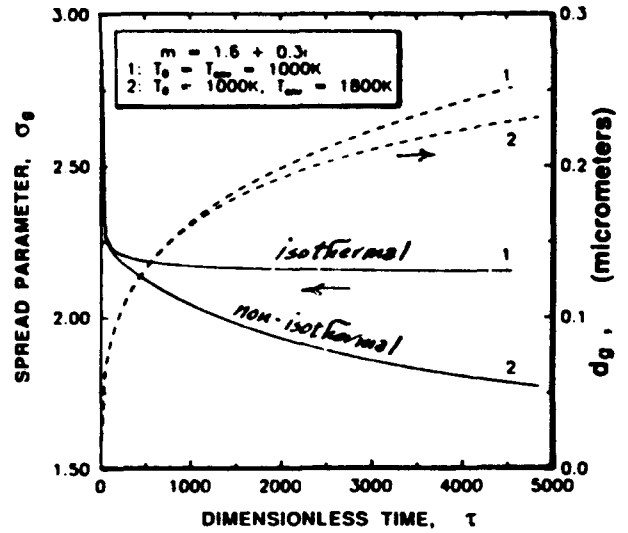

Figure 6. Energy-transfer effects on the evolution of a log-normal population of unequal temperature ("overheated") spherical particles; time dependence of population "spread" and mean particle diameter (after Mackowski et al. (1990a,b, 1991)).

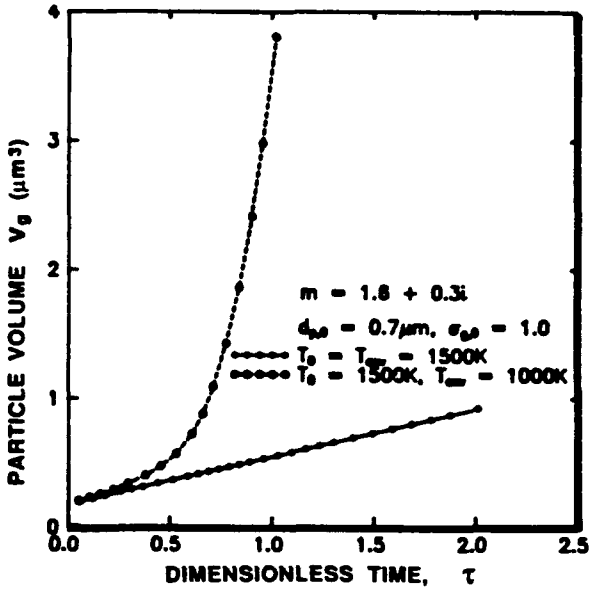

Figure 7. Energy-transfer effects on the evolution of an initially monodisperse population of "undercooled" spherical particles; time dependence of mean particle diameter (after Mackowski et al. (1990a,b)).

case (particle encounters due only to Brownian motion) while curves labeled 2 correspond to the case of "overheated" particles. Note that in the isothermal case the population *spread* (solid curve 1) eventually reaches a constant value corresponding to a "self-preserving" distribution (see, e.g., Lee, 1983). In the case *with* heat transfer "the larger the particles, the larger the repulsive forces", so small particles in the population tend to "catch up" with the larger ones, resulting in a *narrower* PSD with a smaller mean size (dashed curve 2). In view of the above-mentioned fact that electrostatic repulsion and "thermal repulsion" lead to interparticle collision rate laws of identical form (cf. eq 11), this PSD "sharpening" (or "focusing" in size space) should also be observed in the coagulation of unipolar aerosols. In either case the ability to obtain narrower distributions than those ordinarily associated with Brownian coagulation may prove to be useful in the controlled synthesis of fine particles (section 4). Cases involving "undercooled" particles ($T_p < T_g$) may also be of considerable practical interest (Mackowski et al., 1990a,b; 1991), but they require a more general treatment due to significant departures from the single-mode log-normal PSD-shape assumption. We have recently employed a discretized population balance ("sectional") method based on the work of Hounslow et al. (1988) to examine the behavior of radiation-cooled particle populations (Mackowski et al., 1990a,b, 1991). In Figure 7 we show the evolution of the population median particle volume vs dimensionless time for an initially monodisperse aerosol coagulating under isothermal (solid line) and undercooled (dashed line) conditions. After a short "induction" period, after which particle sizes become disparate enough so that thermophoretic forces dominate (see, also, Figure 5), the larger particles grow at significantly higher rates, thus appreciably increasing the population average size.

3.4. Thermophoretic Gas Cleaners. When the "target" surface is *hotter* than the dusty gas stream (i.e., when $T_w > T_g$), the incoming particles are thermally "repelled" and the associated thermophoretic "suction" parameter, $-B_T$, changes sign. This implies dramatically *reduced* particle deposition rates on "overheated" surfaces, and in the limit of negligible inertia and Brownian diffusion, this can bring about a nearly "dust-free" zone in the immediate vicinity of the surface (see, e.g., Friedlander, 1977; Gokoglu and Rosner, 1986a,b; Friedlander et al., 1988; Strattmann et al., 1988; Park and Rosner, 1987). This can be exploited in many ways as, for example, in a continuous "thermophoretic gas cleaner". Thus, if the gas in the "dust-free" zone is continuously "skimmed off", it can be conveyed to dust-sensitive equipment (e.g., a combustion turbine) whereas the remaining gas will, of course, be dust-enriched. Some of the properties of an axisymmetric laminar stagnation flow "hot-wall" configuration, including the effects of high particle mass loading and intermediate Reynolds number, are computed in Park and Rosner (1987, 1989a–c). In effect, of course, this is the same phenomenon which acts to "shut off" the further *coagulation* of "large" overheated particles, as described above (section 3.3).

4. Conclusions and Recommendations

From the representative examples discussed in section 3 and the references cited therein, we conclude that in the presence of radiative and/or diffusive (Fourier) energy transfer small suspended particles in a gas experience unbalanced forces which cause them to drift, usually (but not always) in the direction of the local energy flux. This "phoresis" can cause dramatic changes in the rates at which fine suspended particles are deposited (section 3.1) or scavenged (section 3.2), as well as the rates at which unequal temperature particles coagulate among themselves (section 3.3). Particularly interesting and not yet explored in depth are the phenomena predicted here for unsymmetrical particles in the presence of a heat flux (section 2.3), e.g., unequal sphere agglomerates, which should exhibit "anomalous" thermophoretic coefficients and "effective" Brownian diffusivities, in addition to a tendency to "align" themselves in the direction of the energy flux. Such phenomena, several of which are being experimentally studied in our (HTCRE) laboratory, will inevitably have important implications for the morphology of agglomerates suspended in gases, the deposition (capture) rates of single particles and agglomerates, and the microstructure (hence thermal properties) of resulting deposits.

Because of the particle mass transport mechanisms described here, well-documented methods which have been

successfully used to predict or correlate coagulation and deposition rates in "dusty gas" systems *without* appreciable heat transfer can*not* be straightforwardly applied to situations with appreciable radiative and/or diffusive energy fluxes. Conversely, *by imposing suitable energy fluxes, many of these phenomena can be creatively exploited to improve the performance of devices intended to produce or separate fine particulate matter in/from flowing gases.* We hope that the present contribution will stimulate advances along these lines.

Acknowledgment

It is a pleasure to acknowledge the financial support of DOE-PETC (under Grants DE-FG22-86PC90756 and DE-FG22-90PC90099) and the US AFOSR (under Grant AFOSR 91-0170), as well as the related support of the Yale HTCRE Laboratory by our Industrial Affiliates: Shell, General Electric Co., Du Pont, Union Carbide, and SCM-Chemicals. We have also benefited from the perceptive comments of R. A. Dobbins, A. G. Konstandopoulos, C. Megaridis, J. Fernandez de la Mora, S. Furstenau, M. Sitarski, and A. Gomez. This paper is dedicated to Stuart W. Churchill, whose cumulative research and teaching has strengthened considerably the ability of chemical engineers to predict, rationally correlate, and exploit convective heat transfer. It was presented at the (S. W. Churchill Birthday) Symposium: Advances in Rate Processes, AIChE 1990 National Meeting, Nov 12, 1990, Chicago, IL. Preliminary accounts of portions of this paper were presented as Poster OPF II-18 at the 9th (Intersociety) International Heat Transfer Conference, Jerusalem, Israel, Aug 23, 1990, and as Paper 173, Session 6E.1 at the Annual Meeting of the American Association for Aerosol Research (AAAR), Philadelphia PA, June 18–22, 1990. This manuscript was transmitted on September 25, 1990 to Dr. John Chen to be part of the symposium issue in honor of Dr. Stuart Churchill.

Nomenclature

a = spherical particle radius
$-B_T$ = thermophoretic "suction" parameter, eq 14
B_i = mobility of particle i in the prevailing gas, eq 10
C_c = Cunningham–Millikan correction to Stokes drag
c_{mom} = momentum (tangential) exchange coefficient
c_t = thermal exchange coefficient (gas/solid)
c_p = specific heat of carrier gas
d = diameter
F_{12} = effective interparticle force
J_1 = photophoretic radiative asymmetry factor
J_1 = wavelength integrated photophoretic radiative asymmetry factor
k = Fourier thermal conductivity
k_B = Boltzmann constant
k = imaginary part of complex number m
Kn = Knudsen number (based on l_g and particle diameter)
L = latent heat of vaporization
Le = Lewis number (Fick/thermal diffusivity ratio)
l_g = gas mean free path
M_k = kth moment of aerosol PSD $n(v,t)$; eq 22
m = complex index of refraction of particle
n = real part of m
n = PSD function (of v); $n \equiv dN_p/dv$
N_p = total particle number density ($=M_0$)
Nu_h = heat-transfer Nusselt number
Nu_m = mass-transfer Nusselt number
$\dot{Q}'''$ = radiative energy absorption rate/volume
$\dot{Q}_i$ = net heat source for particle i
$\dot{\mathbf{q}}''_F$ = Fourier energy flux vector
$\dot{\mathbf{q}}''_R$ = radiative energy flux vector
p = pressure
Pr = Prandtl number of gas mixture (momentum-/thermal-diffusivity ratio)
R = center-to-center distance between two spheres
r = radius measured from center of spherical particle or droplet
Re = Reynolds number
Sc = Schmidt number, ν/D_p(Brownian)
T_e = temperature at outer edge of thermal "boundary layer"
T_w = surface temperature at gas/solid interface
T_∞ = temperature far from surface ("upstream infinity")
$\mathbf{v}_T$ = particle thermophoretic velocity
$\mathbf{v}_P$ = particle photophoretic velocity
v = particle volume (treated as a continuous variable)
x = radiative size parameter, $\pi d_p/\lambda$
x = distance between particle 1 and particle 2 (section 2.4)
y = dimensionless thermophoretic "potential"
Z = correction to the Brownian coagulation rate constant

Greek Symbols

α = absorptivity
α_T = thermophoretic diffusion factor
α_{mom} = momentum accommodation factor
β = coagulation rate constant, eq 18
δ = boundary layer thickness
ϵ = emittance
ϕ_p = aerosol particle volume fraction
μ = dynamic viscosity of host gas
ν_g = momentum diffusivity (kinematic viscosity)
ω_p = particle mass fraction in mixture
ρ = mass density
τ = dimensionless time (proportional to $N_{p,0}t$)
σ_g = standard deviation of log-normal PSD
σ_B = Stefan–Boltzmann radiation constant

Subscripts

BFP = body-fixed phoresis
eff = effective
env = environment (radiative)
g = gas
h = heat transfer
i = particle i
k = moment index (k = 0, 1, 2, ...)
m = mass transfer
p = associated with particle (dimension)
rot = rotational
v = vapor
w = evaluated at the gas/target interface
∞ = evaluated far from the target

Abbreviations

BFP = body-fixed phoresis
C = continuum
FM = free molecule
ODE = ordinary differential equation
OWG = optical waveguide
P = photophoretic
PSD = particle size distribution
QS = quasi-steady
T = thermophoretic

Literature Cited

Batchelor, G. K.; Shen, C. J. Thermophoretic Deposition of Particles in Gas Flowing Over Cold Surfaces. *J. Colloid Interface Sci.* **1985**, *107*, 21-37.

Brock, J. R. On the Theory of Thermal Forces Acting on Aerosol Particles. *J. Colloid Sci.* **1962**, *17*, 768-780.

Buckley, R. L.; Loyolka, S. K. Cunningham Correction Factor and Accommodation Factor: Interpretation of Millikan's Data. *J. Aerosol Sci.* **1989**, *20* (3), 347-349.

Castillo, J.; Mackowski, D. W.; Rosner, D. E. Photophoretic Contribution to the Transport of Absorbing Particles Across Com-

bustion Gas Boundary Layers. *Prog. Energy Combust. Sci.* **1990**, *16*, 253-260.

Cohen, E. R.; Vaughn, E. U. Approximate Solutions of the Equations for Aerosol Agglomeration. *J. Colloid Sci.* **1971**, *35*, 612-623.

Cooper, D. W. *Handbook of Multiphase Systems*; Hemisphere: Washington, DC, 1982; Section 9.2.2, pp 9-16 to 9-41.

Dobbins, R. A.; Megaridis, C. M. Morphology of Flame-Generated Soot as Determined by Thermophoretic Sampling. *Langmuir* **1987**, *3*, 254-259.

Einstein, A. *Investigations on the Theory of the Brownian Motion* (reprinted by Dover Press: New York, 1956); 1926.

Eisner, A. D.; Rosner, D. E. Experimental Studies of Soot Particle Thermophoresis in Non-Isothermal Combustion Gases Using Thermocouple Response Techniques. *Combust. Flame* **1985**, *61*, 153-166.

Eisner, A. D.; Rosner, D. E. Experimental and Theoretical Studies of Submicron Particle Thermophoresis in Combustion Gases. *PCH, PhysicoChem Hydrodyn.* **1986**, *7*, (2/3), 91-100.

Fernandez de la Mora, J.; Rosner, D. E. Inertial Deposition of Particles Revisited and Extended; Eulerian Approach to a Traditionally Lagrangian Problem. *PCH, PhysicoChem Hydrodyn.* **1981**, *2*, 1-21.

Flagan, R.; Friedlander, S. K. In *Recent Developments in Aerosol Science*; Davis, J., Ed.; 1978.

Flagan, R. K.; Seinfeld, J. H. *Fundamentals of Air Pollution Engineering*; Prentice-Hall: Englewood Cliffs, NJ, 1988.

Friedlander, S. K. *Smoke, Dust and Haze*; Wiley: New York, 1977.

Friedlander, S. K.; Fernandez de la Mora, J.; Gokoglu, S. A. Diffusive Leakage of Small Particles Across the Dust-Free Layer Near a Hot Wall. *J. Colloid Interface Sci.* **1988**, *125*, 351-355.

Fuchs, N. A. *The Mechanics of Aerosols*; Pergamon: Oxford, England, 1964 (Reprinted 1989 by Dover Press: New York; Paperback 0-486-66055-9).

Garcia-Ybarra, P.; Rosner, D. E. Thermophoretic Properties of Nonspherical Particles and Large Molecules. *AIChE J.* **1989**, *35*, 139-147.

Gokoglu, S. A.; Rosner, D. E. Correlation of Thermophoretically-Modified Small Particle Diffusional Deposition Rates in Forced Convection Systems with Variable Properties, Transpiration Cooling and/or Viscous Dissipation. *Int. J. Heat Mass Transfer* **1984**, *27*, 639-645.

Gokoglu, S. A.; Rosner, D. E. Prediction and Rational Correlation of Thermophoretically Reduced Particle Mass Transfer to Hot Surfaces Across Laminar or Turbulent Forced-Convection Gas Boundary Layers. *Chem. Eng. Commun.* **1986a**, *44*, 107-119.

Gokoglu, S. A.; Rosner, D. E. Thermophoretically-Augmented Forced Convection Mass Transfer Rates to Solid Walls Across Non-Isothermal Laminar Boundary Layers. *AIAA J.* **1986b**, *24* (1), 172-179.

Gomez, A.; Rosner, D. E. Thermophoretic Effects on Particles in Counterflow Laminar Diffusion Flames. Manuscript in preparation, 1992 (based on paper 26f, 1987 AIChE Annual Meeting, New York).

Goren, S. L. Thermophoresis of Aerosol Particles in the Laminar Boundary Layer on a Flat Plate. *J. Colloid Interface Sci.* **1977**, *61*, 77-85.

Hidy, G. *Aerosols—an Industrial and Environmental Science*; Academic: Orlando, FL, 1984.

Hounslow, M. J.; Ryall, R. L.; Marshall, V. R. A Discretized Population Balance for Nucleation, Growth and Aggregation. *AIChE J.* **1988**, *34* (11), 1821-1832.

Konstandopoulos, A.; Rosner, D. E. Inertial Effects on Thermophoretic Transport of Small Particles to Walls with Streamwise Curvature—I. Theory. II. Experiment. *Int. J. Heat Mass Transfer* **1991**. Submitted for publication.

Lee, K. W. Change of Particle Size Distribution During Brownian Coagulation. *J. Colloid Interface Sci.* **1983**, *92*, 315-326.

Mackowski, D. W. Photophoresis of Aerosol Particles in the Free-Molecular and "Slip-Flow" Regimes. *Int. J. Heat Mass Transfer* **1989**, *32* (5), 843-854.

Mackowski, D. W. Phoretic Behavior of Asymmetric Particles in Thermal Nonequilibrium with the Gas: Two-Sphere Aggregates. *J. Colloid Interface Sci.* **1990**, *140* (1), 138-157.

Mackowski, D. W.; Rosner, D. E.; Tassopoulos, M. Coagulation Rates and Evolution of Populations of Unequal Temperature Particles. Presented at Session 6E.1 Annual Meeting of *American Association for Aerosol Research*, Philadelphia, PA, June 18-22, 1990a; paper 173.

Mackowski, D. W.; Tassopoulos, M.; Rosner, D. E. Coagulation Dynamics of Populations of Unequal Temperature Particles. Presented at the session on Aerosol Preparation of Ceramic Precursor Powders, AIChE 1990 Annual Meeting, Chicago, IL, Nov 15, 1990b, paper 213c.

Mackowski, D. W.; Tassopoulos, M.; Rosner, D. E. Effect of Radiative Heat Transfer on the Coagulation Rates of Combustion-Generated Particulates. Presented at the Central States Section Meeting/The Combustion Institute, Nashville, TN, April 21-24, 1991; expanded version prepared for submission to *J. Aerosol Sci.*

Makel, D. B.; Kennedy, I. M. Experimental and Numerical Investigation of Soot Deposition in Laminar Stagnation Point Boundary Layers. *Proceedings of the 23rd International Combustion Symposium*; The Combustion Institute: Pittsburgh, PA, 1991; pp 1551-1557.

Marner, W. J. Progress in Gas-Side Fouling of Heat Transfer Surfaces. In *Proceedings of the A. L. London Symposium on Compact Heat Exchanges*; Hemisphere: Washington, DC, 1989; pp 421-489.

Megaridis, C. M.; Dobbins, R. A. Morphological Description of Flame-Generated Materials. *Combust. Sci. Technol.* **1990**, *71*, 95-109.

Mountain, R. D.; Baum, H.; Mulholland, G. W. Simulation of Aerosol Agglomeration in the Free Molecular and Continuum Flow Regimes. *J. Colloid Interface Sci.* **1986**, *114* (1), 67.

Park, H. M.; Rosner, D. E. "Thermophoretically Induced Phase-Separation in Highly Mass-Loaded "Dusty" Gas Mixtures"; Yale HTCRE Laboratory Publication No. 162, May 1987.

Park, H. M.; Rosner, D. E. Combined Inertial and Thermophoretic Effects on Particle Deposition Rates in Highly Loaded Dusty-Gas Systems. *Chem. Eng. Sci.* **1989a**, *44* (10), 2233-2244.

Park, H. M.; Rosner, D. E. Boundary Layer Coagulation Effects on the Size Distribution of Thermophoretically Deposited Particles. *Chem. Eng. Sci.* **1989b**, *44* (10), 2225-2231.

Park, H. M.; Rosner, D. E. Dopant Redistribution Across Aerosol-laden Laminar Nonisothermal Boundary Layers. *Chem. Eng. Sci.* **1989c**, *44* (3), 603-617.

Pratsinis, S. Simultaneous Nucleation, Condensation and Coagulation in Aerosol Reactors. *J. Colloid Interface Sci.* **1988**, *124* (2), 416-427.

Rohatschek, H. Direction, Magnitude and Causes of Photophoretic Forces. *J. Aerosol Sci.* **1985**, *16*, 29.

Rosner, D. E. Thermal (Soret) Diffusion Effects on Interfacial Mass Transport Rates. *PCH, PhysicoChem. Hydrodyn.* **1980**, *1*, 159-185.

Rosner, D. E. *Transport Processes in Chemically Reacting Flow Systems*; Butterworths-Heinemann: Stoneham, MA, 1986 (third printing, 1990).

Rosner, D. E. Mass Transfer Across Combustion Gas Thermal Boundary Layers—Power Production and Materials Processing Implications. In *Heat Transfer in Fire and Combustion Systems*; ASME HTD No. 45, 1987; pp 3-8.

Rosner, D. E. Total Mass Deposition Rates from "Polydispersed" Aerosols. *AIChE J.* **1989a**, *35*, 1761-1763.

Rosner, D. E. Side-wall Gas "Creep" and "Thermal Stress Convection" in Microgravity Experiments on Film Growth by Vapor Transport. *Phys. Fluids A—Fluid Mech.* **1989b**, *1* (11), 1761-1763.

Rosner, D. E.; Fernandez de la Mora, J. Small Particle Transport Across Turbulent Non-Isothermal Boundary Layers. *ASME Trans.—J. Eng. Power* **1982**, *104*, 885-894.

Rosner, D. E.; Kim, S. S. Optical Experiments on Thermophoretically Augmented Submicron Particle Deposition from "Dusty" High Temperature Gas Flows. *Chem. Eng. J.* **1984**, *29*, 147-157.

Rosner, D. E.; Park, H. M. Thermophoretically Augmented Mass, Momentum and Energy Transfer Rates in High Particle Mass-Loaded Laminar Forced Convection Systems. *Chem. Eng. Sci.* **1988**, *43* (10), 2689-2704.

Rosner, D. E.; Tassopoulos, M. Deposition Rates from "Polydispersed" Particle Populations of Arbitrary Spread. *AIChE J.* **1989**, *35*, 1497-1508.

Rosner, D. E.; Tassopoulos, M. Correction for Sampling Errors Due to Coagulation and Wall Losses in Laminar and Turbulent Tube Flow: Direct Solution of Canonical "Inverse" Problem for Log-Normal Size Distributions. *J. Aerosol Sci.* **1991**, *22* (7), 843-867.

Rosner, D. E.; Mackowski, D. W. Fine Particle Scavenging by Evaporating Droplets: Implications for Wet Scrubber Performance. Manuscript in preparation, 1992.

Rosner, D. E.; Mackowski, D. W.; Garcia-Ybarra, P. Size- and Structure-Insensitivity of the Thermophoretic Transport of Aggregated "Soot" Particles in Gases. *Combust. Sci. Technol.* **1991**, *80* (1-3), 87-101.

Shen, C. Thermophoretic Deposition of Particles Onto Cold Surfaces of Bodies in Two-Dimensional and Axisymmetric Flows. *J. Colloid Interface Sci.* **1985**, *127* (1), 104–115.
Stratmann, F.; Fissan, H.; Papperger, A.; Friedlander, S. K. Suppression of Particle Deposition to Surfaces by the Thermophoretic Force. *Aerosol Sci. Technol.* **1988**, *9*, 115–121.
Talbot, L. Thermophoresis—A Review. In *Rarefied Gas Dynamics, Part I*; Fisher, S. S., Ed.; Progress in Astronautics and Aeronautics 74; AIAA: New York, 1981; pp 467–488.
Tassopoulos, M.; O'Brien, J.; Rosner, D. E. Simulation of Microstructure/Mechanism Relationships in Particle Deposition. *AIChE J.* **1989**, *35*, 967–980.
Viskanta, R.; Menguc, M. P. *Prog. Energy Combust. Sci.* **1987**, *13*, 97–160.
Waldmann, L. in *Rarefied Gas Dynamics*; Talbot, L., Ed.; Academic: New York, 1961; p 323.
Whytlaw-Gray, R.; Patterson, H. S. *Smoke*; Arnold: London, 1932.
Yalamov, Yu. I.; Kutukov, V. B.; Shchukin, E. R. *J. Colloid Interface Sci.* **1976**, *57*, 564–571.
Zebel, G. Coagulation of Aerosols. In *Aerosol Science*; Davies, C. N., Ed.; Academic: New York, 1966; pp 31–58.

Received for review July 25, 1991
Accepted December 12, 1991

HIGH TEMPERATURE CHEMICAL REACTION ENGINEERING LABORATORY
YALE UNIVERSITY
BOX 2159, YALE STATION
NEW HAVEN, CONNECTICUT 06520 U.S.A.

J. Aerosol Sci., Vol 22, No. 7, pp 843 867, 1991
Printed in Great Britain

0021 8502/91 $3.00+0.00

CORRECTION FOR SAMPLING ERRORS DUE TO COAGULATION AND WALL LOSS IN LAMINAR AND TURBULENT TUBE FLOW: DIRECT SOLUTION OF CANONICAL 'INVERSE' PROBLEM FOR LOG-NORMAL SIZE DISTRIBUTIONS*

DANIEL E. ROSNER† and MENELAOS TASSOPOULOS

Yale University, Department of Chemical Engineering, High Temperature Chemical Reaction Engineering Laboratory, New Haven, CT 06520-2159, U.S.A.

(*Received* 22 *February* 1991; *and in final form* 24 *June* 1991)

Abstract—Aerosol sampling from industrial environments (e.g. combustion engines) or natural environments (e.g. the troposphere) frequently involves conveying the sample to a downstream ('sheltered') instrument via an upstream tube or duct. While the instrument may be capable of characterizing, say, the particle size distribution (PSD) of the aerosol actually presented to it, the investigator is, of course, usually more interested in the PSD of the aerosol entering the upstream sampling tube. Invariably, this differs from that measured because of several systematic phenomena—perhaps the two most obvious of which are particle size-dependent losses to the tube walls (i.e. incomplete 'penetration') and PSD distortion due to suspended particle–particle coagulation when the particle concentrations are sufficiently high. We show here how recent research on the use of 'moment methods' to predict the effects of size-dependent walls loss and/or Brownian coagulation in flow systems can now be brought to bear to conveniently solve this 'inverse' problem by numerically integrating the quasi-one-dimensional coupled moment equations in the upstream direction, using downstream (measured) aerosol properties in the definitions of all dimensionless dependent variables and parameters. Illustrative 'universal' graphs are presented here for the sampling of *log-normally distributed 'inertialess'* (Brownian) aerosols in long straight adiabatic ducts for both commonly encountered extremes of particle Knudsen number $Kn_p \gg 1$(free molecule) or $Kn_p \ll 1$ (continuum), as well as convenient rational approximations derived from the leading terms of a Taylor series expansion of the above-mentioned dimensionless moment equations.

NOMENCLATURE

A	cross-sectional area of duct
b	exponent describing dependence of St_m on particle volume v
C	dimensionless coagulation rate parameter (fm or c)
C_f	friction factor (dimensionless wall shear stress)
$C_1^{(k)}$	first order coefficient in Taylor series expansion of $M_k(\xi)$
d_g	particle diameter corresponding to v_g
D	Brownian diffusion coefficient for particle of volume v
d_w	duct diameter
$f_k(u, v)$	function of particle volumes appropriate to moment k
F_k	dimensionless moment shift function (equation (12))
$\bar{F}_e$	entrance effect correction for streamwise averaged mass transfer coefficient
k	moment index (e.g. $k = 0, 1, 2$ are of particular physical interest)
k_B	Boltzmann constant; Table 2
K	environment/mechanism-dependent part of the coagulation rate constant β
Kn_p	Knudsen number based on prevailing gas mean-free path and particle diameter
L	total length of sampling duct (upstream of detector)
m_p	mass of particle of volume v
M_k	k^{th} moment of $n(v, \ldots) \equiv dN_p/dv$
n	size distribution function dN_p/dv
N_p	total particle number density ($\equiv M_0$)
Nu_m	mass transfer Nusselt (Sherwood) number (Rosner, 1986)
P	'wetted' perimeter of the duct of cross-sectional area $A(z)$

* Supported, in part, by AFOSR (Grand 89-0223), DOE-PETC (Grant DE-FG-22-9 0PC90099) and the 1991 Yale HTCRE Lab Industrial Affiliates (Union Carbide, Shell, SCM Chemicals, DuPont, General Electric).
† Professor of Chemical Engineering, Yale Univ.; Director HTCRE Lab.

Re	Reynolds number based on $4A/P$ and mean velocity U
R	radius (of curvature) of centerline of a bend (e.g. elbow) in duct
Sc	particle Schmidt number $(\mu/\rho)_{gas}/D$
St_m	mass transfer Stanton number, $Nu_m/(ReSc)$ (Rosner, 1986)
t	time
t_p	particle stopping time in the prevailing carrier gas
t_p^+	$u_*^2/t_p/\nu$; dimensionless particle stopping time
T	absolute temperature (K)
U	mean velocity of carrier gas in sampling duct
u	particle volume (dummy variable)
u^*	friction velocity $(C_f/2)^{1/2}U$
v	volume of spherical particle
v_g	geometric-mean particle volume in log-normal PSD $n(v, \ldots)$
$\bar{v}$	mean particle volume, ϕ_p/N_p, of local aerosol
x	$L-z$; distance measured upstream from the detector
$\mathbf{x}$	position vector
z	distance measured downstream from the sampling tube inlet
$Z^{(k)}$	collision integral functions defined by coagulation rate law (equation (15))

Greek letters

β	coagulation rate constant in "mass-action" law (equation (14))
ξ	scaled dimensionless distance upstream of the aerosol detector
ϕ_p	particle volume function ($\equiv M_1$)
ρ_p	intrinsic density of a particle (m_p/v_p)
μ_k	dimensionless k^{th} moment of PSD ($\mu_0 = 1$, $\mu_1 = 1$)
μ_{gas}	dynamic Newtonian viscosity of the carrier gas
ν	momentum diffusivity of the carrier gas, μ_{gas}/ρ_{gas}
ζ_m	$(ReSc)^{-1}(L/d_w)$ (in equation (40))
σ_g	geometric standard deviation of the log-normal PSD $n(v, \ldots)$ (see, e.g. Rosner and Tassopoulos, 1989)

Subscripts and superscripts

C	pertaining to interparticle coagulation
c	coagulation
eff	effective
k	pertaining to moment k where k need *not* be an integer nor positive
(k)	pertaining to moment k
g	pertaining to log-normal PSD (geometric)
gas	pertaining to the carrier gas
L	evaluated at $z = L$ (downstream location of aerosol detector)
max	maximum value
meas	measured
p	particle(s)
o	evaluated at the sampling system inlet station ($z = 0$)
WL	pertaining to wall loss
$'$	first derivative with respect to ξ
$''$	second derivative with respect to ξ

Others

$(\hat{\ })$	normalized by the value $(\ )$ at the aerosol detector (at $z = L$)
$(\bar{\ })$	mean value (e.g. $\bar{v} \equiv \phi_p/N_p$, $\bar{d} = (6\bar{v}/\pi)^{1/3}$; $\overline{St}_m$ (streamwise mean))

Abbreviations

c	continuum ($Kn_p \ll 1$)
coag	pertaining to (caused by) coagulation
fm	free molecule ($Kn_p \gg 1$)
GDE	general dynamic equation (population balance)
h.o.t.	higher order terms
ODE	ordinary differential equation
PSD	particle size (volume) distribution
RHS	right hand side (of equation)
WL	pertaining to (caused by) particle loss to walls

1. INTRODUCTION, BACKGROUND AND MOTIVATION

Historically, the need to accurately sample industrial and natural aerosols has led to many advances in the science and technology of fine particulate matter suspended in gases, including the invention and development of a wide variety of clever instruments as well as

ancillary theoretical developments concerning techniques for avoiding or minimizing 'bias' when extracting the sample and delivering it to the instrument (see, e.g. Fuchs, 1964; Davies, 1966; Mercer, 1973; Friedlander, 1977; Hinds, 1982; Hidy, 1984; Vincent, 1989). Some phenomena will cause an unavoidable systematic 'distortion' in the recorded particle size distribution (PSD) which must be corrected for—in particular—the size-dependent loss of particles to the walls of an upstream sampling tube, and any suspended particle–particle coagulation that occurs between the inlet of the sampling tube and the (downstream) monitoring instrument. The present contribution provides rational, yet simple, methods to make such corrections, under conditions that, while deliberately idealized, are frequently encountered. Indeed, one of our goals is to produce a set of generalized graphs which can facilitate making such corrections for Brownian aerosols (in the absence of appreciable inertial- and sedimentation-phenomena), as well as guide the design/selection of sampling systems which will keep future corrections acceptably small.

Wall deposition losses in the absence of interparticle coagulation have been the subject of many early investigations, especially for the case of dilute, steady, fully-developed laminar gas flow in straight, constant-area ducts (see, e.g. Fuchs and Sutugin, 1971). This understanding, in fact, led to the development of the so-called 'diffusion battery' (see, e.g. Mercer and Green, 1974) for estimating PSDs based on the observed penetration characteristics of the aerosol as a function of particle size, duct diameter, length, and gas flow rate. At suspended particle concentrations high enough for non-negligible coagulation (Brownian, shear, . . .) the situation becomes rather more complicated and the computational methods used by earlier investigators to predict PSD distortion effects fail (i.e. assuming that the penetration of one particle size class is not influenced by the simultaneous presence of the others). Indeed, the interesting interactions between coagulation and convective-diffusion deposition rates now comprise an active field of research (see, e.g. Park and Rosner, 1989; Pratsinis and Kim, 1989; Bai and Biswas, 1990; Rosner and Tassopoulos, 1990), to which the present paper contributes. The present work is also an extension and application of techniques we have recently developed for predicting total mass deposition rates from polydispersed aerosol populations formed by coagulation (Rosner, 1989; Rosner and Tassopoulos, 1989), but without the complication of appreciable coagulation within diffusion boundary layers (see, e.g. Park and Rosner, 1989; Bai and Biswas, 1990).

Finally, mention should be made of relevant theoretical studies whose primary purpose was to support interpret fundamentally-oriented experiments on the mechanisms of organic- and inorganic-soot production in laminar flames (see, e.g. Ulrich and Subramanian, 1977; Ulrich and Riehl, 1982; Dobbins and Mulholland, 1984; Dobbins and Megaridis, 1987; Frenklach and Harris, 1987; Megaridis and Dobbins, 1990; Megaridis, 1987; Zachariah and Semerjian, 1989). Indeed, our treatment below of free-molecule regime coagulation in aerosol sampling system *is* equivalent to that of Dobbins and Mulholland (1984) (rather than that of Lee *et al.*, 1984), suitably augmented to include the simultaneous occurrence of particle size-specific convective-diffusion to the walls of the sampling tube.

Rather than explicitly dealing with the 'direct' problem of predicting the 'evolution' of the penetrating (and depositing) aerosol as a function of dimensionless downstream distance and coagulation parameters (see, e.g. Rosner and Tassopoulos, 1990, 1991b) we show here (section 3.6) that by 'backwards' (upstream-) integration of the governing moment equations and the use of dimensionless dependent variables and parameters based on downstream reference quantities, we, in effect, can provide direct solutions to the canonical 'inverse' problem of aerosol sampling theory—i.e. correction factors which allow the investigator to go immediately from PSD-parameters recorded at the downstream instrument to the PSD-parameters that must have characterized the aerosol entering the inlet* of the sampling

* Additional correction factors may be necessary due to peculiarities of the inlet orifice itself, and its geometric surroundings (see, e.g. Vincent, 1989; Mercer, 1973; Hungal and Willeke, 1990; Belyaeu and Levin, 1974; Zabel, 1978; Ivie *et al.*, 1990; Huebert *et al.*, 1990). In considering the need for such additional factors, however, the reader should bear in mind that we emphasize here Brownian particles well below the 'inertial' range. In any case, if necessary, additional 'inlet' correction factors can be superimposed on the present predictions.

tube. Toward this end, in section 2 we spell out our underlying assumptions/idealizations, and in section 3 we state the laws used here to predict the evolution of the three lowest integral moments of the log-normal shape aerosol PSD for (quasi-) steady, (quasi-) one-dimensional gas flow in a straight adiabatic aerosol sampling duct. General results ('universal' graphs and formulae) are presented in section 4, together with a simple numerical ('backward-marching') procedure for dealing with much more complex cases. Some implications and applications of the results of section 4 are provided and briefly discussed in section 5 with the help of two specific numerical air-monitoring examples (nearly isothermal)—one ground-based and one airborne. Section 6 offers a concise defense of many useful idealizing assumptions, as well as an indication of how to relax many of the assumptions exploited here for particular sampling applications which are more complex, such as extractive sampling from high temperature combustors (for further details the reader is referred to the references cited in section 6 and Rosner and Tassopoulos (1990, 1991b)). Our summary recommendations, and an indication of future relevant work are contained in section 7, which concludes the present paper. Extensions based, in part, on section 6 will be the subject of future communications from this laboratory.

2. BASIC ASSUMPTIONS

In keeping with our goal of deriving reasonably general results applicable to a wide variety of intrinsically similar, commonly encountered sampling situations we introduce the following explicit simplifying assumptions and idealizations. These are defended or shown to be relaxable in section 6.

A1: Quasi-one dimensional steady gas flow in a straight adiabatic sampling duct with constant effective diameter $d_{\text{eff}} = 4A/P$.

A2: Aerosol PSD well-represented by a single mode continuous log-normal function of the dense spherical particle volume v.

A3: Axial *diffusion* of particles negligible compared to axial *convection*.

A4: Previously calculated (or measured) fully-developed perimeter-averaged mass transfer coefficients adequately describe local convective-diffusion particle mass transport to the wall, and depend on a single power, b, of the particle volume valid in the high Schmidt number ($\text{Sc} = \nu/D_p \gg 1$) limit.

A5: Negligible interfacial 'barrier' to incident particle capture by the wall, and negligible reentrainment of already deposited particles.

A6: Brownian coagulation occurs primarily in the core of the sampling duct flow according to the mass-action laws of free-molecule transport ($\text{Kn}_p \gg 1$) or continuum transport ($\text{Kn}_p \ll 1$).

As discussed in section 6, Assumptions A3, A4, and A6 can apply to either laminar or turbulent duct flow (perhaps more accurately to the latter than the former (because of A4, see sections 5.2 and 6)). Methods to include the systematic consequences of 'entry' effects, non-power-law deposition, transition regime particle transport and coagulation, diabatic walls, bends (in a 'piecewise-straight' sampling system) and non-spherical 'aggregated' solid particles are taken up briefly in section 6, and in greater detail in Rosner and Tassopoulos (1990, 1991). It should also be remarked that in the continuum limit ($\text{Kn}_p \ll 1$) many of our methods/results will apply to particle suspensions in flowing *liquid* (hydrosals).

3. MOMENT METHODS AND LOG-NORMAL PSDs

Rather than dealing directly with the complete suspended particle population balance or 'general dynamic equation' (GDE) governing the continuous size distribution function $n(v, \mathbf{x}, t) = \mathrm{d}N_p/\mathrm{d}v$ (presumed to be measurable at the location of the downstream aerosol instrument) the predictions made below are based on solving a closed set of coupled

differential equations for the three lowest integral 'moments' of $n(v, \ldots)$, defined by:

$$M_k \equiv \int_0^\infty v^k n(v, \ldots) \mathrm{d}v \qquad (k = 0, 1, 2). \tag{1}$$

This strategy, and its implementation for the case of steady quasi-one dimensional duct flow, are the subjects of sections 3.1–3.6 below. Owing tc more extensive discussions elsewhere (see, e.g. the mass deposition-oriented work of Rosner, 1989; Rosner and Tassopoulos, 1989, 1990, 1991) only the most important conclusions/results are stated below for completeness.

3.1. *Method of moments*

The use of differential equations for the moments of $n(v, \ldots)$ to construct rational approximate solutions to the GDE (an integro–differential equation) is a subject that has been under intense development in the past two decades, and progress continues unabated. Moment methods have been especially successful in elucidating many aerosol situations involving coagulation (see, e.g. Cohen and Vaughn, 1971; Lee *et al.*, 1984; Dobbins and Mulholland, 1984; Megaridis and Dobbins, 1989, 1990; Pratsinis and Kim, 1989; Frenklach and Harris, 1987, . . .). Although different authors use somewhat different methods to achieve closure, especially when coagulation occurs near or in the 'free-molecule' regime, almost all authors derive/use equations for M_0, M_1, and M_2, which are, indeed, particularly simple (see sections 3.4 and 3.5). The first two moments also have the merit of being of direct physical significance, with $M_0 = N_p$ (the total particle number density) and $M_1 = \phi_p$ (the total particle volume fraction). In the present case of steady quasi-one-dimensional flow in a sampling duct we therefore focus our attention on the coupled ordinary differential equations governing the $M_k(z)$, where $k = 0, 1, 2$, and z is the axial coordinate down the sampling tube (measured from the inlet). When use is made of the known laws of particle deposition (section 3.4) we encounter terms involving additional moments M_k, where $k \neq 0, 1, 2$ so that it becomes necessary to interrelate moments to obtain a closed set of integrable equations. In the present case this is accomplished using the log-normal PSD shape approximation, as discussed in section 3.2, and defended in section 6 for this class of problems.

3.2. *Implications of log-normality*

It is now well known that 'coagulation-aged' populations of aerosol particles closely approach single-mode log-normal size distributions (i.e. Gaussian in $\ln(v)$). Moreover, it is easy to demonstrate that power-law wall removal processes (see A4 and section 3.3) will not alter this situation. Hence, for our present purposes the single-mode log-normal approximation is a particularly appropriate and convenient starting point. For such single-mode log-normal PSDs it can also be shown that all moments are necessarily interrelated as follows:

$$M_k = v_g^k \cdot N_p \cdot \exp\left(\left(\frac{k^2}{2}\right)\ln^2 \sigma_g\right), \tag{2}$$

where v_g is the median (geometric mean) particle volume and σ_g is the corresponding geometric standard deviation of the PSD. These PSD parameters can be related to N_p, ϕ_p, and M_2 *via*:

$$\ln^2 \sigma_g = \ln\left(\frac{M_2 \cdot N_p}{\phi_p^2}\right) \tag{3}$$

and

$$v_g = \left(\frac{\phi_p}{N_p}\right)^{3/2} \cdot (M_2)^{-1/2} \tag{4}$$

but any other desired moment $M_k (k \neq 0, 1, 2)$ can now be obtained in terms of either N_p, ϕ_p, and M_2, or N_p, v_g and σ_g. We will also have frequent need for the relation:

$$v_g = \bar{v} \cdot \exp\left(-\left(\frac{1}{2}\right) \ln^2 \sigma_g \right), \tag{5}$$

where $\bar{v} \equiv \phi_p / N_p$ is the mean particle volume.

While not discussed further here, the assumption of log-normality in effect also allows us to escape the numerical problems often encountered in 'inverting' aerosol population measurements (see, e.g. Cooper and Wu, 1990). Thus, our "upstream" integrations (section 3.6) are perfectly straightforward, but deliberately limited to cases where the required PSD-parameter 'correction' factors are well within one decade of unity.

3.3. *Modeling particle size-dependent particle wall losses*

For steady quasi-one-dimensional (z-direction) flow in a duct of area $A(z)$ and wetted perimeter $P(z)$ the wall loss contribution can be written (see, e.g. Rosner and Tassopoulos, 1990)

$$\left\{ \frac{1}{A} \frac{d}{dz} (AUM_k) \right\}_{\text{wall loss}} = -\frac{P}{A} U \cdot \int_0^\infty \text{St}_m(v) \cdot v^k n(v) \, dv, \tag{6}$$

where $\text{St}_m(v)$ is the appropriate perimeter-mean particle volume-dependent dimensionless mass transfer coefficient (Stanton number = $\text{Nu}_m/(\text{ReSc})$), Rosner (1986) at station z, and $n(v, z)$ is the PSD describing the bulk (mixing-cup averaged) suspended particle–gas mixture at this same streamwise station. As shown and exploited in our recent work (see, e.g. Rosner, 1989; Rosner and Tassopoulos, 1989) in the submicron particle size range of primary interest here it is often possible to accurately represent the v-dependence of $\text{St}_m(v, \ldots)$ by simple power-law:

$$\text{St}_m \cong \text{St}_m(\bar{v}) \cdot \left(\frac{v}{\bar{v}} \right)^b \tag{7}$$

where, e.g. for $\text{Sc} \gg 1$ turbulent convective-diffusion (see, e.g. Rosner (1986, 1990) equation (6.5–11b)) $\text{Nu}_m \sim \text{Sc}^{0.296}$, $\text{St}_m \sim \text{Sc}^{-0.704}$ and therefore:

$$b = 0.704 \left(\frac{\partial \ln D}{\partial \ln v} \right) \tag{8}$$

and, for fully-developed laminar flow $\text{Nu}_m = \text{const}$, $\text{St}_m \sim \text{Sc}^{-1}$, so that:

$$b = \left(\frac{\partial \ln D}{\partial \ln v} \right). \tag{9}$$

Since $D \sim v^{-2/3}$ for dense spherical particles in the free-molecule regime ($\text{Kn}_p \gg 1$), and $D \sim v^{-1/3}$ for dense spherical particles in the continuum limit, the exponents b used in our calculations below are readily obtained and summarized in Table 1. For isothermal convective-diffusion they are seen to fall between the extremes of -0.235 and -0.667. Other mechanisms of particle transport to the sampling tube wall (e.g. eddy impaction, or particle thermophoresis) and other types of particles (e.g. aggregates comprised of smaller diameter 'primary' particles) will, of course, be characterized by rather different b-values, as discussed elsewhere (Rosner, 1989; Rosner and Tassopoulos, 1989; Rosner, 1991).

Taking into account this power-law behavior, and considering the particular case of constant area adiabatic duct flow, we find that equation (6) can be simplified to:

$$\left\{ U \frac{dM_k}{dz} \right\}_{\text{wall loss}} = -\frac{P}{A} U \cdot \text{St}_m(\bar{v}) \cdot \bar{v}^{-b} \cdot M_{k+b}, \tag{10}$$

where, in the equations below $k = 0, 1, 2$. In practice (see, e.g. section 3.5) we rewrite

Table 1. Values of the exponent b for fully-developed convective diffusion in straight ducts

	Flow regime	
Particle Knudsen number	Laminar*	Turbulent†-smooth wall
Free-molecule (fm)	−2/3	−0.469
Continuum (c)	−1/3	−0.235

* In this case $Nu_m \sim$ constant so that $St_m \sim Sc^{-1}$.
† Based on $Sc \gg 1$ transport by Brownian motion within the viscous sublayer.

equation (10) in the formally simple way:

$$\left\{U\frac{dM_k}{dz}\right\}_{\text{wall loss}} = -\frac{P}{A}U\cdot St_m(\bar{v})\cdot F_k\cdot M_k, \tag{11}$$

where F_k is the dimensionless 'moment-shift' function* defined by:

$$F_k \equiv \frac{\bar{v}^{-b}M_{k+b}}{M_k} = \frac{\mu_{k+b}}{\mu_k} \tag{12}$$

where we have introduced the dimensionless moments:

$$\mu_k \equiv \exp\left\{\frac{k(k-1)}{2}\cdot\ln^2\sigma_g\right\}. \tag{13}$$

Equations (12) and (13) follow from the PSD-condition of log-normality.

3.4. *Inclusion of coagulation processes at high particle number densities*

If the coagulation rate between $n(v)dv$ particles/volume of volume $v \pm dv/2$ and $n(u)du$ suspended particles/volume of volume $u \pm du/2$ is taken to be of the 'mass-action' form $\beta(u, v)n(u)n(v)du\,dv$ then it is known that (in a well-mixed, transient situation):

$$\left(\frac{dM_k}{dt}\right)_{\text{coag.}} = \frac{1}{2}\int_0^\infty\int_0^\infty f_k(u, v)\cdot\beta(u, v)n(v)\cdot n(u)\,dv\,du. \tag{14}$$

Clearly $f_0 = -1$ and $f_1 = 0$, and it can be shown that $f_2 = 2uv$ (see, e.g. Cohen and Vaughn (1971)). Following Dobbins and Mulholland (1984), for log-normal distributions, once the rate constant $\beta(u, v)$ is specified the right-hand side of equation (14) can always be calculated numerically and the results expressed in the form:

$$\left(\frac{dM_k}{dt}\right)_{\text{coag.}} = \frac{1}{2}K\cdot N_p^2\cdot Z^{(k)}(v_g, \sigma_g), \tag{15}$$

where the coefficient K is independent of particle size and number density but dependent on environmental conditions and perhaps particle material properties. Values of K and the so-called collision integrals $Z^{(k)}$ for the free-molecule (fm) coagulation of hard spheres (Dobbins and Mulholland, 1984) are reproduced (in our notation) in the top rows of Table 2. In the continuum (c) limit it is well known that $(dM_0/dt)_{\text{coag}}$ is proportional to $-(M_0^2 + M_{1/3}M_{-1/3})$ and $(dM_2/dt)_{\text{coag}}$ is proportional to $(M_1^2 + M_{4/3}M_{2/3})$ (see, e.g. Cohen and Vaughn (1971) or Flagan and Seinfeld (1988)) with the proportionality constant (hence K-value) depending on the combination $k_B T/\mu_{\text{gas}}$. When these results are recast in terms of equation (15) using equation (5) we obtain/use the values of K_c and $Z_c^{(k)}$ shown in the bottom row of Table 2. Thus, in the equations below we set the Brownian coagulation contribution to $U\,dM_k/dz$ equal to the RHS of equation (15), and, for $\sigma_g < 3.32$, used the

* In our previous papers (Rosner, 1989; Rosner and Tassopoulos, 1989) particular attention was focused on F_1 $(= \mu_{1+b})$, which was shown to be equal to the physically interesting ratio of the actual total mass deposition rate to the total mass deposition rate if all particles in the population had the mean volume $\bar{v}$.

Table 2. Summary of factors*†‡ appearing in the coagulation rate term [equation (15)]

Coagulation regime§	$K(T,\ldots)$	$Z^{(0)}$	$Z^{(1)}$	$Z^{(2)}$
Free-molecule* ($Kn_p \gg 1$)	$\left(\frac{3}{4\pi}\right)^{1/6}\cdot\left(\frac{6k_BT}{\tilde{\rho}_p}\right)^{1/2}$	$-4\sqrt{2}\bar{v}_g^{1/6}\cdot\exp\left[\frac{3}{16}\ln^2\sigma_g\right]$	0	$8\sqrt{2}\bar{v}_g^{13/6}\cdot\exp\left[\frac{65}{48}\ln^2\sigma_g\right]$
Continuum ($Kn_p \ll 1$)	$\frac{4k_BT}{3\mu_{gas}}$	$-2\left\{1+\exp\left(\frac{1}{9}\ln^2\sigma_g\right)\right\}$	0	$4\bar{v}^2\cdot\left[1+\exp\left(\frac{1}{9}\ln^2\sigma_g\right)\right]$

* Values taken from Dobbins and Mulholland (1984); see, also, Megaridis and Dobbins (1990a) for $\sigma_g > 3.32$.

† As a consequence of the assumed conservation of volume when two particles collide and coalesce $Z^{(1)}$ vanishes for all cases. (Recall that $M_1 = \phi_p$ = particle volume fraction.)

‡ Note that, according to equation (15) only the products $KZ^{(k)}$ necessarily have the same dimensions (in the fm and c cases). However, as is clear from the entries above, the K-factors (and the corresponding $Z^{(k)}$ factors) themselves do not have the same dimensions in the free-molecule and continuum cases.

§ For intermediate Kn_p-values (transition regime), see Rosner and Tassopoulos (1991b) and section 6.6.

values of K and $Z^{(k)}$ assembled in Table 2. If necessary, this approach could clearly be extended to other coagulation mechanisms (see, section 6, i.e. other rate constants $\beta(u, v, \ldots)$ (cf. equation (14)) appropriate to the mechanism of interest (see, e.g. Mackowski *et al.*, 1991).

3.5. *Coupled ODEs for free-molecule and continuum coagulation; steady, quasi-one-dimensional duct flow with simultaneous wall losses*

Combining the results of sections 3.1–3.4 above, we see that, subject to the assumptions of section 2, in all cases the PSD moments M_k ($k = 0, 1, 2$) will satisfy the coupled ODEs:

$$U\frac{dM_k}{dz} = -\frac{P}{A}\cdot U\cdot \mathrm{St}_m(\bar{v})\cdot F_k M_k + \frac{1}{2}KM_0^2 Z^{(k)}, \tag{16}$$

where F_k is the above-mentioned moment shift function appropriate to the mass transfer law (section 3.3) and the appropriate values of $K(T,\ldots)$ and $Z^{(k)}$ appearing in the coagulation rate terms can be read from Table 2. All of the conclusions we derive and state below follow from these coupled non-linear ordinary differential equations and the abovementioned moment interrelations. Before proceeding it is worth noting that the coagulation term (second term on RHS) will not appear in the ODE governing $M_1 (\equiv \phi_p)$; i.e. $Z^{(0)} = 0$. Moreover, if instead of an axial position variable z measured downstream from the sampling duct inlet $z = 0$ (with $0 < z < L$) we introduce a position variable x measured upstream from the aerosol instrument at $z = L$ then $x = L - z$ and $dx = -dz$. Thus, introduction of such a variable (to form the corresponding $U(dM_k/dx)$ equations) will merely change the sign of all terms on the RHS of equation (16). This sets the stage for the 'backward' integration of equation (16) to find the upstream dependence of the aerosol PSD moments based on a knowledge (measurement) of their downstream (instrument) values.

3.6. *Non-dimensionalized inverse problem ODEs*

In Rosner and Tassopoulos (1990, 1991b) we illustrated the use of equation (16) to calculate the downstream evolution of the aerosol PSD in terms of inlet values and associated dimensionless coagulation parameters for a variety of flow conditions (laminar, turbulent, free-molecule transport, continuum transport). To solve the 'inverse' problem of aerosol sampling theory, we merely redefine our dimensionless variables and parameters using downstream values (presumed measured) and integrate in the upstream direction. Thus, we here introduce $\tilde{N} \equiv N_p/N_{p,L}$, $\tilde{\phi} \equiv \phi_p/\phi_{p,L}$, $\tilde{M}_2 \equiv M_2/M_{2,L}$ and define the 'rescaled' axial distance variable:

$$\xi \equiv \left\{\frac{P}{A}\mathrm{St}_m(\bar{v}_L)\cdot F_{o,L}\right\}\cdot(L-z). \tag{17}$$

The coupled ODEs satisfied by $\tilde{N}(\xi, \ldots)$, $\tilde{\phi}(\xi, \ldots)$ and $\tilde{M}_2(\xi, \ldots)$ can be obtained from the dimensionless ODEs of Rosner and Tassopoulos (1990, 1991) by making the appropriate parameter replacements and sign changes, with the following results. Let us introduce the coagulation parameter:

$$C \equiv \frac{(-Z_L^{(0)}) \cdot (\frac{1}{2}K) \cdot N_{p,L}^2}{\left\{\left(\frac{P}{A}\right) \cdot U \cdot \mathrm{St}_m(\bar{v}_L) \cdot F_{o,L} \cdot N_{p,L}\right\}} \tag{18}$$

(a measure of the relative importance of coagulation and wall loss in altering the PSD parameters). Then, subject to the 'initial' normalization conditions: $\tilde{N}(0) = 1$, $\tilde{\phi}(0) = 1$, $\tilde{M}_2(0) = 1$ and the assumptions of section 2, the coupled dimensionless moment equations become the non-linear first order system:

$$\frac{d\tilde{N}}{d\xi} = \left(\frac{\tilde{\phi}}{\tilde{N}}\right)^b \cdot \frac{F_0}{F_{0,L}} \cdot \tilde{N} + C\tilde{N}^2 \cdot \frac{(-Z^{(0)})}{-Z_L^{(0)}} \tag{19}$$

$$\frac{d\tilde{\phi}}{d\xi} = \left(\frac{\tilde{\phi}}{\tilde{N}}\right)^b \cdot \frac{F_1}{F_{0,L}} \cdot \tilde{\phi} \tag{20}$$

$$\frac{d\tilde{M}_2}{d\xi} = \left(\frac{\tilde{\phi}}{\tilde{N}}\right)^b \cdot \frac{F_2}{F_{0,L}} \cdot \tilde{M}_2 - C\tilde{\phi}^2 \cdot \left\{\frac{2}{\exp(\ln^2 \sigma_{g,L})} \cdot \frac{(-Z^{(0)})}{(-Z_L^{(0)})}\right\}, \tag{21}$$

where the subscript L implies evaluation of the appropriate function at $z = L$ ($x = 0$). These same equations formally hold for either the free-molecule or continuum case provided the appropriate coagulation parameters/functions are introduced according to Table 2. Similarly, subject to the assumptions indicated in section 2 and discussed in section 6, they hold for either turbulent or laminar flow in a straight duct.

3.7. *Similitude implications*

Inspection of the above-mentioned moment equations governing the present simplified model reveals that the idealizations of section 2 lead to correction factors of the functional form:

$$N_{p,o}/N_{p,L} = \mathrm{fct}_0(\xi_{max}, \sigma_{g,L}, b, C) \tag{22}$$

$$\phi_{p,o}/\phi_{p,L} = \mathrm{fct}_1(\xi_{max}, \sigma_{g,L}, b, C) \tag{23}$$

$$M_{2,o}/M_{2,L} = \mathrm{fct}_2(\xi_{max}, \sigma_{g,L}, b, C) \tag{24}$$

from which we can also calculate the interesting correction factors:

$$\sigma_{g,o}/\sigma_{g,L} = \mathrm{fct}_3(\xi_{max}, \sigma_{g,L}, b, C) \tag{25}$$

$$v_{g,o}/v_{g,L} = \mathrm{fct}_4(\xi_{max}, \sigma_{g,L}, b, C), \tag{26}$$

where relevant values of the exponent b are given in Table 1, the value of the PSD spread parameter $\sigma_{g,L}$ is presumed to be measured, ξ_{max} is the value of the 'scaled' length coordinate ξ (equation (17)) evaluated at the sampling tube inlet ($z = 0$) and C is the relevant dimensionless coagulation parameter (which is seen to scale linearly with $N_{p,L}$). In section 4 we present the results of numerical integrations of (equations (19–21)) for many combinations of physical interest to display the explicit sensitivity of the desired correction factors to macroscopic flow regime (laminar, turbulent) and the Knudsen regime of particle transport. We also present an extensive set of graphical results for the commonly encountered limiting case of negligible Brownian coagulation (i.e. $N_{p,L}$ is low enough to cause $C \ll 1$). Note that, although all of our graphs deliberately go beyond the range of ξ_{max} values where the leading term of a small-ξ Taylor series expansion is valid (see section 4.2), rather frequently ξ_{max}-values of physical interest *will* be small enough to allow the simple explicit formulae of section 4.2, thus circumventing the need for the above-mentioned graphs, or specific numerical integrations (see, e.g. the numerical examples discussed in section 5).

4. RESULTS

4.1. *'Universal' graphs for convective-diffusion wall losses without (and with) appreciable particle coagulation*

In this section we display and briefly comment upon the results of our numerical integrations of the coupled set of ODEs explicitly given by equations (19)–(21) in the text,

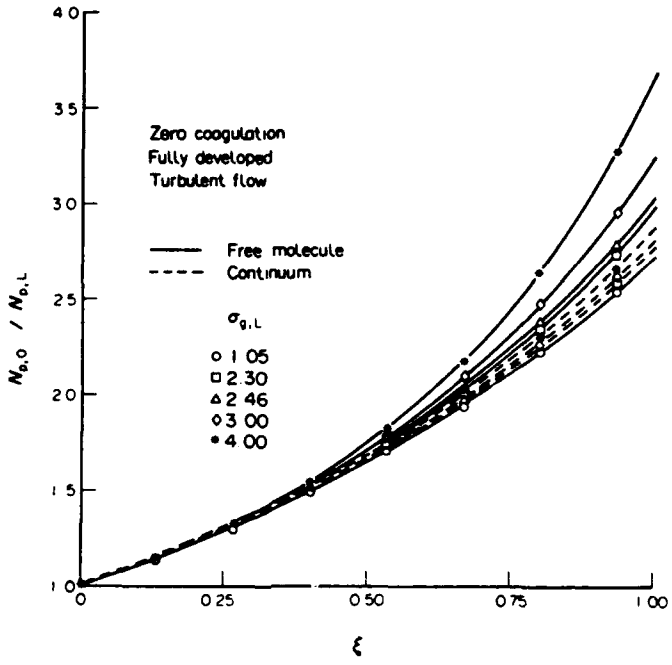

Fig. 1. Effects of particle size dependent convective-diffusion wall loss, Knudsen number regime, and PSD spread on the particle number density correction factor $N_{p,0}/N_{p,L}$ for turbulent gas flow in straight sampling tubes of scaled length ξ in the absence of appreciable Brownian coagulation.

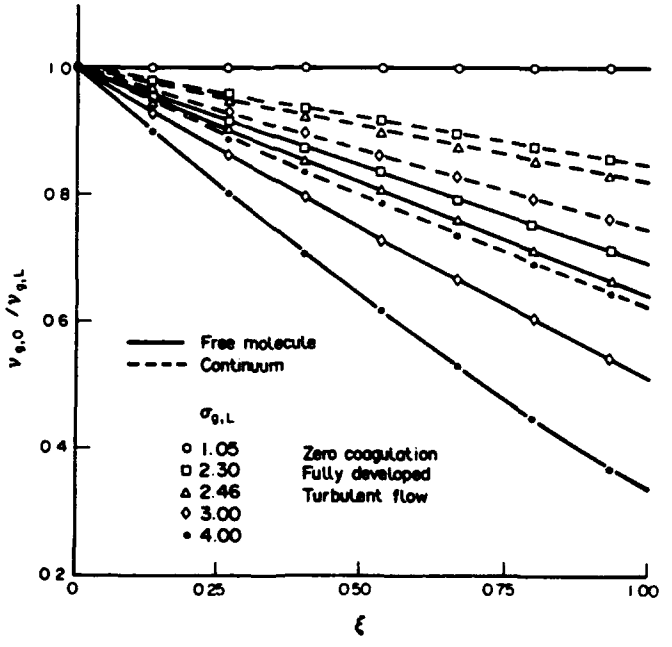

Fig. 2. Effects of particle size dependent convective-diffusion wall loss, Knudsen number regime, and PSD spread on the geometric mean particle volume correction factor $v_{g,0}/v_{g,L}$ for turbulent gas flow in straight sampling tubes of scaled length ξ in the absence of appreciable Brownian coagulation.

subject to their initial (normalization) conditions. Results are grouped as follows: Figs 1–6 pertain to PSD-parameter corrections in the limit of negligible coagulation, with the first three dealing with turbulent carrier gas flow. These graphs allow N_p-, v_g- and σ_g-corrections to be made for scaled sampling tube lengths $\xi_{max} \leq 1$ with either free-molecule or continuum

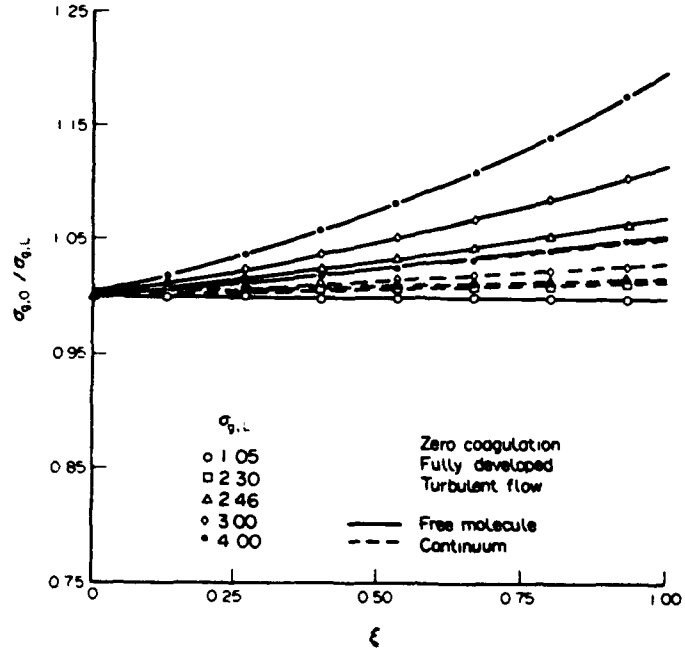

Fig. 3. Effects of particle size dependent convective-diffusion wall loss, Knudsen number regime, and PSD spread on the correction factor to the geometric PSD-spread, $\sigma_{g,0}/\sigma_{g,L}$, for turbulent gas flow in straight sampling tubes of scaled length ξ in the absence of appreciable Brownian coagulation.

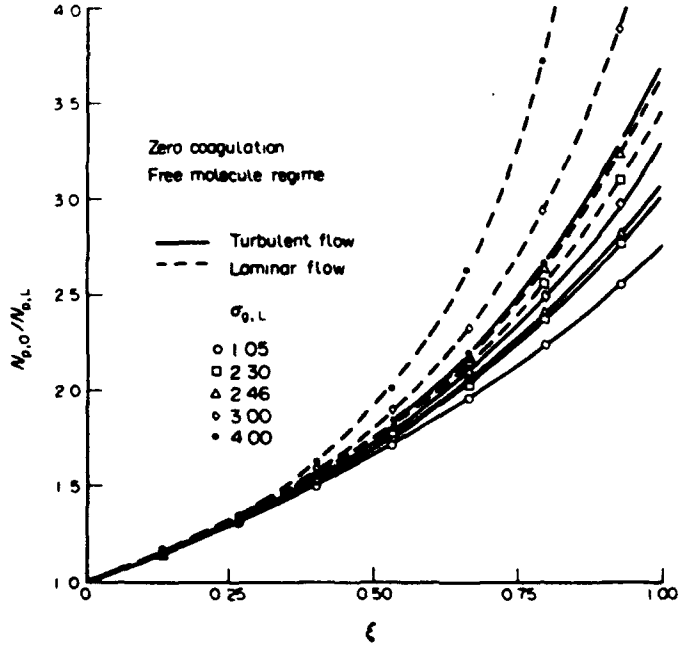

Fig. 4. Effects of particle size dependent wall loss by convective-diffusion, gas flow regime and PSD spread parameter on the total particle number density correction factor $N_{p,0}/N_{p,L}$ for gas flow in straight sampling tubes of scaled length ξ in the absence of appreciable free-molecule regime interparticle coagulation.

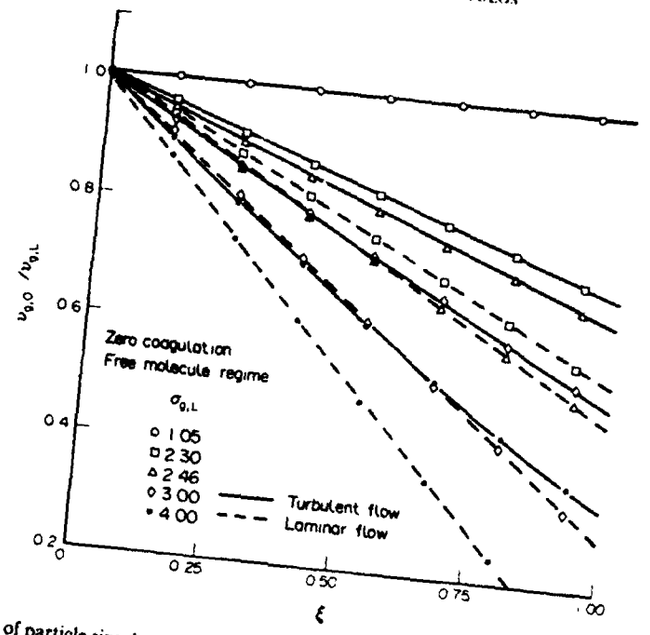

Fig. 5. Effects of particle size dependent wall loss by convective-diffusion, gas flow regime and PSD spread parameter on the geometric mean particle volume correction factor $t_{g,0}/t_{g,L}$ for gas flow in straight sampling tubes of scaled length ξ in the absence of appreciable free-molecule regime interparticle coagulation.

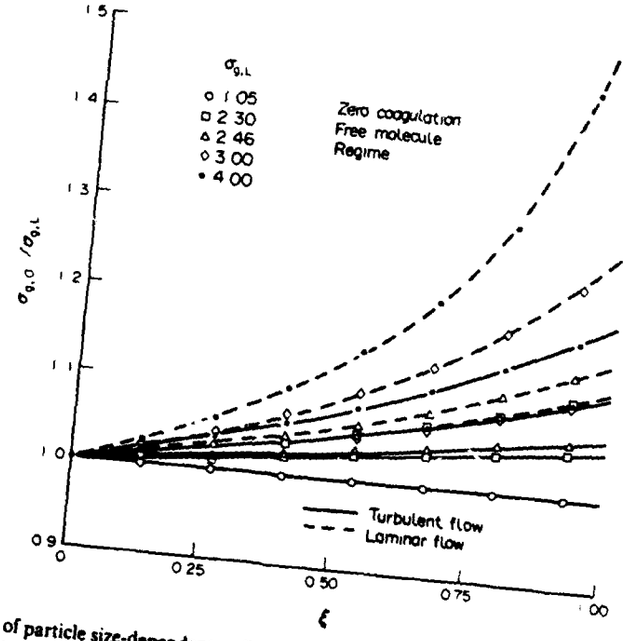

Fig. 6. Effects of particle size-dependent wall loss by convective-diffusion, gas flow regime and PSD spread parameter on the correction factor to the geometric mean PSD-spread, $\sigma_{g,0}/\sigma_{g,L}$ for gas flow in straight sampling tubes of scaled length ξ in the absence of appreciable free-molecule regime interparticle coagulation.

transport over a range of observed PSD spread parameters $\sigma_{g,L}$ at the aerosol detector. In the limit $\sigma_{g,L} \to 1$ (monodispersed) the dependence of the correction factors on Kn-regime drops out due to our choice of (scaled-) variables. For 'polydispersed' cases the correction factors are seen to depart further from unity in the free-molecule limit owing to the

increased size dependence of the Brownian diffusivity $D(v)$ when $Kn_p \to \infty$. Figures 3–6 also pertain to negligible coagulation but compare laminar flow results to those for turbulent flow when the particle transport mechanism is free-molecule. As discussed in sections 5.2 and 6.1, for the laminar flow cases 'entrance effects' may dictate the need for b_{eff}-values not explicitly included in these graphs. When $\xi_{max} < 0.5$ (say), these effects can be dealt with by using the small ξ_{max} Taylor series formulae presented in section 4.2 (below) and Appendix A. For $\xi_{max} = O(1)$ one expects $b_{eff} \to b$ (Table 1) and Figs 4–6 may be useful in their present form. Note that the PSD-correction factors depart further from unity for laminar flow cases when compared at the same value of the scaled sampling system length, ξ_{max}.

Figures 7–9 display our computed PSD-correction factors in the presence of appreciable interparticle Brownian coagulation effects (non-negligible C) when the gas flow is turbulent and the PSD spread parameter at the particle detector is near the appropriate 'self-preserving' value. Clearly, for any value of ξ_{max}, these correction factors depart further from unity when the coagulation parameter C is increased, in either the free-molecule or continuum regimes. Particularly interesting is the rapid rise in the spread correction factor $\sigma_{g,o}/\sigma_{g,L}$ which sets in at sufficiently large ξ_{max}-values (see Fig. 9). This can be shown to be a consequence of equation (3), given the sensitivity of $\tilde{N}_p$ (compared to $\tilde{\phi}_p$ and $\tilde{M}_2$) to coagulation in the sampling system.

4.2. *Small-ξ expansions*

As will be appreciated from several numerical examples (sections 5.1 and 5.2) the maximum value of ξ (the 'scaled' distance measured upstream from the aerosol instrument to the sampling tube inlet) is frequently a small number, often less than 10^{-1}. This suggests that even the above-mentioned universal graphs or the numerical integrations on which they are based can be bypassed by using a small ξ Taylor series expansion, the first terms of which can be written down by inspection of equations (20, 21). Thus, if we write:

$$\tilde{M}_k = 1 + C_1^{(k)}(C, \sigma_{g,L}, b)\xi + \text{h.o.t.} \tag{27}$$

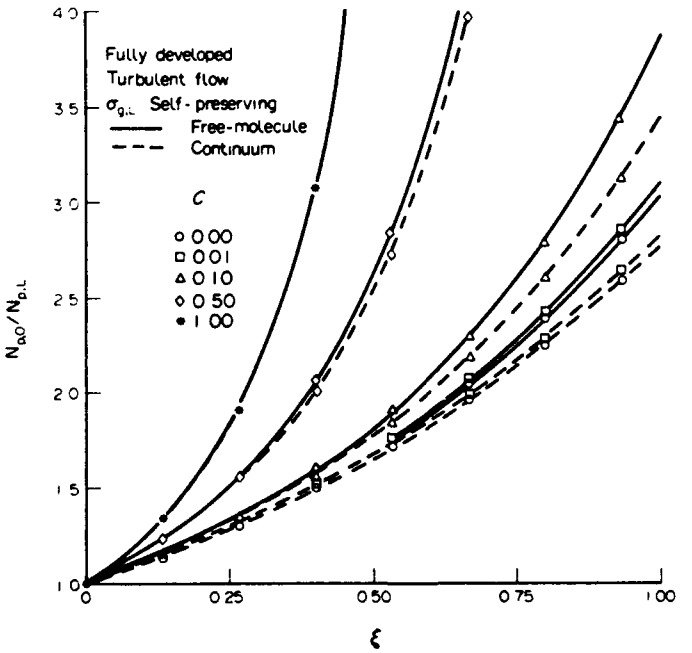

Fig. 7. Effects of Brownian coagulation, particle size-dependent convective-diffusion wall loss and particle/gas Knudsen number regime on the correction factor for total particle number density $N_{p,o}/N_{p,L}$ for turbulent gas flow in straight sampling tubes of scaled length ξ. Curves shown pertain to nearly self-preserving PSDs at the detector (i.e. $(\sigma_{g,L})_{fm} = 2.46$ and $(\sigma_{g,L})_c = 2.3$).

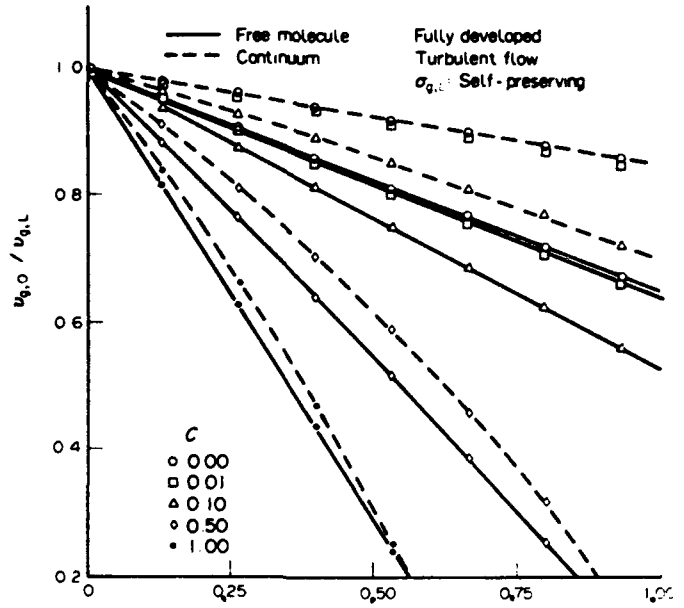

Figure 8. Effects of Brownian coagulation, particle size-dependent wall convective-diffusion loss and particle/gas Knudsen number regime on the correction factor to geometric mean particle volume $v_{g,0}/v_{g,L}$, for turbulent gas flow in straight sampling tubes of scaled length ξ. Curves shown pertain to nearly self-preserving PSDs at the detector (i.e. $(\sigma_{g,L})_{fm} = 2.46$ and $(\sigma_{g,L})_c = 2.3$).

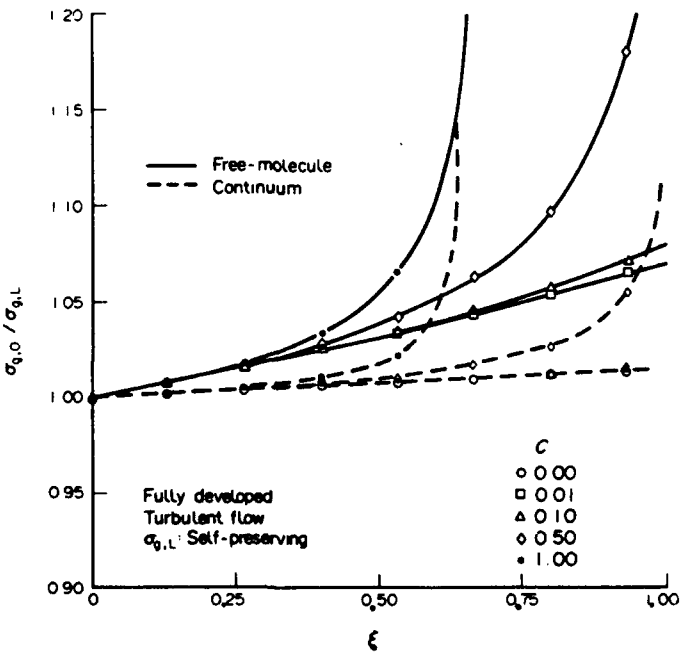

Fig. 9. Effects of Brownian coagulation, particle size-dependent wall convective-diffusion loss and particle/gas Knudsen number regime on the correction factor for to the PSD spread, $\sigma_{g,0}/\sigma_{g,L}$. Curves shown pertain to nearly self-preserving PSDs at the detector (i.e. $(\sigma_{g,L})_{fm} = 2.46$ and $(\sigma_{g,L})_c = 2.3$).

we find that the first-order coefficients† $C_1^{(k)}$ are explicitly:

$$C_1^{(0)} = 1 + C \qquad (k = 0)$$
$$C_1^{(1)} = 1 \qquad (k = 1) \tag{28}$$

and

$$C_1^{(2)} = \exp(-2b\ln^2\sigma_{g,L}) - 2C\exp(-\ln^2\sigma_{g,L}) \quad (k = 2).$$

Under circumstances for which assumptions A1–6 are reasonable and the 'higher order terms' of equation (27) can be neglected† we can therefore state the following potentially useful rational explicit correction factor-relations:

$$\frac{N_{p,o}}{N_{p,L}} \cong 1 + (1 + C)\xi_{max} \qquad \text{(number density)} \tag{29}$$

(independent of b and $\sigma_{g,L}$)

$$\frac{\sigma_{g,o}}{\sigma_{g,L}} \approx 1 + \frac{(C_1^{(2)} + C_1^{(0)} - 2C_1^{(1)})\xi_{max}}{2\ln\sigma_{g,L}} \qquad \text{(spread)} \tag{30}$$

and, since $\bar{v} \equiv (\phi_p/N_p)$ we find:

$$\frac{\bar{v}_0}{\bar{v}_L} \cong 1 - C\xi_{max} \qquad \text{(mean size).} \tag{31}$$

The last two equations, when combined with equation (5), immediately yield the corresponding correction to the geometric mean particle size: $v_{g,o}/v_{g,L}$,

i.e.
$$\frac{v_{g,o}}{v_{g,L}} \cong 1 - [C + \tfrac{1}{2}(C_1^{(2)} + C_1^{(0)} + C_1^{(1)})]\,\xi_{max}. \tag{32}$$

Thus, it would appear that when $\xi_{max} \leq 0.3$ (say) and the assumptions A1–7 are simultaneously reasonable equations (29)–(31) can provide acceptable rational corrections to measured aerosol data to account for the systematic effects of upstream coagulation and/or wall losses. It is interesting to note that while in the explicit forms stated they appear to be valid for either‡ laminar or turbulent gas flow, and free-molecule or continuum particle transport, in practice they would often incur unacceptably large errors for laminar flow systems due to so-called 'entrance'-effects on the mass transfer coefficient (see, e.g. sections 5.2 and 6.1, and Rosner (1986)). A numerical procedure to effectively eliminate such errors without introducing any new parameters has been developed (Rosner and Tassopoulos, 1991b) but is beyond the scope of the present paper. However, the present results can be approximately corrected for this effect by simply replacing the 'fully-developed' value of $\mathrm{St}_m(\bar{v}_L)$ $(= \mathrm{Nu}_m/(\mathrm{ReSc}))$ by the streamwise-integrated average value $\bar{F}$(entrance) $\cdot$ Nu_m(fully developed)/$(\mathrm{Re}\cdot\mathrm{Sc}(\bar{v}_L))$ and by introducing an effective value of the St_m-exponent b, written b_{eff}, which varies between $-4/9$ and $-2/3$ (Table 1) according to the value of $\bar{F}$(entrance). This correction procedure for the present laminar results, using Nu_m(fully developed) $= 3.657$ for a straight circular duct, is illustrated in section 5.2.

4.3. *Direct numerical integration for particular cases*

The 'universality' of the results derived and presented above, and the relatively small number of dimensionless parameters on which they depend (section 3.7), of course follow from our underlying idealizations, made explicit in section 2. However, the basic moment-method approach (section 3), together with our treatment of wall losses (section 3.3) and

† Closed-form expressions are available for the $C_2^{(k)}$ coefficients (of ξ^2) (see Appendix A).

‡ These physical differences do, of course, affect the results, but only implicitly via establishment of the appropriate values of ξ_{max} (equation (3.6-1)) and the St_m exponent b (see Table 1).

interparticle coagulation (section 4, and the primary references cited therein) can clearly be used to obtain PSD-parameter correction factors in much more complicated aerosol sampling duct situations, such as for example, systems which are cooled near the inlet (to prevent thermal failure) and subsequently heated (to prevent water vapour condensation) for extracting carbonaceous soot (smoke) aerosols from gas turbine engine combustors (see, e.g. Colket *et al.* (1977), and section 6). In such cases the recommended procedure would be to integrate the appropriate coupled set of ODEs (of the form of equation (16), but with the LHS written $\{(1/A)\mathrm{d}(AUM_k)/\mathrm{d}z\}$ and introduction of the 'upstream' position variable $x = L - z$), after incorporating the required special features of the sampling system of particular interest (see sections 6.1–6.12).

5. IMPLICATIONS AND APPLICATIONS

To fix ideas, become familiar with typical orders-of-magnitude, and illustrate how to use the results calculated/presented in section 4 it is useful to briefly consider at least two specific numerical examples that arise in conveying aerosol samples to a 'remote' instrument via a constant area duct. The first (section 5.1) is based on an exercise in Friedlander's 1977 textbook involving turbulent gas flow in a ground-based aerosol sampling system. The second example involving laminar gas flow is based on conditions encountered in a proposed system for sampling the Earth's atmosphere from a research aircraft flying at ca. 8 km altitude. In both cases we examine log-normal distributions of highly submicron particles for which wall losses are often non-negligible even for relatively 'short' ducts. We also define the total concentration levels beyond which Brownian coagulation processes of such particles within the duct will become non-negligible. Explicit applications to more complex (e.g. diabatic) systems, as frequently encountered in sampling combustion engines, are beyond the scope of this paper (see sections 4.3 and 6).

5.1. *Turbulent flow in duct of ground-based air monitoring station*

Exercise 5, Chapter 3 of Friedlander (1977) deals with a ground-based air monitoring station. Outside air is delivered to the aerosol instruments via a 2-in diameter, 12-ft long duct at a mean velocity of 10 ft s^{-1}. The goal is to "calculate the correction factor that must be applied for submicron particles as a result of diffusion to the walls of the duct, e.g. the percentage by which the measured concentration must be altered to provide the true (ambient) concentration as a function of particle size". To illustrate our procedures let us imagine that the aerosol instrument 'sees' a sub-micron aerosol PSD which is log-normal with a spread of $\sigma_g = 2.46$ and a geometric mean diameter corresponding to $\bar{d}_p = 0.02\ \mu$m, i.e.:

$$d_g = \bar{d}_p \cdot \exp[-\tfrac{1}{6}\ln^2 \sigma_g] = (0.02\ \mu\mathrm{m}) \cdot \exp[-\tfrac{1}{6}\ln^2(2.46)] = 0.0175\ \mu\mathrm{m}. \qquad (33)$$

The Brownian diffusivity D_p for a 0.02 μm diameter particle in, say, 20°C air at 1 atm is (see, e.g. Table 2.1, Friedlander (1977)) 1.34×10^{-4} cm^2 s^{-1} and (since the momentum diffusivity of air is 1.50×10^{-1} cm^2 s^{-1} under these same conditions) we also find that $\mathrm{Sc}(\bar{v}_{p,L}) \equiv \nu/D_p(v_{p,L}) = 1.12 \times 10^3$ for the mean particle diameter. The mass transfer coefficient St_m appropriate to this case can be estimated once the Reynolds number Ud_w/ν characterizing this air flow is determined. Converting to metric units we find that $d_w = 5.08$ cm, $U = 3.05 \times 10^2$ cm s^{-1} and, therefore, $\mathrm{Re} = 1.03 \times 10^4$, which is well into the turbulent range. For a smooth wall straight duct and particles in this size range (see section 6.7) St_m can therefore be estimated from, say, equation (6.5–11b) of Rosner (1986), i.e.:

$$\mathrm{St}_m \approx 0.0889\left(\frac{C_f}{2}\right)^{1/2} \cdot \mathrm{Sc}^{-0.704} \qquad (\mathrm{Sc} \gg 1), \qquad (34)$$

where $C_f(\mathrm{Re})$ is the friction factor (non-dimensional time-averaged shear stress at the hydraulically smooth duct wall) corresponding to the prevailing Reynolds number. This can be estimated as $0.079\ \mathrm{Re}^{-1/4}$ so that $C_f = 0.783 \times 10^{-2}$, $(C_f/2)^{1/2} = 0.626 \times 10^{-1}$ and, hence,

$St_m(\bar{v}_{p,L}) \approx 3.97 \times 10^{-6}$ (via equation (34)). We are now in a position to calculate the decisive dimensionless 'scaled' length of the sampling tube, i.e.:

$$\xi_{max} \equiv 4\left(\frac{L}{d_w}\right) \cdot \mathrm{St}_m(\bar{v}_{p,L}) \cdot F_{0,L} \tag{35}$$

$$\xi_{max} \equiv 4\left(\frac{L}{d_w}\right) \cdot \mathrm{St}_m(\bar{v}_{p,L}) \cdot \exp\left[\frac{b(b-1)}{2} \cdot \ln^2 \sigma_{g,L}\right] = 1.51 \times 10^{-3},$$

where we have used the fact that $L = 3.66 \times 10^2$ cm, $L/d_w = 72$ and (see Table 1) $b \cong -0.469$ for particles which are small compared to the prevailing gas-free-path (0.065 μm). In this case, since ξ_{max} is small, the Taylor series results of section 4.3 will be useful, i.e.:

$$\frac{N_{p,0}}{N_{p,L}} \cong 1 + (1 + C_{fm})\xi_{max}, \tag{36}$$

so that if coagulation is negligible (i.e. $C_{fm} \ll 1$ (see below)) then $N_{p,0}/N_{p,L} = 1 + 1.51 \times 10^{-3} = 1.0015$. Thus, under such conditions total number densities in the ambient atmosphere would only be about 0.15% above those present at the detector. Based on the definition of the dimensionless coagulation parameter C_{fm} it is also possible to calculate the level of particle number density, $N_{p,L}$ at which coagulation effects and wall loss effects on $N_{p,0}/N_{p,L}$ would be comparable—i.e. conditions corresponding to $C_{fm} = 1$. In the present case:

$$C_{fm} \equiv \frac{(-Z^{(0)}_{fm,L})(\frac{1}{2}K_{fm})N_{p,L}}{4/d_w \cdot U \cdot \mathrm{St}_m(\bar{v}_{p,L}) \cdot F_{0,L}}. \tag{37}$$

Setting $C_{fm} = 1$ and evaluating the factors $(-Z^{(0)}_{fm,L})$ and $\frac{1}{2}K_{fm}$ from their respective definitions (see Table 2, first row) we find that $C_{fm} = 1$ when $N_{p,L} \cong \mathrm{O}(1.1 \times 10^7$ particles $\mathrm{cm}^{-3})$, a level that could be experienced near pollutant sources. However, on the assumption that particle concentrations are frequently much lower than this we proceed to calculate the (small) corrections needed to arrive at the ambient PSD parameters $\sigma_{g,0}$ and $v_{g,0}$. These can be obtained from equations (30) and (32), respectively. In this case: $C_1^{(0)} = 1$, $C_1^{(1)} = 1$, $C_1^{(2)} = \exp[-2(-0.469)\ln^2(2.46)] = 2.138$ so that:

$$\frac{\sigma_{g,0}}{\sigma_{g,L}} \approx 1 + \frac{(2.138-1)(1.51 \times 10^{-3})}{2\ln(2.46)} = 1.00095$$

and:

$$\frac{(d_{p,g})_0}{(d_{p,g})_L} \approx \exp(-\tfrac{1}{6}(2.138-1)(1.51 \times 10^{-3})) = 0.9997,$$

i.e. when $\bar{d}_{p,L} = 0.02$ μm and $\sigma_{g,L} = 2.46$ the systematic corrections are modest indeed. However, the present formulation has the merit that it allows rapid calculations of corrections under other conditions of $d_{p,L}$, $\sigma_{g,L}$, L/d_w, U, . . . for which the corresponding corrections due to wall loss and/or coagulation may be appreciable, including cases requiring the graphs of sections 4.1 and 4.2 rather than the small ξ_{max} expansions of section 4.3 and Appendix A.

5.2. *Laminar flow in sampling tube upstream of an airborne condensation nucleus counter*

As our second specific example consider the following set of conditions typical of an airborne condensation nucleus particle counter (CNC) system for flight at an altitude of 25,000 ft. Suppose the cabin instrument package sees an aerosol with a mean particle diameter $\bar{d}_{p,L} \cong 0.014$ μm and a spread parameter of 2.46 in air at a volume flow rate of 24 $\mathrm{cm}^3\,\mathrm{s}^{-1}$, with the pressure and temperature levels established at 0.4 atm and 244 K,

respectively. If the insulated upstream tube that conveys the aerosol sample to the instrument has a length of 121 cm and an internal diameter of 0.953 cm then we seek to estimate the correction factors $N_{p,o}/N_{p,L}$, $\sigma_{g,o}/\sigma_{g,L}$ and $d_{g,o}/d_{g,L}$ to be applied to data recorded at the instrument in order to estimate the corresponding aerosol properties in the local troposphere.

If we tentatively assumed 'fully-developed' particle mass transfer in this $L/d_w = 128$ sampling tube system (see, however, section 6.1 and below) we would proceed as follows: Under the stated conditions the Reynolds number Ud_w/ν can be calculated to be only 1.165×10^2 so the gas flow will be *laminar*. The prevailing mean-free-path under the above-mentioned conditions is about 0.2 μm so that $\mathrm{Kn}_p(\bar{v}_{p,L}) = 14.4$ and most particles will experience conditions appropriate to free-molecule (fm) flow. In particular, the mean size particle will be characterized by a Brownian diffusivity of about $0.93 \times 10^{-3}\ \mathrm{cm^2\,s^{-1}}$, corresponding to a Schmidt number $\mathrm{Sc} = \nu/D_p$ of about 2.96×10^2. For fully-developed steady laminar flow in a straight circular duct it is well known that $\mathrm{Nu}_m = 3.657$ (Nusselt) so that:

$$\mathrm{St}_m(\bar{r}_L) = \frac{\mathrm{Nu}_m}{\mathrm{Re}\cdot\mathrm{Sc}} = \frac{3.657}{(1.165\times 10^2)(2.96\times 10^2)} = 1.06\times 10^{-4}. \tag{38}$$

It would follow that:

$$\xi_{max} = 4\left(\frac{L}{d_w}\right)\cdot \mathrm{St}_m(\bar{r}_L)\cdot \exp\left[\frac{b(b-1)}{2}\ln^2\sigma_g\right] = 0.852\times 10^{-1} \tag{39}$$

since (Table 1) $b = -2/3$. If the coagulation parameter $C_{fm} \ll 1$ (see below) then this would correspond to $N_{p,o}/N_{p,L} \cong 1.085$ due to particle size-dependent wall loss (based, again, on equation (29)). Noting that $C_1^{(2)} = \exp\{-2(-2/3)\ln^2(2.46)\} = 2.947$ we find (equation (30)) that the remaining correction factors are: $\sigma_{g,o}/\sigma_{g,L} \approx 1.09$ and $d_{g,o}/d_{g,L} \approx 0.973$ (equation (32)). Returning to the possibility of coagulation effects, we can calculate what particle number density $N_{p,L}$ would be required to cause $C_{fm} \approx 10^{-1}$, say. Since this turns out to be *ca* $3\times 10^6\ \mathrm{cm^{-3}}$ in the present case (a value very far in excess of ambient atmosphere particle number densities ($O(10^{-2}\ \mathrm{cm^{-3}})$ at such altitudes) the neglect of coagulation in such sampling tubes is seen to be self-consistent.

Returning to the question of the validity of our tentative assumption of 'fully-developed' particle mass transfer (i.e. A4, negligible 'entrance effect') we note that while the viscous flow itself would become fully-developed (z/d_w-independent) beyond a L/d_w of only about $0.2\mathrm{Re} = 23$, the value of St_m will not approach the fully-developed asymptote until L/d_w is about $0.2\mathrm{ReSc} = 6900$. Since the actual L/d_w of the system is 128 we see *a posteriori* that A4 is not justified under such laminar flow conditions (see section 6.1). All is not lost, however, since there is good reason to believe that if ξ_{max} is recalculated using the actual length-averaged transfer coefficient, and an effective value of b appropriate to the magnitude of the entrance effect, then our previous formulas (or graphs) will provide a useful first approximation. The 'entrance-effect' correction factor $\bar{F}_e$ to the fully-developed value of $\overline{\mathrm{Nu}}_m$ or $\overline{\mathrm{St}}_m$ is known to depend upon the dimensionless distance variable:

$$\frac{1}{\mathrm{Re}\cdot\mathrm{Sc}}\cdot\frac{L}{d_w} \equiv \zeta_m(\text{say}). \tag{40}$$

For fully-developed laminar flow in a straight circular duct a convenient approximation to $\bar{F}$(entrance) is (see, e.g. Rosner, 1986)

$$\bar{F}_e \approx [1 + (7.60\zeta_m)^{-8/3}]^{1/8}, \tag{41}$$

which, in the present case, gives $\bar{F}_e = 3.29$ corresponding to $\overline{\mathrm{St}}_m(\bar{v}_L) = 3.49\times 10^{-4}$. Using the appropriate "effective" value of b obtained from

$$b_{eff} = -\frac{2}{3}\cdot\left[1 + \frac{d\ln\bar{F}_e}{d\ln\zeta_m}\right] \cong -\frac{2}{3}\left[1 - \frac{1}{3}(1-\bar{F}_e^{-8})\right] \approx -\frac{4}{9} \tag{42}$$

(see, e.g. Rosner and Tassopoulos, 1991) we then recalculate the values of ξ_{max}, this time obtaining $\xi_{max} = 0.30$, corresponding to $N_{p,o}/N_{p,L} \cong 1.3$. Recomputing the remaining correction factors now gives $\sigma_{g,o}/\sigma_{g,L} \cong 1.18$ and $d_{g,o}/d_{g,L} \approx 0.95$. Based on the present work this would provide the best current estimate of the required correction factors in this laminar flow aerosol sampling system. More rigorous calculations (now underway) will be necessary to test the accuracy of this plausible, proposed correction procedure (for relaxing A4).

In the light of these two simple numerical examples, both involving highly submicron, dense (*ca* $\tilde{\rho}_p = 1.83\ \mathrm{g\,cm^{-3}}$) spherical particles in straight nearly adiabatic sampling ducts but one with laminar flow (section 5.2) and one with turbulent flow (section 5.1), it is now appropriate to briefly discuss many of the abovementioned assumptions, indicating, where possible, methods to generalize the treatment to include less 'idealized' cases often encountered in sampling from industrially important devices (e.g. combustors for propulsion or power generation).

6. DISCUSSION OF ASSUMPTIONS AND GENERALIZATIONS

It is prudent to consider the domain of validity of the underlying assumptions of section 2 and useful to indicate here how readily some of these assumptions can be relaxed, thereby opening the door to the quantitative treatment of much more complex sampling duct situations.

6.1. *Entry effects*

Even apart from development of the viscous gas flow itself, the mass transfer boundary layers within the sampling tube require a 'development length' before $\mathrm{St_m}$ (equation (6)) becomes essentially independent of z/d_w. For laminar mass transfer boundary layers the required number of duct diameters is approximately:

$$\left(\frac{L}{d_w}\right)_{req} = 0.2(\mathrm{Re}\cdot\mathrm{Sc}), \tag{43}$$

which, for the example of section 5.2, is about 6900, far in excess of the actual L/d_w of the sampling system (128) or the L/d_w required for development of the host gas flow itself (*ca* 23). Thus, unless much smaller particles are of interest, Assumption 4 will *not* be defensible for many *laminar* flow sampling systems. A rational 'correction' for this can, however, be made when coagulation is negligible (using the actual length-averaged $\overline{\mathrm{St}}_m$-value in the definition of ξ and modifying the effective exponent b, as discussed in section 5.2) or specific results can be generated for laminar sampling systems by accurately including such mass transfer 'entrance effects' (Rosner and Tassopoulos, 1991a). For *turbulent*, high Sc systems the situation is much improved and $(L/d_w)_{req}$ will ordinarily be less than about 30, a condition which is frequently met*, and certainly met in the ground-based air monitoring application discussed in section 5.1.

6.2. *Variable* $\mathrm{d_{eff}} \equiv 4\mathrm{A}(z)/\mathrm{P}(z)$

If the effective duct diameter d_{eff} is not constant, but sufficiently slowly varying, then the quasi-one-dimensional equations (equation (16)) remain valid, and such geometric effects can clearly be incorporated in the numerical integrations. In many situations d_{eff} will be piecewise-constant, in which case our analysis would apply to each *segment* of the system but with the effective lengths of the segments modified to allow for the inevitable 'entrance-effects' near each juncture (see, e.g. section 6.1).

* Colket *et al.* (1977) describe a diabatic system with $L/d_w \approx 2200$ for sampling from gas turbine combustors.

6.3. *Bends*

Because of the secondary flows and turbulence modulation associated with bends in a "piecewise straight" sampling system $St_m(z/d_w, Re, Sc)$ will be modified in accord with the curvature d_w/R and included angle of the bend. Recent (vapor) mass transfer data of this type (see, e.g. Sparrow and Chrysler (1986) and Ohadi and Sparrow (1989, 1990)) are now being mobilized and recast so that it may be conveniently used in the present type of quasi-one dimensional, $Sc \gg 1$ analysis (Rosner *et al.*, 1991).

6.4. *Heated (cooled) ducts*

Inadvertent or deliberate heat transfer can dramatically alter the rates of fine particle loss to the wall, and the particle size-dependence of this rate (cf. the St_m exponent b) as a result of particle thermophoresis. The laws of particle thermophoresis (drift down the transverse temperature gradient) have been under extensive development in the last 15 years (see, e.g. the recent review of Rosner *et al.*, 1990) and it has been shown that for submicron particles deliberately heated ducts can be used to sharply reduce wall deposition rates [see, e.g. Gokoglu and Rosner (1986) (before the gas temperature 'catches up' with the wall temperature]. While beyond the scope of the present paper, it can be shown that in some cases (e.g. constant wall heat flux (addition)) the present results can be used as a first approximation with a suitably reduced St_m-value and a modified (more negative) b_{eff}-value (Rosner and Tassopoulos, 1991b). In some cases wall cooling may be necessary near the inlet to prevent local probe failure (as in extracting samples from high temperature combustors (Colket *et al.* (1977), arcjets, etc.). This can cause appreciable local particle losses to the wall unless the wall cooling is accomplished by foreign gas transpiration (see, e.g. Gokoglu and Rosner, 1985). Sometimes downstream heating is also used to prevent the condensation of a co-present vapor, as in sampling the combustion products of a gas turbine combustor.

6.5. *Single mode log-normality*

Aerosols formed from several distinct mechanisms may exhibit a multi-modal PSD, each mode of which can be represented by a log-normal distribution. If (as is often the case) further coagulation can be neglected within the aerosol sampling tube then our present results can be applied without modification to each mode. In the presence of appreciable coagulation this is no longer possible and results would have to be obtained using an extended coagulation rate theory along the lines of Megaridis and Dobbins (1990a) to deal with particular cases of interest.

6.6. Kn_p-*interpolation*

If an appreciable portion of the aerosol is in the transition regime of $Kn_p = O(1)$, then neither of the above-mentioned asymptotic regime results ($Kn_p \gg 1$ called free-molecule, or $Kn_p \ll 1$ called continuum) would provide an accurate description. This influences both the wall loss behavior (via its effect on the Brownian diffusion law $D(v)$) and the coagulation rate behavior (via the collision rate constant β, which will differ from either of the previously considered asymptotes β_{fm} and β_c). A general treatment of this regime is possible, which will introduce an additional parameter like the Knudsen number based on the median diameter $(6v_{g,L}/\pi)^{1/3}$. In the absence of coagulation the principal effects are to modify $St_m(\bar{v}_L)$ and the effective values of the St_m-exponent b. In the presence of coagulation, use can be made of the simple and successful so-called 'harmonic-average' approximation for the coagulation rate constant, i.e. $\beta^{-1} \approx \beta_{fm}^{-1} + \beta_c^{-1}$ which can be introduced to generalize the moment-method treatment of section 3.4 (Rosner and Tassopoulos, 1991b) (for an alternative but closely related approach, see Pratsinis and Kim (1989) and Biswas *et al.* (1989)).

6.7. *Eddy-impaction*

When the sampling duct flow is turbulent ($Re > 2.3 \times 10^3$, say) and a significant portion of the aerosol is associated with dimensionless particle stopping times $t_p^+ (\equiv u_*^2 t_p/\nu)$ greater than about $16.5\,(Sc)^{-0.352}$ then time-averaged wall losses will be enhanced by the mechanism of 'eddy-impaction' (see, e.g. the brief summary of available correlations contained in Rosner and Tassopoulos (1989)), which also modifies the effective value of the exponent b for that portion of the aerosol. Only when eddy-impaction is the dominant mechanism and $St_m \sim (t_p^+)^2$ for most of the prevailing particles can our present formulation be retained, but with $b = +1.333$ (see Rosner and Tassopoulos, (1989)). However, for the illustrative problem discussed in section 5.1 we find that eddy-impaction would not set in until $d_p = 3.8\ \mu m$, a size beyond which there are few particles indeed. Thus, the previous treatment is self-consistent in this respect. Other effects associated with the mass of the suspended particles (e.g. sedimentation and/or inertial impaction in bends) are likewise expected to be negligible.

6.8. *Turbulent coagulation*

In principle, new mechanisms of suspended particle–particle coagulation/coalescence occur in turbulent flows (Friedlander, 1977) which could be incorporated within our moment method calculation of coagulation via the appropriate $\beta(u, v, \ldots)$ functions. However, even in turbulent flows sufficiently small suspended particles (the ones likely to be numerous enough) will still coagulate according to the Brownian laws discussed in section 2, especially in initially well-mixed (homogeneous) submicron aerosol situations at the inlet. In many cases even such small particles may not be numerous enough to warrant the inclusion of coagulation within the sampling tube (see the examples of sections 5.1 and 5.2).

6.9. *Axial dispersion*

For radially nonuniform velocity steady flow in a duct the effective axial diffusivity is known to be larger than the true Brownian diffusivity by the Taylor-contribution (see, e.g. Butt, 1980; Denbigh and Turner, 1971; Probstein, 1989)

$$(D_{eff})_{Taylor} = \begin{cases} \dfrac{Re \cdot Sc}{192} \cdot U d_w & \text{(laminar)} \\ 5\left(\dfrac{C_f}{2}\right)^{1/2} \cdot U d_w & \text{(turbulent)} \end{cases} \tag{44}$$

so that Assumption 3 (section 2) is equivalent to satisfying the inequality:

$$\left(\frac{D_{eff}}{UL}\right) \cdot \left(\frac{N_{p,0}}{N_{p,L}} - 1\right) \ll 1. \tag{45}$$

This criterion is readily satisfied in the turbulent flow example (section 5.1) but is only marginally satisfied in the laminar flow example (section 5.2). In both examples the effective axial diffusivity in completely dominated by the fluid-dynamic (Taylor) contribution. These results again suggest (cf. section 6.1) that the idealizations exploited in the present work are more appropriate to turbulent flow sampling systems (section 5.1) than laminar flow sampling systems (section 5.2), and that many laminar systems will warrant a more accurate treatment than that indicated in section 5.2, even including the above-mentioned 'entrance-effect' correction (section 6.1).

6.10. *Aggregate deposition/coagulation*

For non-coalesced aggregates comprised of primary particles of volume v_1 each depositing 'particle' will have the total volume $v = nv_1$, where n is some integer (see, e.g. Megaridis

and Dobbins, 1990b). Such aggregated particles will have orientation-averaged Brownian diffusivities which will depend not only upon v but also on the particular morphology (arrangement of the primary particles). In each case we can write:

$$b \equiv \frac{\partial \ln \mathrm{St}_m}{\partial \ln v} = -\frac{\partial \ln \mathrm{St}_m}{\partial \ln \mathrm{Sc}} \cdot \left(\frac{\partial \ln D}{\partial \ln v} \right). \tag{46}$$

Thus, when coagulation is negligible, a knowledge of $\mathrm{St}_m(v)$, where $v = nv_1$ and of the appropriate value of $\partial \ln D / \partial \ln v$ for the morphology is question will also allow useful predictions to be made for aggregated particles (see, e.g. Rosner, 1991; Rosner *et al.*, 1991). A treatment of suspended aggregate–aggregate coagulation analogous to that outlined in section 3.4 is apparently not yet available.

6.11. *Non-power law capture*

If the Schmidt number dependence of St_m deviates from a simple power law and/or $D(v)$ departs from a simple power-law then the value of the exponent b will not be a constant (cf. equation (46)) and corrections to the convenient computational procedures exploited here will be necessary. In Rosner (1989) we showed that these corrections depend upon $(\partial^2 \ln \mathrm{St}_m / \partial \ln^2 v)_{\bar{v}}$ and the local spread of the PSD. This provides either a testable criterion for the validity of power-law behavior in any particular case or the basis of a systematic correction procedure for the calculation of the factor F_k (cf. equation (12)) (see, e.g. Rosner and Tassopoulous (1991b)). For straight duct high Schmidt number turbulent convective-diffusion transport in either the free-molecule (fm) or continuum (c) limits these corrections vanish and the exponents (b-values) presented in the second row of Table 1 are true constants. However, it should be realized that no single mechanism of particle transport (hence $\mathrm{St}_m(v)$-law) is strictly valid over the entire range of particle sizes (see, e.g. Rosner and Tassopolous, 1989). Furthermore, even when a single deposition mechanism dominates, departures from simple power-law behavior may be associated with fluid-dynamic non-idealities, such as developing-(section 6.1) and/or secondary-flows (cf. section 6.3)

6.12. *Vapor growth/particle evaporation*

In the present analysis we assumed that the suspended particles are stable with respect to evaporation or growth by vapor condensation in the prevailing carrier gas environment (A7). In "diabatic" sampling tube cases (often encountered in extractive sampling from hostile environments, such as gas turbine engine combustors) this may not be valid and the analysis of section 3 would then have to be generalized by including the contribution to the $U dM_k/dz$ due to vapor growth (see, e.g. Friedlander, 1977; Megaridis, 1987; Megaridis and Dobbins, 1989) coupled with balance equations for the vapor concentration and the bulk (mixing cup-averaged) gas temperature. The present class of moment methods would also make specific calculations of this type feasible, however, the assumption of log-normality could prove overly restrictive in many such instances (see, e.g. Landgrebe and Pratsinis, 1989; Landgrebe, 1989; Biswas *et al.*, 1987; Mackowski *et al.*, 1991).

7. CONCLUSIONS, RECOMMENDATIONS AND FUTURE WORK

A simple, rational, moment-based method is presented for correcting aerosol sampling data for the systematic upstream effects of particle size-dependent wall losses and, if necessary, particle–particle coagulation. 'Universal' graphs and rational formulae are developed and provided for the commonly encountered cases of log-normally distributed aerosols in straight adiabatic ducts of constant cross-section/'wetted' perimeter for the limiting cases of free-molecule particle transport ($\mathrm{Kn}_p \gg 1$) and continuum particle transport ($\mathrm{Kn}_p \ll 1$). In many cases the leading terms of a Taylor series expansion in the dimensionless distance (proportional to $(L/d_w)\mathrm{St}_m(\bar{v})$) will be adequate to provide the

desired correction factors: $N_{p,o}/N_{p,meas}$, $\phi_{p,o}/\phi_{p,meas}$ and $M_{2,o}/M_{2,meas}$ as well as $r_{g,o}/r_{g,meas}$ and $\sigma_{g,o}/\sigma_{g,meas}$. In more general cases backward numerical integration of the relevant coupled moment equations is recommended, allowing several of the idealizations discussed in sections 2 and 6 to be simultaneously relaxed. In addition to providing a simple yet rational basis for correcting aerosol sampling instrument data (i.e. a direct solution to the canonical 'inverse' problem of aerosol sampling theory), the present results can also be used to provide preliminary design information for a prospective aerosol sampling system to circumvent the future need for uncomfortably large correction factors (predicted or laboriously measured) in the ambient environment of interest.

The present approach opens the door to several generalizations which will be of practical interest (see, also, Rosner and Tassopoulos, 1990, 1991b)—especially the inclusion of additional deposition and/or coagulation mechanisms, effects of sampling duct bends, variable cross-sectional area, diabatic walls, departures from single-mode log-normality, and the presence of suspended particulate aggregates. Several of these extensions, beyond the scope of this introductory presentation but of importance in sampling from combustion turbines, rockets, and stationary fossil energy power plants (necessarily only briefly discussed in section 6), will be the subject of future communications from this laboratory.

Acknowledgements - This research was supported, in part, by AFOSR (Grant 89-0223), DOE-PETC (Grant DE-FG-2290PC90099), as well as the Yale HTCRE Laboratory Industrial Affiliates (SCM-Corporation, DuPont, Shell, GE and Union Carbide Corporations). It is also a pleasure to acknowledge helpful discussions and/or correspondence with J. Fernandez de la Mora, M. B. Colket, S. Grinshpun, A. G. Konstandopoulos, L. J. Forney and S. W. Rosner.

REFERENCES

Abuzucid, S., Busnaina, A. A. and Ahmadi, G. (1990) Wall deposition of aerosol particles in a turbulent channel flow. *J. Aerosol Sci.*

Bai, H. and Biswas, P. (1990) Diffusional deposition of continuous size distribution aerosols. *J. Aerosol Sci.* **21**, 629–640.

Belyaeu, S. P. and Levin, L. M. (1974) Techniques for collection of representative aerosol samples. *J. Aerosol Sci.* **5**, 325–338.

Biswas, P., Jones, C. L. and Flagan, R. C. (1987) Distortion of size distributions by condensation and evaporation in aerosol instruments. *Aerosol Sci. Technol.* **7**, 231–246.

Biswas, P., Li, X. and Pratsinis, S. E. (1989) Optical waveguide preform fabrication: silica formation and growth in a high temperature aerosol reactor. *J. appl. Phys* **65**, 2445–2450.

Butt, J. B. (1980) *Reaction Kinetics and Reactor Design*. Prentice-Hall, Englewood Cliffs, New Jersey.

Chow, K. H. and Lee, P. S. (1982) *Atmos. Envir.* **16**, 1513–1522.

Cohen, E. R. and Vaughan, E. U. (1971) Approximate solution of the equations for aerosol agglomeration. *J. Colloid Interf. Sci.* **35**, 612–623.

Colket, M. B., Stefucza, J. M., Peters, J. E. and Mellor, A. M. (1977) Radiation and smoke from gas turbine flames. U. S. Army Tank Automotive Command Propulsion Systems Lab (Warren MI) Tech. Report 12163; see, also, *J. Energy (AIAA)* **1**, 115.

Cooper, D. W. and Wu, J. J. (1990) The inversion matrix and error estimation in data inversion: application to diffusion battery measurements. *J. Aerosol Sci.* **21**, 217–226.

Davies, C. N. (1966) Deposition from moving aerosols, chap. 7 in *Aerosol Science* (Edited by Davies, C. N.), pp. 293–446. Academic Press, London.

Davies, C. N. (1968) The entry of aerosols into sampling tubes and heads. *Brit. J. Appl. Physics–J. Phys. D.* **1**, 921.

Denbigh, K. G. and Turner, J. C. R. (1971) *Chemical Reactor Theory*, second edition. Cambridge Univ. Press, Cambridge.

Dobbins, R. A. and Megaridis, C. (1987) Morphology of flame-generated soot as determined by thermophoretic sampling. *Langmuir (ACS)* **3**, 254.

Dobbins, R. A. and Mulholland, G. W. (1984) Interpretation of optical measurements of flame generated particles. *Combust. Sci. Technol.* **40**, 175–191.

Flagan, R. C. and Seinfeld, J. H. (1988) *Fundamentals of Air Pollution Engineering*. Prentice-Hall, Englewood Cliffs, New Jersey.

Frenklach, M. and Harris, S. (1987) Aerosol dynamics modeling using the method of moments. *J. Colloid Interf. Sci.* **118**, 252 (General Motors Res. Lab. Public. GMR-5504, 13 August 1986).

Friedlander, S. K. (1977) *Smoke, Dust and Haze*. John Wiley, New York.

Friedlander, S. K. and Wang, C. S. (1966) The self-preserving particle size distribution for coagulation by Brownian motion–small particle slip correction and simultaneous shear flow. *J. Colloid Interf. Sci.* **22**, 126–132.

Friedlander, S. K. and Wang, C. S. (1967) The self-preserving particle size distribution for coagulation by Brownian motion small particle slip correction and simultaneous shear flow. *J. Colloid Interf. Sci.* **24**, 170–179.

Fuchs, N. A. (1964) *Mechanics of Aerosols*. Pergamon Press, London.

Fuchs, N. A. and Sutugin, A. G. (1971) Highly dispersed aerosols. In *Topics in Current Aerosol Research* (Edited by Hidy, G. M. and Brock, J. R.), pp. 1–60. Pergamon Press, Oxford.

Hidy, G. (1984) *Aerosols—An Industrial and Environmental Science*. Academic Press, New York.
Hinds, W. C. (1982) *Aerosol Technology—Properties, Behavior and Measurement of Airborne Particles*. John Wiley, New York.
Huebert, B. J., Lee, G. and Warren, W. L. (1990) Airborne aerosol inlet passing efficiency measurement. *J. Geophys. Res.* **95**, 16,369–16,387.
Hungal, S. and Willeke, K. (1990) Aspiration efficiency: unified model for all sampling angles. *Envir. Sci. Technol.* **24**, 688–691.
Ivie, J. J., Forney, L. J. and Roach, R. L. (1990) Supersonic particle probes: measurement of internal wall losses. *Aerosol Sci. Technol.* **13**, 10.
Lai, F. S., Friedlander, S. K., Pich, J. and Hidy, G. M. (1971) The self-preserving particle size distribution for Brownian coagulation in the free-molecule regime. *J. Colloid Interface Sci.* **39**, 395–405.
Landgrebe, J. D. (1989) Gas-phase particulate manufacture: the interplay of chemical reaction and aerosol coagulation. MS Dissertation. Univ. of Cincinnati, Dept. ChE/Nuclear Eng.
Landgrebe, J. D., Pratsinis, S. E. and Mastrangelo, S. V. R. (1990) Nomographs for vapor synthesis of ceramic powders. *Chem. Eng. Sci.* **45**, 2931–2941.
Lee, K. W., Chen, H. and Gieseke, J. A. (1984) Log-normality preserving size distribution for Brownian coagulation in the free-molecule regime. *Aerosol Sci. Technol.* **3**, 53–62.
Liu, B. Y. H. and Agarwal, J. K. (1974) Experimental observations of aerosol deposition in turbulent pipe flow. *J. Aerosol Sci.* **5**, 145–155.
Mackowski, D. W., Tassopoulos, M. and Rosner, D. E. (1991) Effect of radiative heat transfer on the coagulation rates of combustion-generated particulates. Combustion Inst-Central States Section, Spring Meeting 21–24 April 1991, Nashville, TN.
Megaridis, C. M. (1987) Thermophoretic sampling and soot aerosol dynamics of an ethene diffusion flame, PhD Dissertation, Brown Univ., Providence, RI; see, also NBS-(now NIST-) Report NBS-GCR-87-532.
Megaridis, C. M. and Dobbins, R. A. (1989) An integral solution of the aerosol dynamic equation including surface growth reactions. *Comb. Sci. Technol.* **63**, 153–167.
Megaridis, C. M. and Dobbins, R. A. (1990a) A bimodal integral solution of the dynamic equation for an aerosol undergoing particle inception and coagulation. *Aerosol Sci. Technol.* **12**, 240–255.
Megaridis, C. M. and Dobbins, R. A. (1990b) Morphological description of flame-generated materials. *Comb. Sci. Technol.* **71**, 95–109.
Mercer, T. T. (1973) *Aerosol Technology in Hazard Evaluation*. Academic Press, New York.
Mercer, T. T. and Greene, T. D. (1974) Interpretation of diffusion 'battery' data. *J. Aerosol Sci.* **5**, 251–255.
Mitchell, J. P., Edwards, R. T. and Ball, M. H. E. (1989) The penetration of aerosols through fine capillaries. Atomic Energy Authority Report AEEW-R-2558. Winfrith, U.K.
Ohadi, M. M. and Sparrow, E. M. (1989) Heat transfer in a straight tube situated downstream of a bend. *Int. J. Heat Mass Transfer* **32**, 201–212.
Park, H. M. and Rosner, D. E. (1989) Boundary layer coagulation effects on the size distribution of thermophoretically deposited particles. *Chem. Eng. Sci.* **44**, 2225–2231.
Pratsinis, S. E. and Kim, K. S. (1989) Particle coagulation, diffusion and thermophoresis in laminar tube flows. *J. Aerosol Sci.* **20**, 101–111.
Probstein, R. (1989) *Physicochemical Hydrodynamics—An Introduction*. Butterworth-Heinemann, Stoneham, Massachusetts.
Rosner, D. E. (1986) *Transport Processes in Chemically Reacting Flow Systems*. Butterworth-Heinemann, Stoneham, Massachusetts.
Rosner, D. E. (1989) Total mass deposition rates from 'polydispersed' aerosols. *AIChE J.* **35**, 164–167.
Rosner, D. E. (1991) Structure-sensitivity of total mass deposition rates from streams containing coagulation-aged populations of aggregated primary particles (in preparation).
Rosner, D. E. and Tassopoulos, M. (1989) Deposition rates from 'polydispersed' particle populations of arbitrary spread. *AIChE J.* **35**, 1497–1508.
Rosner, D. E., Konstandopolous, A. G., Tassopoulos, M. and Mackowski, D. W. (1991) Deposition dynamics of combustion-generated particles: summary of recent studies of particle transport mechanisms, capture rates and resulting deposit microstructure/properties, Proc. Engineering Foundation Conference: *Inorganic Transformations and Ash Deposition During Combustion* (in press).
Rosner, D. E., Mackowski, D. W., Tassopoulos, M., Castillo, J. and Garcia-Ybarra, P. (1990) Effects of heat transfer on the dynamics and transport of small particles in gases, I/EC-Research (in press). (Paper 293e AIChE 1990 Annual Mtg., Chicago, IL, 12 Nov.).
Rosner, D. E. and Tassopoulos, M. (1990) Moment methods to predict coagulation effects on deposition rate phenomena, Paper 5E.5, 1990 Meeting of the Amer. Assoc. Aerosol Res., 18–22 June, Philadelphia, PA.
Rosner, D. E. and Tassopoulos, M. (1991a) Moment method calculation of mass transfer entrance effects on wall-loss corrections in laminar flow aerosol sampling systems (in preparation).
Rosner, D. E. and Tassopoulos, M. (1991b) Moment methods in the theory of 'polydispersed' particle deposition from flowing suspensions. (in preparation.)
Rosner, D. E. *et al.* (1991) Use of available sublimation, electrochemical and heat transfer data to estimate ultrafine particle losses in sampling systems containing bends. Yale Univ. HTCRE Lab. Publication (in prep.).
Seinfeld, J. H. (1986) *Air Pollution*. Wiley, New York.
Sparrow, E. M. and Chrysler, G. M. (1986) Turbulent flow and heat transfer in bends of circular cross-section. *ASME Trans.-J. Heat Trans.* **108**, 40–47.
Ulrich, G. D. and Riehl, J. W. (1982) Aggregation and growth of submicron oxide particles in flames. *J. Colloid Interface Sci.* **87**, 257.
Ulrich, G. D. and Subramanian, N. S. (1977) Particle growth in flames, III. Coalescence as a rate-controlling process. *Comb. Sci. Technol.* **17**, 119–126.
Vincent, J. H. (1989) *Aerosol Sampling and Practice*, chap. 10. John Wiley, Chichester.

Zachariah, M. and Semerjian, H. (1989) Simulation of ceramic particle formation: comparison with *in situ* measurements. *AIChE J.* 35, 2003–2012.
Zebel, Z. (1978) Some problems in the sampling of aerosols. In *Recent Developments in Aerosol Science* (Edited by Shaw, D. T.). Wiley-Interscience, New York.

APPENDIX A: $C_2^{(k)}$ COEFFICIENTS

In this Appendix we provide the second-order terms, $C_2^{(k)\dagger}$, of the small-ξ expansions (see equation (27)). The wall-loss (WL) terms, clearly the same for free-molecule and continuum coagulation, are:

$$\tilde{N}''_{p,WL}(L)=\left[b\tilde{\phi}'_p+(1-b)\tilde{N}'_p+\frac{(b-1)b(-2\tilde{\phi}'_p+\tilde{M}'_2+\tilde{N}'_p)}{2}\right]_L$$

$$\tilde{\phi}''_{p,WL}(L)=\left[-(1+b)[\tilde{\phi}'_p]^2+b\tilde{N}'_p\tilde{\phi}'_p-\frac{(b-1)b(-2\tilde{\phi}'_p+\tilde{N}'_p+\tilde{M}'_2)\tilde{\phi}'_p}{2}\right]_L$$

$$\tilde{M}''_{2,WL}(L)=\left[b(\tilde{\phi}'_p-\tilde{N}'_p)+\tilde{M}'_2+\frac{b(3+b)(-2\tilde{\phi}'_p+\tilde{M}'_2+\tilde{N}'_p)}{2}\right]_L\cdot\exp(2b\ln^2\sigma_{g,L}),$$

where $\tilde{N}'_p$, $\tilde{\phi}'_p$ and $\tilde{M}'_2$ are the first-order expansion coefficients* defined in equations (28). Next we provide the coefficients associated with coagulation†. For free-molecule coagulation we find:

$$\tilde{N}''_{p,C}(L)=\left[\frac{1}{6}\tilde{\phi}'_p+2\tilde{N}'_p+\frac{5(-2\tilde{\phi}'_p+\tilde{M}'_2+\tilde{N}'_p)}{48}\right]_L\cdot\frac{C}{(\ln\sigma_{g,L})^{1/3}\exp(\frac{1}{12}\ln^2\sigma_{g,L})}$$

$$\tilde{\phi}''_{p,C}(L)=0$$

$$\tilde{M}''_{2,C}(L)=C\cdot\left\{-\frac{2\left[\frac{13}{6}\tilde{\phi}'_p+2\tilde{N}'_p+\frac{13}{48}(-2\tilde{\phi}'_p+\tilde{N}'_p+\tilde{M}'_2)\right]_L}{(\ln\sigma_{g,L})^{13/3}\cdot\exp\left(\frac{37}{12}\ln^2\sigma_{g,L}\right)}\right\}.$$

The corresponding coefficients for continuum coagulation are:

$$\tilde{N}''_{p,C}(L)=C\cdot\frac{2[1+\exp(\frac{1}{9}\ln^2\sigma_{g,L})]\tilde{N}'_p+\frac{1}{9}\exp(\ln^2\sigma_{g,L})(-2\tilde{\phi}_p+\tilde{M}'_2+\tilde{N}'_p)}{1+\exp(\frac{1}{9}\ln^2\sigma_{g,L})}$$

$$\tilde{\phi}''_{p,C}(L)=0$$

$$\tilde{M}''_{2,C}(L)=C\left\{-\frac{2\left[2\left(1+\exp\left(\frac{1}{9}\ln^2\sigma_{g,L}\right)\right)+\frac{1}{9}\exp(\ln^2\sigma_{g,L})(-2\tilde{\phi}_p+\tilde{M}'_2+\tilde{N}'_p)\right]}{\exp(\ln^2\sigma_{g,L})\cdot[1+\exp(\ln^2\sigma_{g,L})]}\right\}.$$

These coefficients can prove useful to evaluate correction factors when ξ_{max} exceeds, say 0.2, but does not exceed about 0.6. For values of ξ_{max} much above 0.6 direct use should be made of the figures of section 4.2 or specific numerical integrations in accord with section 4.3.

HIGH TEMPERATURE CHEMICAL REACTION ENGINEERING LABORATORY
YALE UNIVERSITY
BOX 2159, YALE STATION
NEW HAVEN, CONNECTICUT 06520 U.S.A.

* In the present notation $C_1^{(0)}\equiv\tilde{N}_{p,L}$, $C_1^{(1)}\equiv\tilde{\phi}'_{p,L}$, $C_1^{(2)}\equiv\tilde{M}'_{2,L}$.
† Note that $C_2^{(0)}\equiv\tilde{N}''_{p,WL}(L)+\tilde{N}''_{p,C}(L)$, etc.